DEVELOPMENT OF PEPTIDE BASED MATERIALS AS A SYNTHETIC SCAFFOLD TO MIMIC EXTRACELLULAR MATRIX

A DISSERTATION SUBMITTED TO

THE GRADUATE SCHOOL OF ENGINEERING AND SCIENCE

OF BILKENT UNIVERSITY

IN PARTIAL FULFILLMENT OF THE REQUIREMENTS FOR

THE DEGREE OF

DOCTOR OF PHILOSOPHY

IN

MATERIALS SCIENCE AND NANOTECHNOLOGY

By

MELİKE SEVER

July 2017

DEVELOPMENT OF PEPTIDE BASED MATERIALS AS A SYNTHETIC SCAFFOLD TO MIMIC EXTRACELLULAR MATRIX

By Melike Sever
July 2017

We certify that we have read this dissertation and that in our opinion it is fully adequate, in scope and in quality, as a dissertation for the degree of Doctor of Philosophy.

Ayşe Begüm Tekinay (Advisor)

Çağlar Elbüken

Yusuf Şükrü Çağlar

Nülüfer Tülün Güray

Michelle Marie Adams

Approved for the Graduate School of Engineering and Science:

Ezhan Karaşan

Director of the Graduate School

ABSTRACT

DEVELOPMENT OF PEPTIDE BASED MATERIALS AS A SYNTHETIC SCAFFOLD TO MIMIC EXTRACELLULAR MATRIX

Melike Sever

Ph.D. in Materials Science and Nanotechnology

Advisor: Ayşe Begüm Tekinay

July, 2017

Biomaterials obtained through self-assembling process of peptide amphiphile (PA) molecules provide great potential to introduce new therapeutic approaches in regenerative medicine through mimicking the natural environments of different types of tissues. The ability of self-assembled PA nanofibers to mimic natural extracellular matrix (ECM) renders them attractive for regenerative medicine applications. The materials-cell interactions can be modulated through the surface modification of the materials such as introducing the bioactivity via short bioactive peptide sequences derived from natural ECM proteins, which regulate cell behavior through controlling of cellular activities such as proliferation and differentiation.

Herein, I described my studies on the development of PA nanofibers in order to mimic natural ECM with differentiation and regeneration purposes. Heparan sulfate mimetic and laminin mimetic PA nanofibers were used as a potential therapeutic approach in Parkinson's disease (PD). These bioactive PA nanofibers were found to reduce the progressive cell loss in SH-SY5Y cells caused by 6-hydroxydopamine treatment *in vitro*, and improve neurochemical and behavioral consequences of Parkinsonism in

rats and provide a promising new strategy for treatment of PD. These nanofibers also proved to be effective in enhancing the viability of Schwann cells and increase nerve growth factor (NGF) release from these cells *in vitro*. Since NGF has a crucial role in nerve injury repair and myelination in the regenerating nerve, the bioactive epitopes used in this study present also a promising approach as guidance cues for regenerating axons.

Tenascin-C is another multifunctional ECM glycoprotein common in both nerve and bone tissue. By decorating peptide nanofibers with tenascin-C derived epitope and using in three-dimensional (3D) system, this tenascin-C mimetic 3D cell culture system was found to provide both the biochemical and physical aspects of the native environment of neural cells, thereby filling the gap between 2D cell culture models and *in vivo* environments and contributing to more tissue-like structure and more predictive approaches to organogenesis and tissue morphology.

Within the scope of this thesis, tenascin-C mimetic nanofibers were also used for osteogenic differentiation of mesenchymal stem cells (MSCs). They were found to significantly enhance the attachment, proliferation, and osteogenic differentiation of MSCs even in the absence of any external bioactive factors and regardless of the suitable stiff mechanical properties normally required for osteogenic differentiation.

Keywords: Peptide nanofibers, extracellular matrix, Parkinson's disease, neural differentiation and regeneration, osteogenic differentiation

ÖZET

HÜCRELER ARASI MATRİSİN TAKLİT EDİLMESİ İÇİN SENTETİK İSKELE OLARAK PEPTİT TABANLI MALZEMELERİN GELİŞTİRİLMESİ

Melike Sever

Malzeme Bilimi ve Nanoteknoloji, Doktora

Tez Danışmanı: Ayşe Begüm Tekinay

Temmuz, 2017

Peptid amfifil (PA) moleküllerinin kendiliğinden bir araya gelmesiyle elde edilen biyomalzemeler, farklı doku türlerinin doğal ortamlarını taklit ederek rejeneratif tıpta yeni terapötik yaklaşımlar getirme potansiyeli taşımaktadır. Kendiliğinden oluşan PA nanofiberlerin doğal hücre dışı matrisi (HDM) taklit etme yeteneği onları rejeneratif tıp uygulamaları için çekici kılmaktadır. Biyoaktif sinyaller taşıyan ve kendiliğinden oluşan peptit nano yapılar, sentetik HDM malzemeleri olarak yaygın bir şekilde kullanılmaktadır. Malzeme-hücre etkileşimlerini geliştirmek amacıyla proliferasyon ve farklılaşma gibi hücresel aktivitelerin modülasyonu yoluyla hücre davranışını düzenleyen doğal HDM proteinlerinden türetilen kısa biyoaktif peptit sekansları materyallerin yüzeylerini biyoaktifleştirmede kullanılmıştır.

Bu tezde, farklılaşma ve rejenerasyon amaçlarıyla doğal hücre dışı matrisi taklit edebilmek için PA nanofiberlerin gelişimi üzerine uygulamalar anlatılmıştır. Parkinson hastalığında (PH) potansiyel bir tedavi yaklaşımı olarak heparan sülfat ve laminin taklidi PA nanofiber kullanılmıştır. Bu biyoaktif PA nanofiberlerin, *in vitro*

olarak 6-hidroksidopaminin neden olduğu SH-SY5Y hücrelerindeki ilerleyici hücre kaybını azalttığı ve sıçanlarda PH'nin nörokimyasal ve davranışsal sonuçlarını düzelttiği ve PH'nin tedavisinde umut verici yeni bir strateji sağladığı bulunmuştur. Bu nanofiberlerin ayrıca Schwann hücrelerinin canlılığı üzerinde etkili oldukları ve *in vitro* olarak bu hücrelerden sinir büyüme faktörü salımını arttırdığı gösterilmiştir. Sinir büyüme faktörünün yenilenen sinirde, sinir hasarının onarımı ve miyelinasyonunda önemli rolü olduğu için, bu çalışmada kullanılan biyoaktif epitoplar, yenilenen aksonların yol gösterici ipuçları olarak umut verici bir yaklaşım sunmaktadır.

Tenascin-C, hem sinir hem de kemik dokusunda ortak olan, çok işlevli bir hücre dışı matris glikoproteinidir. Tenascin-C türevli epitop ile peptit nanofiberlerin biyoaktif hale getirilmesi ve üç boyutlu (3B) sistemde kullanılmasıyla, tenascin-C mimetik 3B hücre kültürü sisteminin sinir hücrelerinin doğal ortamını hem biyokimyasal hem de fiziksel yönleriyle taklit ettiği ve böylece iki boyutlu hücre kültürü modelleriyle *in vivo* ortamlar arasındaki boşluğu doldurduğu ve organogeneze ve doku morfolojisine daha akıllı yaklaşımlar getirdiği gösterilmiştir.

Bu tez kapsamında tenascin-C mimetik nanofiberler mezenkimal kök hücrelerin (MKH) osteojenik farklılaşması için de kullanılmıştır. Bu nanofiberlerin, normal olarak osteojenik farklılaşma için gerekli olan dış biyoaktif faktörlerin yokluğunda ve yumuşak mekanik özelliklere bakılmaksızın MKH'lerin bağlanma, çoğalma ve osteojenik farklılaşmasını önemli ölçüde arttırdığı bulunmuştur.

Anahtar kelimeler: Peptid nanofiberler, hücre dışı matris, Parkinson hastalığı, sinirsel farklılaşma ve rejenerasyon, osteojenik farklılaşma

Acknowledgement

I would like to express my deepest appreciation to my thesis advisors Prof. Ayşe Begüm Tekinay and for their scientific knowledge, guidance, encouragement and support throughout my PhD thesis studies. In addition to guiding my PhD studies, she has preened me as a scientist, and fully supported my professional development in any way she could. I would like to thank Prof. Mustafa Özgür Güler for his scientific support during my studies. I would also like to acknowledge my jury members for their contributions to my thesis.

I would like to express my special thanks to Prof. Dr. Mehmet Cansev, Dr. Büşra Mammadov, Mesut Türkyılmaz and Gökhan Günay for their support and great collaboration.

I would like to acknowledge The Scientific and Technological Research Council of Turkey (TÜBİTAK BIDEB 2211-E) for the financial support. Also, our experimental studies were supported by TÜBİTAK projects 111M410, 113S038 and 113S538.

I would like to acknowledge my previous and present lab members Dr. Gözde Uzunallı, Öncay Yaşa, Yasin Tümtaş, Ceren Garip Yaşa, Didem Mumcuoğlu, Elif Arslan, Dr. Hakan Ceylan, Dr. Göksu Çınar, Dr. Melis Şardan, Dr. Berna Şentürk, Seren Hamsici, Egemen Deniz Eren, Ayşegül Dede, Çağla Eren, Mustafa Beter, Nuray Gündüz, İdil Uyan, Zeynep Orhan, İbrahim Çelik, Canelif Yılmaz, Özüm Şehnaz Günel, Dr. Gülcihan Gülseren, Melis Göktaş, Özge Uysal, Dr. M. Aref Khalily, Nurcan Haştar, Fatih Yergöz, Merve Şen, Oğuz Tuncay, Begüm Dikeçoğlu, Alper Özkan, Ahmet Emin Topal, Aygül Zengin, Meryem Hatip, Dr. Ruslan Garifullin, Dr.

Rashad Mammadov, Dr. Özlem Erol, Dr. Ashif Shaikh, Hatice Kübra Kara, Hepi Hari Susapto, Şehmus Tohumeken, Burak Demircan, Dr. Seher Yaylacı and Dr. Hilal Ünal Gülsüner for creating such a warm working environment. I would like to thank Dr. Gülistan Tansık and Dr. Canan Kurşungöz for their friendships and support during my PhD studies at UNAM. Also, I would like to thank Zeynep Erdoğan and Mustafa Guler for their technical contribution to my thesis.

I would like to extend my special thanks to İsmail Cem Yılmaz, İrem Sevgi Öztürk, Eren Öztürk, Sinan Tarık Türesay, Latif Serkan Atabey, Beril Özbalcı, Utku Aslan and Orbay Tuğ who are always with me during those years and creating unforgettable memories with me. I also thank to Oya Gül and Ahu Durmuşçelebi for their endless friendship, help and support. I also thank to Temiz İş Band for their perfect sound and being my models to improve my photography skills.

I would like to thank Bahçekapılı, Kazan and Metinbaş families for their love and support. I especially thank to Ayşen Kazan, my new little sister, for making all the times enjoyable with her emotional support and cheerfulness.

I would like to express my most sincere gratitude to my parents, my mother Birsen Sever and my father Saffet Sever for their endless love, motivation, support and encouragement. I would not be where I am today without their help and support. My special thanks for my life partner, my love Oytun Bahçekapılı. We were right by each other side through all the highs and lows. Thank you so much for being a huge part of my life. Last but not least, I would like to thank to my little brother. He is my best friend and always supports me whenever I need. I am so lucky to have a brother like him. I dedicate this thesis to my beloved brother, Oğuz Sever.

Contents

List of Figures

List of Tables

Abbreviations

6-OHDA	6-hydroxydopamine
ALP	Alkaline phosphatase
ANOVA	Analysis of variance
BSA	Bovine serum albumin
CD	Circular dichroism
CNS	Central nervous system
DAB	3,3′-diaminobenzidine
DCM	Dichloromethane
DIEA	*N*,*N*-diisopropylethylamine
DIT	Digital integration time
DMEM	Dulbecco's modified Eagle's medium
DMF	*N*,*N*-Dimethylformamide
ECM	Extracellular matrix
ETD	Everhart–Thornley detector
FBS	Fetal bovine serum
Fmoc	9-Fluorenylmethoxycarbonyl
GAPDH	Glyceraldehyde 3-phosphate dehydrogenase
HBTU	*N*,*N*,*N*′,*N*′-Tetramethyl-O-(1*H*-benzotriazole-1-yl) uronium hexafluorophosphate
HCl	Hydrochloric acid
H&E	Hematoxylin and eosin
HPLC	High pressure liquid chromatography
HRP	Horseradish peroxidase
HS	Horse serum
HSPG	Heparan sulfate proteoglycans
i.p.	intraperitoneally
LC-MS	Liquid chromatography-mass spectroscopy
MEM	Minimum essential medium
MSC	Mesenchymal stem cell
Mtt	4-methytrityl

NGF	Nerve growth factor
NSC	Neural stem cell
PA	Peptide amphiphile
PBS	Phosphate buffered saline
PD	Parkinson’s disease
PLL	Poly-L-lysine
PNS	Peripheral nervous system
PVDF	Polyvinylidene fluoride
P/S	Penicillin/streptomycin
rMSC	Rat mesenchymal stem cell
RPMI	Roswell Park Memorial Institute medium
qRT-PCR	Quantitative real-time polymerase chain reaction
sem	Standard error of mean
SEM	Scanning electron microscopy
STEM	Scanning transmission electron microscopy
SYN1	Synaptophysin I
TBST	Tris-buffered saline and Tween 20
TCP	Tissue culture plate
TFA	Trifluoroacetic acid
TH	Tyrosine hydroxylase
TIS	Triisopropyl silane
TN	Tenascin
UV	Ultraviolet

Chapter 1

1. Introduction

1.1 Neurodegenerative Diseases

Neurodegenerative diseases are characterized by progressive neuronal degeneration, intracellular or extracellular protein aggregation, and motor and cognitive dysfunctions. The prevalence of most of the neurodegenerative diseases increases with age. For instance, ~15 million people are affected worldwide by Alzheimer disease, which is a common neurodegenerative disease. Since there are currently no available therapeutic approaches in order to prevent the progression of the disease, it is predicted that this will increase to 13.2 million and 16.2 million in the United States and Europe by 2050, respectively [1, 2]. Therefore, development of effective strategies for prevention or treatment of neurogenerative diseases are essential in order to deal with social and financial costs of neurodegeneration.

1.2 Extracellular Matrix (ECM) of the Nervous System

ECM is the noncellular collection of extracellular molecules secreted by the cells, and provides physical support for the cells and affects the intracellular signaling cascades through biomechanical and biochemical cues that are essential for cell fate including proliferation, adhesion, differentiation and cell death. ECM components show synergy with the signals coming from growth factors and hormones and are involved in tissue-specific gene expression control via transduction mechanisms [3, 4]. Also, ECM displays a dynamic structure by being remodeled by the cells and constantly altering its composition and structure during development, remodeling, repair and aging [5].

1.2.1 Components of ECM of the Nervous System

Although some components of ECM such as water, proteins and polysaccharides are common in all tissues, ECM of each tissue has a specific structure in terms of physical, topological, and biochemical composition. ECM is mainly composed of two types of macromolecules which are fibrous proteins and proteoglycans [6, 7]. Collagens, elastins, laminins and fibronectins are the main proteins found in ECM. The ECM shows different degrees of stiffness, which varies several orders of magnitude from brain tissue to bone tissue. This variation occurs as a result of concentration of some ECM components such as collagen and elastin. Collagen is the most abundant fibrous protein of ECM and has different functions including providing tensile strength, regulation of cell adhesion, support for migration, and tissue development [8]. Elastin, which is another protein, provides recoil for the tissue during repeated stretching while fibronectin directs the ECM organization and has an important role in cell attachment [9]. As a non-fibrous protein, laminin plays a role in tissue structure and cell function including cell adhesion, migration, and differentiation [10]. Proteoglycans are the glycosylated proteins which form the majority of the extracellular space and display different functions [6]. While some proteoglycans are specific to different tissue types, some of them are common and distributed widely. For instance, aggrecan is the major type of proteoglycan found in cartilage tissue while perlecan is a heparan sulfate proteoglycan (HSPG) present in basement membrane [11]. Composition of ECM also varies according to the developmental stage and aging. For instance, levels of some junctional proteins such as cadherin decrease during aging and gaps occur between the epithelial cells, which affects the junctional integrity [12]. Therefore, composition and

dynamic structure of ECM must be taken into consideration while designing synthetic materials.

1.2.2 Challenges to Nerve Regeneration

Nervous system is the most complex and highly organized system in the body and is composed of a complex network of nerves. Since the nervous system has very limited regeneration capacity, any damage in this system induced by either physical injuries or neurological disorders can cause degeneration and neuronal cell death due to loss of communications between the healthy cells. Following the injuries or traumas in the nervous system, patients generally suffer from the loss of sensory or motor function, and neuropathic pains.

Although the current therapeutic approaches provide regeneration up to a certain point, they are not quite effective. For the development of new therapies for nervous system, it is important to understand the nature and requirements of the cells, including physical, chemical and biological signals, and to induce regeneration process while preventing the formation of glial scars, which makes it a complex process. Peripheral nervous system (PNS) and central nervous system (CNS) respond to injury differently. In the PNS, a series of pathophysiological events occur after the Wallerian degeneration in the distal end. The distal part of the nerve is degenerated and the remaining cellular debris is removed by the macrophages and monocytes [13]. In PNS injuries, direct end-to-end reconnection through surgical sutures is a common method for the treatment of small injury gaps. For larger nerve defects, autografts are used as a gold standard to bridge the gaps. However, there are still problems which limit the use of autografts such as loss of function at donor sites and limited number of donor

grafts. Allografts and xenografts may be considered [14, 15], but they also have problems including transfer of several diseases and immunological rejections. CNS has much lower regeneration capacity compared to PNS. Following the injury in CNS, glial scar formation and release of inhibitory molecules occur at the injury site. Removal of cell debris is slower in CNS than PNS due to the limited infiltration levels of macrophages through the brain-spinal cord barrier [16]. Because of these reasons, the scaffolds constructed by tissue engineering strategies may offer an alternative strategy to facilitate neural repair. The studies about neural regeneration generally focus on the inhibitory nature of the nervous system after the injuries and combination of multiple cues in order to increase regeneration capacity of nervous system. In nervous system, regeneration occurs through mechanisms to recover the function of degenerated cells. The limited regeneration capacity of nervous system is aimed to be improved by using biomaterials designed for stem cell culture, differentiation and *in vivo* regeneration. The strategies to construct biomaterials for nerve repair should include the removal of inhibitory environment after the damage, induction of axon guidance, managing the cell signaling, increasing the local concentration of neurotrophic factors and providing an artificial microenvironment by mimicking the native ECM of the cells in order to fill the gap originating from the injury [17].

1.3 Approaches in the Design of ECM-Mimetic Scaffolds for Neural Differentiation and Regeneration

Biomaterials, that are generated as a result of self-assembling process and include short peptides and peptide derivatives, have significant potential in regenerative medicine applications. Mimicking native ECMs which have regulatory functions in tissue

formation and regeneration is a promising strategy for the design of synthetic biomaterials. Synthetic materials are commonly used in tissue engineering applications because of their specific properties such as modifiable elasticity, high water content and ability for encapsulation of cells. Cell adhesion, proliferation and differentiation are other important significant criteria to be considered when designing a nanomaterial for neural tissue engineering. The main goal of regenerative medicine is to enhance tissue regeneration and healing after injury or disease leading to degeneration of the tissue of interest. Guidance of cell behavior by the features of a material at cell-biomaterial interfaces has significant importance, and developing novel biomaterials with certain surface modifications to induce controlled cell function would be beneficial for improving therapeutic potential of current regenerative medicine protocols. The biodegradability and biocompatibility are the most important features of synthetic biomaterials. These synthetic materials must also be multifunctional in order to mimic the natural ECM both biochemically and biophysically.

1.3.1 Biochemical Functionalization of the Scaffolds for Neural Differentiation and Regeneration

Mimicking the cytoarchitecture of native ECM of neural cells has become a common approach in tissue engineering applications. ECM is the non-cellular component of organisms which provides vital physical support and presents the biological cues for tissue development and differentiation [6]. ECM-mimetic scaffolds can be decorated with a number of different peptide motifs derived from the components of ECM at very high density in order to introduce bioactivity to the system and direct the

biochemical signaling cascade. Especially cell-binding epitopes of fibrous proteins of ECM including RGDS, YIGSR, and IKVAV, are widely used in the literature since they have both structural and adhesive roles [18]. In addition to bioactive moieties for initial attachments of the cells, further proliferation, migration and differentiation signals or degradable sites such as hydrolysable ester linkages [19] and enzyme-mediated degradable sequences [20] may also be incorporated into the scaffolds. Among these scaffolds, peptide amphiphiles (PA), which can self-assemble into nanofibers through non-covalent interactions and introduce bioactive epitopes on their surface, have great potential to mimic the regulatory characteristics of natural environment of the cells for biological studies as well as therapeutic applications. PA molecules can form self-organized biocompatible fibers at nanoscale and their surface can be tailored in order to induce biochemical responses in a desired way [21, 22]. Moreover, two or more PAs can be used to form nanofibers with multiple cues in order to obtain cumulative effects [23].

When compared to other systems in the body, nervous system has a very unique structure due to different compositions of ECM and its mechanical properties. While designing a bioactive scaffold for neural regeneration purposes, it is important to consider its biological and chemical properties as well as its physical structure. In order to introduce bioactivity into the system, bioactive epitopes of ECM proteins can be incorporated into the scaffold. Within the concept of biomaterials, use of peptide nanofibers has become extensive in neural regeneration applications. Decorating the peptide molecules with different bioactive epitopes derived from ECM proteins such as, isoleucine-lysine-valine-alanine-valine (IKVAV) and tyrosine-isoleucine-glycine-

serine-arginine (YIGSR) derived from laminin, arginine-glycine-aspartate (RGD) derived from fibronectin and valine-phenylalanine-aspartate-asparagine-phenylalanine-valine-leucine-lysine (VFDNFVLK) peptide derived from tenascin-C (TN-C) makes the scaffolds biofunctional and has been shown to induce neural differentiation, attachment and migration [23-26]. These peptides have become favorable for regenerative medicine applications, since they are more stable and easy to synthesize than the bulk proteins.

Incorporation of the bioactive epitopes into PA molecules and self-assembly of these molecules into nanofibrous scaffolds through non-covalent interactions can provide an artificial microenvironment which is similar to the natural ECM [27, 28]. Arginine–alanine–aspartate (RAD)16-I and RAD16-II were used in the form of self-assembled peptide nanofibrous scaffolds for neural cell cultures. RAD16 peptide scaffolds functionalized with RGD and laminin-derived motifs, GFLGFPT and BMHP were used for differentiation of neural stem cells (NSCs) [27]. IKVAV sequence, which is known to promote and direct neurite outgrowth, was used in different studies as a part of self-assembling peptide nanofibers. Silva et al. cultured neural progenitor cells on IKVAV-bearing scaffolds to study cellular differentiation of these cells *in vitro,* and they selectively induced neuronal differentiation while they suppressed differentiation to astrocytes [29]. In addition to *in vitro* studies, animal models have been used in order to investigate the potential of self-assembling peptide nanofibers for repair and regeneration of nervous system in several studies. Tysseling-Mattiace *et al.* inhibited the glial scar formation, promoted axon elongation and facilitated regeneration with significant behavioral improvement after spinal cord injury using IKVAV-bearing

peptide nanofibers [30]. Also, self-assembling peptide nanofibers functionalized with IKVAV sequence were used to encapsulate NSCs and enhance stem cell survival as well as to reduce formation of glial astrocytes in a rat brain surgery model to demonstrate the damage in cerebral neocortex/neopallium loss [31].

1.3.2 Physical Functionalization of the Scaffolds for Neural Differentiation and Regeneration

When designing biomaterials for tissue-engineering applications, physical properties of a material should also be taken into account in addition to biological and chemical properties. Physical characteristics including stiffness, dimensionality, substrate topography and electrical conductivity are important parameters for scaffold functionalization to induce neural differentiation.

Mechanical properties of the microenvironment are important regulators of cellular characteristics including morphology [32] and motility [33] of the cells as well as differentiation [34]. Normally, brain and spinal cord are the softest tissues in the body with elastic moduli of about 2000 Pa. However, when glial scar forms as a result of injury, it increases the stiffness of this area which leads to problems in neurite extension and neural regeneration. Soft materials have become more favorable for regeneration studies in CNS, because neurons and astrocytes give different responses to matrix stiffness. When designing a scaffold for neural differentiation, the mechanical properties of the scaffold should be similar to that of brain tissue, which is below 1 kPa [35]. It was shown that stiff substrates having elastic moduli between 1,000 and 10,000 Pa caused the differentiation of adult NSCs into glial cells, while soft substrates with elastic moduli between 100-500 Pa induced primarily neuronal

differentiation [36]. Also, spinal cord and cortical brain neurons prefer soft materials in order to be able to extend their neurites [36, 37] while astrocytes form stress fibers and favor the surfaces with high elastic modulus [35]. The effect of stiffness was also studied on human mesenchymal stem cells. This effect was investigated by using three-dimensional (3D) porous scaffolds generated by type I collagen and hyaluronic acid. Using different concentration of 1-ethyl-3(3-dimethylaminopropyl) carbodiimide as a crosslinking agent, the elastic modulus of the 3D substrates was modified and the stiffness was controlled in the range of 1–10 kPa. Results showed that mesenchymal stem cells (MSCs) were likely to differentiate into neurons at 1 kPa while they preferred glial lineage in the scaffold at 10 kPa stiffness verified with experiments focused on up-regulation of neuronal mid- and late protein markers after longer mechanical induction time for 21 days [38].

In vitro models are important tools to study cell behavior and fate in a highly-controlled manner. Although two-dimensional (2D) cell cultures are commonly used in differentiation studies, three-dimensional cell cultures are important *in vitro* models to fill the gap between 2D cell culture experiments and *in vivo* studies. To study regeneration of neural tissue which has a very low regeneration capacity, use of 3D models is important. They better mimic the ECM of neural cells in terms of providing support and enhanced diffusion of oxygen and nutrients. There are fundamental differences between cells grown on a monolayer surface and in 3D manner. The 3D cultures have been shown to display longer neurite outgrowth, higher levels of survival as well as different patterns of differentiation when compared to 2D monolayers [39, 40]. Also, hippocampal neurons cultured on a 3D aragonite matrix displayed higher survival as compared to 2D counterparts with higher-density network formation [41].

In another study, 3D cell culture systems with the functional motifs of RGD (Arg-Gly-Asp), bone marrow homing peptide 1 and 2 were developed for the culture of adult NSCs. The proliferation and differentiation of NSCs were supported by these scaffolds by allowing a satisfactory supply of nutrients and oxygen [42].

Nanotopography is an important tool to guide cell differentiation and it can be modified in size and shape according to desired application. Interaction of the cells with nanotopographies can induce different responses including changes in cell morphology [43], adhesion [44], proliferation [45] and gene regulation [46]. It is important to understand that neurite growth along topographical patterns is important for tissue engineering applications in neurology. In one study, nanotopographic control of neuronal polarity was studied and the interaction between focal adhesions and topographic features were exploited to design a set of scaffolds made of cyclic olefin copolymer yielding control over neuronal polarity establishment and neurite pathfinding. By this way, specific neuronal polarity states were selectively favored by a set of biocompatible textured scaffolds and it was demonstrated that this selection can be tailored through varying the topographical constraint applied to the maturation of focal adhesions during neuritogenesis [47].

Neurons are electrically excitable cells and as a result of their inherent nature, they are capable of transmitting electrochemical signals throughout the nervous system making them highly sensitive to electrical stimuli. The action potential generated at the synapse is the key component of neural communication, so electrical conductivity is an important physical property to enhance neural cell activity [48]. Providing electrical conductivity to the scaffolds and electrical stimulation of the cells cultured on these scaffolds might be useful to improve synaptic connections. One of the new approaches

in scaffold generation is the design of conductive substrates which provide external electrical stimuli to the stem cells, because these stimuli can affect the cell behavior including proliferation, migration and differentiation [49, 50]. Electrical conductivity can be provided to the scaffold through utilization of conductive polymers and carbon based materials which include carbon nanotubes, graphite and graphene [51]. Combining the conductivity of carbon nanotubes with the alignment of the poly(lactic acid) nanofibers supports and increases the neural differentiation of mouse embryonic stem cells which was detected by enhanced expression of mature neuronal markers even in the absence of direct electrical stimulation [52].

Overall, self-assembled nanofibrous scaffolds provide different perspectives in neural regeneration processes. The fibrous structure is quite similar to natural ECM, and tailoring the biochemical and physical properties of the scaffolds enables the manipulation of cellular functions depending of the type of the injury or degeneration. Altogether, these bioactive nanofibrous scaffolds hold great potential for neural regeneration both after injury and for neurodenerative diseases.

Chapter 2

2. Regenerative Effects of Peptide Nanofibers in an Experimental Model of Parkinson's Disease

This chapter of thesis was published in the following article [53]; Reproduced from "Regenerative effects of peptide nanofibers in an experimental model of Parkinson's disease"; Sever, M.; Turkyilmaz, M.; Sevinc, C.; Cakir, A.; Ocalan, B.; Cansev, M.; Guler, M. O.; Tekinay, A. B., *Acta Biomaterialia*, 2016, 46, 79-90, with permission from Elsevier.

2.1 Introduction

Neurodegenerative diseases caused by infection, stroke and acute trauma are the fourth leading cause of death in the world after cardiovascular diseases, cancer and stroke [54]. Among the neurodegenerative diseases, Parkinson's disease (PD) is the second most common neurodegenerative disease after Alzheimer's disease. PD is a severe, chronic and progressive disease associated with symptoms such as tremor, postural instability, rigidity and bradykinesia [55]. PD is characterized by diminished levels of striatal dopamine as a consequence of dopaminergic neuron loss in the substantia nigra pars compacta. Beside the degeneration of dopaminergic neurons, Lewy body formation can be included as pathologic hallmarks of PD [56]. In addition, several studies have shown that activation of apoptosis is one of the mechanisms that underlie progressive striatal neurodegeneration [57-60]. A recent study has provided strong evidence for this hypothesis by showing that *in vivo* suppression of Caspase-3, an apoptotic marker, by RNA interference in a rat model of PD reduced striatal

dopaminergic cell loss and improved locomotor activity [61]. Millions of people in US and Europe suffer from PD, but the pharmaceutical agents used for PD treatment including levodopa, Monoamine oxidase-B inhibitors (selegiline and rasagiline), Catechol-O-methyl transferase inhibitors (tolcapone and entacapone) and dopamine agonists (pramipexole and ropinirole) just relieve and modify the symptoms. In addition, since they are administered orally, they can cause systemic toxicity with different adverse effects [62]. There are no therapies yet available for PD to slow down the degeneration process in the brain and recover the lost function. Besides these current strategies, there are various experimental approaches to improve the efficacy of currently available treatment strategies. Uses of adenosine A2A receptor antagonists, glutamate receptor antagonists, monoamine oxidase inhibitors, anti-apoptotic agents, antioxidants and coenzyme Q10 are among the emerging pharmacotherapies at different stages of preclinical and clinical trials [63]. Also, there are several non-pharmacological approaches offering alternative strategies for the treatment of PD. Viral vectors were studied to silence the over-expressed defective genes considered as risk factors in PD or to transfer the genes such as glutamic acid decarboxylase gene [64]. Stem cell transplantation is another promising approach for the replacement of dopaminergic neurons progressively lost in PD. Induced pluripotent stem cells, NSCs and MSCs are the most commonly studied resources to generate dopaminergic neurons as a treatment strategy for PD [65]. However, there are some drawbacks for this technique such as selecting tumor-free cell type for transplantation, which limits the potential therapeutic benefits. Additionally, some surgical procedures are within the emerging techniques for PD treatment, including deep brain stimulation, pallidotomy and thalamotomy, especially for PD patients having severe disabling

problems and not responding to traditional treatment options. However, these procedures also have high risks and require close post-operative follow-up period [63].

Although repairing the damaged area in the brain is extremely challenging, recent advances in regenerative medicine and tissue engineering provide new therapeutic approaches for neurodegenerative disease treatment. Biomaterials, which are designed to interact with biological systems provide new platforms to replace the damaged neurons or slow down the progression of the diseases [66]. Biomaterial scaffolds can be modified with physical or/and chemical cues depending on the aim of the study. Cell attachment, adhesion, migration and spreading as well as cell differentiation into specific lineages can be achieved through physical or chemical modification of the surface of the scaffold, including stiffness, topography, charge and interactions with ECM proteins or cells [67].

Laminins are heterotrimeric proteins and the major non-collagenous components of the basal lamina. They bind to cell membrane through interaction with integrin receptors on the cell surface, and by this way, they can influence diverse biological activities including cell adhesion, migration and differentiation [68]. Moreover, laminin has a fundamental role in axonal growth and myelination [69] and functions as a neurite-outgrowth promoting factor for peripheral and central neurons [70]. Laminin also interacts with other matrix elements such as HSPG through noncovalent interactions, and laminin-HSPG complex was found to be involved in neurite outgrowth [71, 72]. Heparan sulfates are highly sulfated glycosaminoglycans and function as cell–ECM interface to modify cell signaling. They also interact with

various ECM molecules such as growth factors. They act as a reservoir of such growth factors and increase their local concentration [73-76].

The self-assembled PA nanofibers provide suitable platforms to mimic ECM. As a result of the hydrophobic interaction between alkyl tails and β-sheet formation between peptide segments, they self-assemble into nanofibers in aqueous environment. Also, biochemical signals provided by a specific protein can be introduced into the nanofiber system through addition of bioactive epitopes into individual PA molecules instead of use of bulk protein [77]. The peptide sequences Ile-Lys-Val-Ala-Val (IKVAV) of cell-binding domain of laminin was discovered and found to facilitate neurite extension [78]. After the discovery of this small peptide sequence, IKVAV-carrying PAs were used in both *in vitro* and *in vivo* studies for neural differentiation [29] and spinal cord regeneration [30, 79], respectively. We previously reported that combination of IKVAV-carrying PAs along with heparan-sulfate-mimicking PA nanofibers displayed dual bioactivity and promoted much longer neurite outgrowth compared to the scaffold with laminin-derived signals alone, even in the presence of inhibitory conditions provided by chondroitin sulfate proteoglycans [23]. Although bioactive PA nanofibers were shown to enhance *in vitro* neurite extension or peripheral nerve regeneration, there is no study on the therapeutic effects of bioactive PA nanofibers on PD.

Here we investigated whether these heparan sulfate and laminin mimetic PA nanofibers have potential therapeutic effect for both protection of SH-SY5Y cells against 6-hydroxydopamine (6-OHDA)-induced apoptosis in *in vitro* studies and for reducing striatal injury and enhancing dopaminergic nerve regeneration in

experimental PD model. Six weeks following treatment with bioactive PA nanofibers, rats with 6-OHDA-induced Parkinsonism displayed improvements in behavioral functions, i.e., reductions in forelimb asymmetry, contralateral forelimb akinesia and d-amphetamine-induced rotational behavior in cylinder, stepping and rotation tests, respectively. Moreover, brain dopamine content and tyrosine hydroxylase (TH) levels increased, while cleaved-Caspase-3 levels decreased in rats treated with PA nanofibers compared to sucrose control. Histological assessment also showed that PA injection to the striatum provided better tissue integrity by reducing the progressive cell loss caused by 6-OHDA toxicity, which makes this bioactive nanofiber system a promising new platform for PD treatment.

2.2 Experimental Section

2.2.1 Materials

All protected amino acids, lauric acid, 4-[α-(2′,4′-dimethoxyphenyl) 9-Fluorenylmethoxycarbonyl (Fmoc)-aminomethylphenoxyacetomidonorleucyl-MBHA resin (Rink amide MBHA resin), *N,N,N′,N′*-Tetramethyl-O-(1H-benzotriazole-1-yl) uronium hexafluorophosphate (HBTU) and *N*,*N*-diisopropylethylamine (DIEA) were purchased from Nova-Biochem, ABCR, or Sigma-Aldrich. 6-OHDA was purchased from Sigma Aldrich. Alamar Blue, viability assay reagents and other cell culture materials were purchased from Invitrogen. Apoptosis assay reagents were purchased from Biotium. All other chemicals and materials used in this study were purchased from Thermo Scientific or Sigma Aldrich.

2.2.2 Synthesis of PA Molecules

PA molecules were synthesized on Rink Amide MBHA Resin or Fmoc-Glu(OtBu)-Wang Resin by using Fmoc-protected solid phase peptide synthesis method. Amino

acid couplings were performed with 2 equivalents of amino acids activated with 1.95 equivalents of HBTU and 3 equivalents of DIEA for 2 h. Fmoc removal was performed with 20% piperidine–*N*,*N*-dimethylformamide (DMF) solution for 20 min. 10% acetic anhydride–DMF solution was used to permanently acetylate the unreacted amine groups after each coupling step. DMF and dichloromethane (DCM) were used as washing solvents after each step. p-Sulfobenzoic acid was coupled to the side chain of lysine to synthesize sulfonated PAs. A lysine residue with 4-methytrityl (Mtt) side chain protection was used for selective deprotection of amine groups. Mtt removal was performed by shaking resins for 5 min with trifluoroacetic acid (TFA):triisopropyl silane (TIS):H_2O:DCM in the ratio of 5:2.5:2.5:90. Cleavage of the PAs and protection groups from the resin was carried out with a mixture of TFA:TIS:H_2O in the ratio of 95:2.5:2.5 for 3 h. Excess TFA removal was carried out by rotary evaporation. PAs in the remaining solution were precipitated in ice-cold diethyl ether overnight. The precipitate was collected by centrifugation next day and dissolved in ultrapure water. This solution was frozen at -80 °C for 4 h and then lyophilized for 4–5 days. PAs were characterized by liquid chromatography–mass spectrometry (LC–MS). Mass spectrum was obtained with Agilent LC-MS equipped with Agilent 6530 Q-TOF with an ESI source and Zorbax Extend-C18 2.1 × 50 mm column for basic conditions and Zorbax SB-C8 4.6 × 100 mm column for acidic conditions. A gradient of water (0.1% formic acid or 0.1% NH_4OH) and acetonitrile (0.1% formic acid or 0.1% NH_4OH) was used. In order to remove residual TFA, positively-charged PAs were treated with 0.1 M hydrochloric acid (HCl) solution and lyophilized. To purify the peptides, Agilent preparative reverse-phase high pressure liquid chromatography (HPLC) system equipped with Zorbax Extend-C18 21.2 × 150 mm column was used for basic

conditions and Zorbax SB-C8 21.2 × 150 mm column was used for acidic conditions. A gradient of water (0.1% TFA or 0.1% NH_4OH) and acetonitrile (0.1% TFA or 0.1% NH_4OH) was used. All peptide batches were freeze-dried and reconstituted in ultrapure water at pH 7.4 before use.

2.2.3 Scanning Electron Microscopy (SEM) Imaging of PA Nanofibers

PA nanofiber networks were observed by SEM imaging. Oppositely charged PA solutions (1 wt%) were mixed in appropriate volume ratio (final volume being 30 μL) to produce gels with neutral charge. Gels were formed on silicon wafer and dehydrated by transferring to 20%, 40%, 60%, 80% and 100% v/v ethanol, sequentially. They were critical point-dried afterwards by using Autosamdri 815B equipment from Tousimis. Dried PA gels were coated with 4 nm Au/Pd and SEM (FEI Quanta 200 FEG) images were taken by using an Everhart–Thornley Detector (ETD) at high vacuum mode at 5 keV beam energy.

2.2.4 Scanning Transmission Electron Microscopy (STEM) Imaging of PA Nanofibers

Samples for STEM imaging were prepared by mixing equal volumes of negatively and positively charged PA molecules with appropriate concentrations for charge neutralization and placing them on a 200-mesh carbon TEM grid for 10 min followed by 2 wt% uranyl acetate staining for 2 min and drying. STEM images at HAADF mode were acquired with FEI Tecnai G2 F30 TEM at 300 kV.

2.2.5 Secondary Structure Analysis

A JASCO J815 circular dichroism (CD) spectrometer was used at room temperature. Oppositely charged 2.5×10^{-4} M PA solutions were mixed in appropriate volume

ratios (final volume being 500 μL) to produce nanofibers with net neutral charge. Measurements were carried out from 300 nm to 190 nm; data interval and data pitch being 0.1 nm, and scanning speed being 100 nm min^{-1}. All measurements were performed with three accumulations. Digital Integration Time (DIT) was selected as 1 s, band width as 1 nm, and the sensitivity was standard.

2.2.6 Oscillatory Rheology

Oscillatory rheology measurements were performed with Anton Paar Physica RM301 Rheometer operating with a 25 mm parallel plate configuration at 25 °C. 250 μL total volume with 1 wt% of each PA component was carefully loaded onto the center of the lower plate and incubated for 10 min for gelation before measurement. After equilibration, the upper plate was lowered to a gap distance of 0.5 mm. Storage moduli (G′) and loss moduli (G″) values were scanned from 100 rad s^{-1} to 0.1 rad s^{-1} of angular frequency, with a 0.5% shear strain. Three samples were measured for each PA gel.

2.2.7 Cell Culture and Maintenance

SH-SY5Y cells (kindly provided by Prof. Dr. Fikrettin Sahin, Yeditepe University, Istanbul, Turkey) were used in cell culture experiments. They were cultured in 75 cm^2 flasks at 37 °C in a humidified incubator and supplied with 5% CO_2. Cells were maintained in 1:1 mixture of Eagle's minimum essential medium and F12 medium supplemented with 10% fetal bovine serum (FBS) and 1% penicillin/streptomycin (P/S). All cell experiments were carried out after reaching 90% confluency. The culture medium was changed every 3–4 days.

2.2.8 Drug Treatment and Viability Assay

6-OHDA was dissolved in 0.3% l-ascorbic acid/0.9% NaCl solution to create a stock concentration of 5 mM and was used at a final concentration of 25, 50, 100, 200 and 500 μM. SH-SY5Y cells were seeded at a density of 2×10^4 cells/well on 96-well plate and incubated for 24 h. Then, they were treated with 6-OHDA (25, 50, 100, 200 and 500 μM) for 24 h. Medium was discarded after 24 h of incubation and replaced with medium containing 10% Alamar blue. Blank group contained only Alamar blue medium without cells. After 3 h incubation at 37 °C, absorbance measurement was performed by using Spectramax M5 microplate reader at 570 and 600 nm as reference.

After determining the toxic dose, the viability test of SH-SY5Y cells was performed after 24 h of 6-OHDA treatment by using calcein-AM/ethidium homodimer 1 (EthD-1) staining. In brief, cells were incubated on PA-coated and uncoated 96 well-tissue culture plates (TCPs) at a density of 5×10^3 cells/well. After 24 h, the cells were exposed to 50 μM 6-OHDA dissolved in 0.3% l-ascorbic acid/saline solution or vehicle (0.3% L-ascorbic acid/saline solution). After 24 h of incubation, cell medium was discarded; cells were washed with phosphate buffered saline (PBS) and then incubated with 2 μM calcein-AM and 2 μM EthD-1 in PBS for 30 min at room temperature. Finally, five random images were taken at 100x magnification from each well for both qualitative and quantitative analysis by using Zeiss Axioscope fluorescence microscope. Cells were counted with Image J system for analyzing proliferation.

2.2.9 Flow Cytometry Analysis of Apoptosis

Apoptosis in SH-SY5Y cells seeded on different PA combinations was measured using the Annexin V-FITC Apoptosis Detection kit. After 24 h incubation in 6-well plates

at a density of 5×10^5 cells/well, the cells were exposed to 50 μM 6-OHDA dissolved in 0.3% l-ascorbic acid/saline solution. After 24 h exposure to 6-OHDA, flow cytometry protocol for Annexin V and propidium iodide was performed. Medium was discarded; cells were washed with cold PBS and resuspended in 1X annexin-binding buffer. 100 μL of 1X annexin-binding buffer per assay was added with 5 μL Alexa Fluor® 488 annexin V and 1 μL of 100 μg/mL propidium iodide. Cells were incubated at room temperature for 15 min. The stained cells were analyzed by flow cytometry, measuring the fluorescence emission at 530 nm (FL1 channel) and >575 nm (FL3 channel).

2.2.10 *In Vivo* Surgery

2.2.10.1 Animals

A total of 32 male Sprague Dawley rats (weighing 300–350 g) were housed individually in each cage with free access to food and water in a 12/12 h light/dark cycle. Experimental procedures conformed to the National Institute of Health Guide for the Care and Use of Laboratory Animals and were approved by the Local Ethics Committee on Experimental Animal Research of Uludag University, Bursa, Turkey (Approval ID: 2012-10/1).

2.2.10.2 Surgical Procedure

Rats (n = 24) anesthetized with ketamine and xylazine (80 and 10 mg/kg, respectively) were placed into the stereotaxic apparatus (David Kopf Instruments, Tujunga, CA, USA). Their heads were shaved and a 2-cm incision was made on the skull under aseptic conditions ensured with 70% alcohol. After visualization of the bregma, two burr holes were drilled and hand-made guide cannulas (each 4 mm long) were placed (first one +0.48 mm anterior and second one -0.40 mm posterior to bregma). The

cannulas were plugged and rats were returned to their cages after injection with a single dose of analgesic (buprenorphine; 0.05 mg/kg; s.c.). A group of rats (n = 8) underwent the same operation without placement of guide cannulas in order to serve as sham controls.

2.2.10.3 Intrastriatal lesioning with 6-OHDA and PA Injection

24 h after the placement of guide cannulas, two injection apparatus were placed into the right striata of rats through the guide cannulas at the following coordinates: first at anteroposterior: +0.48 mm, mediolateral: −2.2 mm and vertical: −4.6 mm and second at anteroposterior: −0.40 mm, mediolateral: −4.0 mm and vertical: −6.0 mm according to the Rat Brain Atlas [80]. Freely-moving rats were injected intrastriatally through polyethylene tubing (PE 20; Becton Dickinson, Franklin Lakes, NJ, USA) attached to the apparatus at the given coordinates with either 8 μg of 6-OHDA (dissolved in saline containing 0.3% L-ascorbic acid, n = 16) or its solvent 0.3% L-ascorbic acid (n = 8) at a volume of 2 μL using an injection pump with a flow rate of 1 μL/min. The cannulas were plugged and rats were followed up in individual cages with free access to food and water.

The dose and stereotaxic coordinates for 6-OHDA injections were selected from previous studies [81, 82] which showed that this protocol is adequate for consistent depletion of approximately 70–80% of striatal dopamine and induce Parkinsonism in rats resembling the early phase of PD in clinical setting.

One week later, rats receiving intrastriatal 6-OHDA injections were tested for d-amphetamine-induced rotational behavior. Rats were injected intraperitoneally (i.p.) with d-amphetamine (5 mg/kg) and ipsilateral rotations between 15 and 45 min were

recorded using an automated Rotameter system (TSE Systems, Germany). Initial behavioral task was performed in order to ensure that the unilateral striatal 6-OHDA lesion was established and the data were used to randomize the 6-OHDA-lesioned rats into two treatment groups (i.e., 6-OHDA + Sucrose [n = 8] and 6-OHDA + PA [n = 8] groups) with almost equal mean number of ipsilateral rotations (275 ± 11 and 275 ± 6, respectively) in this task. No rotational behavior was observed in rats in "Sham" and "L-Ascorbic Acid + PA" groups.

Rats were followed-up in their cages for three days after the initial rotational behavior task in order to allow for wash-out of d-amphetamine from the brain and then allocated into treatment groups as follows: (i) Sham group, (ii) L-Ascorbic Acid + PA group, (iii) 6-OHDA + Sucrose group and, (iv) 6-OHDA + PA group.

In rats receiving intrastriatal 6-OHDA or L-ascorbic acid injections, PA (1% aqueous solutions) or sucrose (0.25 M) injections were made using the same coordinates of the right striata through the existing guide cannulas. The 1% solutions dissolved in sucrose of both the heparan sulfate-mimicking (GAG) and laminin-derived (LN) PA nanofibers were injected consecutively by the help of the polyethylene tubing attached to the injection apparatus with a 5 min interval in between two injections. After injection, rats were followed-up for a period of 6 weeks in individual cages with free access to food and water.

2.2.11 Behavioral Analysis

Rotation Test

On completion of 6 weeks, rats were subjected to rotational test as described above.

Cylinder Test

Cylinder test was performed in order to evaluate the forelimb asymmetry in rats using a modified version [83] of the initially-described procedure [84]. Briefly, rats were put individually in a glass cylinder (21 cm diameter, 34 cm height) and video recorded for 5 min without prior habituation. To stimulate rats that showed little or no tendency to explore, the following methods were used in the given order: (i) turning the lights in the room on and off 2 ± 3 times; (ii) mildly shaking the cylinder for 2 ± 3 s; (iii) taking the rat out of the cylinder for approximately 30 s and then putting it back, as described previously [85]. Ipsilateral or contralateral forelimb touches to the cylinder wall were counted by a blinded observer from the video recordings.

Stepping Test

Stepping test (Adjusting Steps Test) was performed in order to evaluate forelimb akinesia three times on the same day with 30 min intervals in between tests according to the procedure described previously [86]. Briefly, rats were held by the experimenter with one hand fixing the hindlimbs and slightly raising the hind part above the surface of a table with a width of 100 cm. The other hand fixed the forelimb not to be monitored. The rats were moved sideways with one paw touching the table at a speed of 100 cm/5 s first in the forehand and then in the backhand direction. The number of adjusting steps was counted for both paws in both directions by a blinded observer from the video recordings.

2.2.12 Animal Perfusion and Tissue Acquisition

Three days after the behavioral tests to allow for the wash-out of d-amphetamine, rats in all groups were sacrificed either with or without transcardiac perfusion using 4% paraformaldehyde solution under ketamine and xylazine anesthesia. Brains were

obtained and striata were excised in rats sacrificed without perfusion. Striata were homogenized using 0.4 N HCl, and homogenates were kept for future analyses of dopamine, TH and cleaved-Caspase-3. Brains of rats obtained following paraformaldehyde perfusion were sectioned and processed for immunohistochemical analyses.

2.2.13 Histological Analyses

Sections were deparaffinized in xylene and rehydrated in serial ethanol series for hematoxylin & eosin (H&E) staining according to the standard protocol. For immunohistochemistry experiments, sections were stained with anti-TH (1:250; Millipore AB152) and anti-Iba1 (1:2000 Sigma ab178846) antibodies. After primary antibody staining, horseradish peroxidase (HRP) conjugated goat anti-rabbit secondary antibody (1:500; Millipore) was used followed by 3,3′-diaminobenzidine (DAB) staining. All samples were mounted onto glass slides using xylene based mounting medium. Digital images were acquired via Zeiss Axio Scope A1. Images were acquired by using 10x and 20x objectives.

2.2.14 Dopamine Analyses

Dopamine contents of striata were analyzed using HPLC coupled with an electrochemical detector and an analytical column as described previously [81]. The samples were run at a rate of 1 mL/min using a mobile phase containing 0.15 M Na_2HPO_4, 0.5 mM sodium octasulfate and 0.1 mM Na_2EDTA dissolved in 10% methanol solution.

2.2.15 Western Blot Analyses

Laemmli loading buffer was added to the homogenates obtained from striata of the brain tissues in equal volumes, they were mixed well and boiled. Equal volumes of the mixtures including the same amount of protein content were loaded into SDS-PAGE (4–20%; Bio-Rad, Hercules, CA, USA) and separated. After separation of the proteins with SDS-PAGE, they were transferred to polyvinylidene fluoride (PVDF) membranes (Millipore, Billerica, MA, USA). Blocking of the membrane was performed with 4% non-fat dry milk (Carnation, Glendale, CA, USA) prepared in Tris-buffered saline and Tween 20 (TBST). After blocking, membranes were incubated with primary antibodies (rabbit anti-TH [Millipore, Billerica, MA, USA] and rabbit anti-cleaved-Caspase-3 [Cell Signaling, Danvers, MA, USA]) in TBST solution overnight. On the following day, the membrane was incubated with peroxidase-conjugated secondary antibody and visualized with the enhanced chemiluminescence system (Millipore, Billerica, MA, USA) using a Licor C-Digit blot scanner (LI-COR Biotechnology, Lincoln, NE, USA). The membranes were incubated with anti-β-tubulin antibody (Sigma-Aldrich, St. Louis, MO, USA) used for normalization after stripping with stripping buffer (Thermo Fisher Scientific, Rockford, IL, USA).

2.2.16 Statistical Analyses

Statistical analyses were performed using Sigma Plot version 12.0 software. Data were expressed as mean ± standard error of mean (sem). Comparisons between two groups were made using Student's t-test and those between multiple groups were made by using one-way analysis of variance (ANOVA) followed by post hoc Tukey test and one-way ANOVA or two-way ANOVA with Bonferroni multiple comparison test. A

p-value of less than 0.05 was considered significant (*$p < 0.05$; **$p < 0.01$; ***$p < 0.001$).

2.3 Results and Discussion

2.3.1 Characterization of Peptide Nanofibers

For both *in vitro* and *in vivo* studies, four different PA molecules were synthesized. All PA molecules had a hydrophobic alkyl tail composed of lauric acid and a β-sheet forming peptide sequence, VVAG. Lauryl-VVAGIKVAV-Am (LN-PA) was synthesized as laminin mimetic PA molecule and Lauryl-VVAGEGDK(pbs)S-Am (GAG-PA) was developed to mimic heparan sulfates with its sulfonate, hydroxyl and carboxylic acid groups incorporated as amino acid side chains. LN-PA/GAG-PA scaffolds bear two bioactive epitopes to mimic both laminin and heparan sulfates. The other two PA molecules used in this study were Lauryl-VVAGE (E-PA) and Lauryl-VVAGK-Am (K-PA) (Figure 2.1). These two PAs did not have any bioactive epitope sequences and they were used for gel formation with oppositely charged PAs to obtain K-PA/GAG-PA and LN-PA/E-PA nanofibers. K-PA/E-PA nanofibers were used as an epitope-free gel control. The PA molecules were synthesized by solid phase peptide synthesis, purified with preparative HPLC and characterized by LC-MS (Figure 2.2).

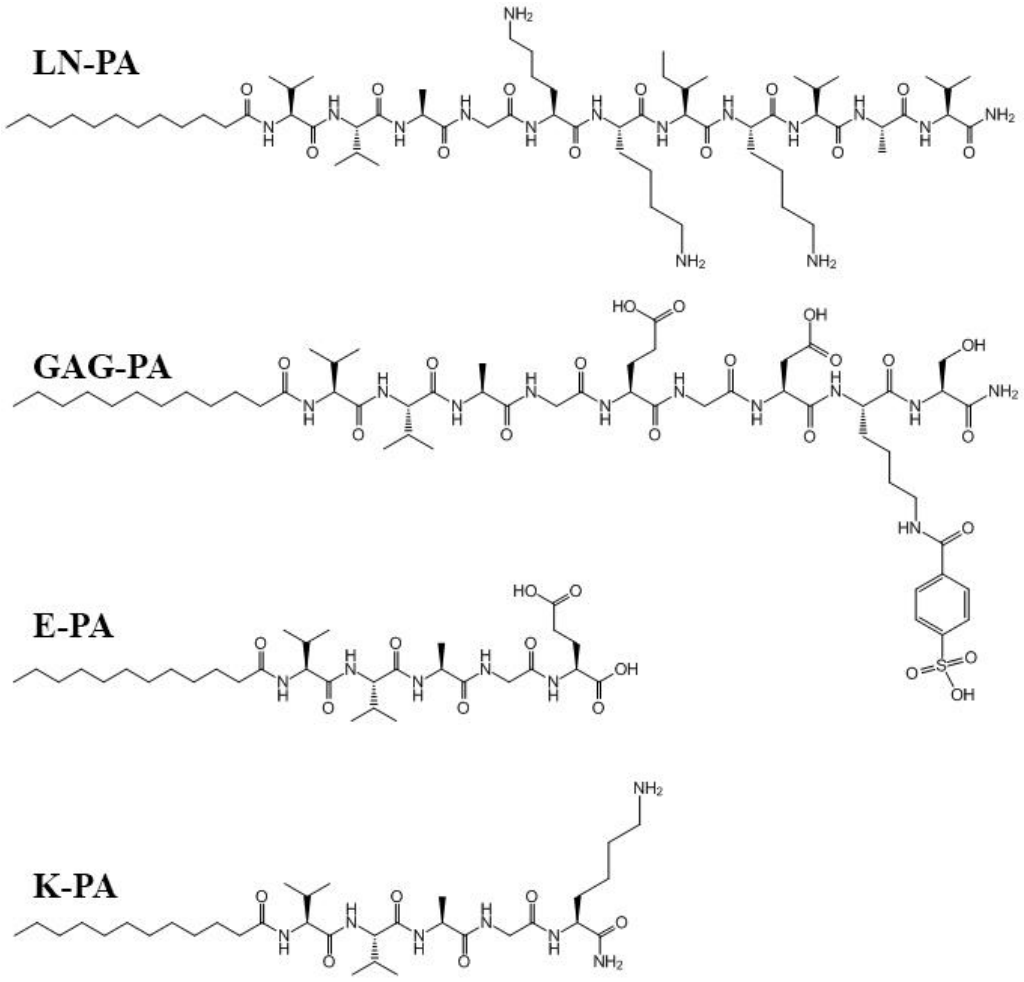

Figure 2. 1 Chemical structures of PA molecules.

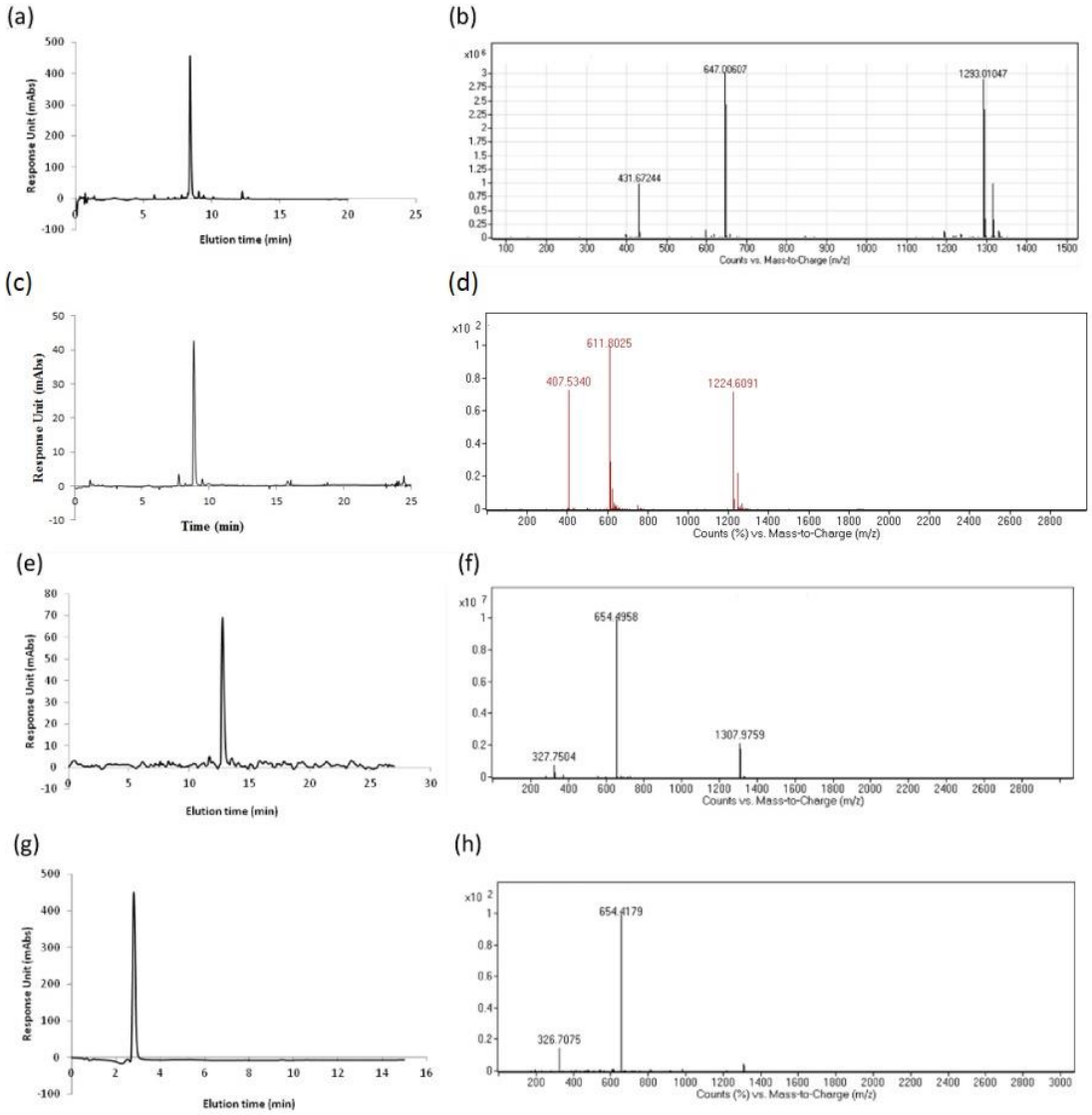

Figure 2. 2 LC-MS of LN-PA (a,b), GAG-PA (c,d), K-PA (e,f) and E-PA (g,h). Mass spectrometry of LN-PA; $[M+H]^+$ (calculated): 1292.93, $[M+H]^+$ (observed): 1293.01, $[M+2H]^{+2}/2$ (calculated): 646.96, $[M+2H]^{+2}/2$(observed): 647.01, $[M+3H]^{+3}/3$ (calculated): 431.64, $[M+3H]^{+3}/3$(observed): 431.67. Mass spectrometry of GAG-PA; $[M-H]^-$ (calculated): 1225.59, $[M-H]^-$ (observed):1224.61, $[M-2H]^{-2}/2$ (calculated): 612.29, $[M-2H]^{-2}/2$ (observed): 611.80, $[M-3H]^{-3}/3$ (calculated): 407.86, $[M-3H]^{-3}/3$(observed): 407.53. Mass spectrometry of K-PA; $[2M+H]^+$ (calculated): 1307.96, $[2M+H]^+$ (observed): 1307.98, $[M+H]^+$ (calculated): 654.48, $[M+H]^+$ (observed):

654.50, $[M+2H]^{+2}/2$ (calculated): 327.74, $[M+2H]^{+2}/2$(observed): 327.75. Mass spectrometry of E-PA; $[M-H]^{-}$ (calculated): 654.42, $[M-H]^{-}$ (observed): 654.42, $[M-2H]^{-2}/2$ (calculated): 326.71, $[M-2H]^{-2}/2$(observed): 326.71.

By SEM imaging, it was revealed that nanofiber networks in PA gels had morphological similarity to natural ECM that surrounds the cells in tissues (Figure 2.3). In addition, STEM imaging showed that all nanofibers were uniform in diameter (10−20 nm) and several micrometers in length (inner frames of Figure 2.3).

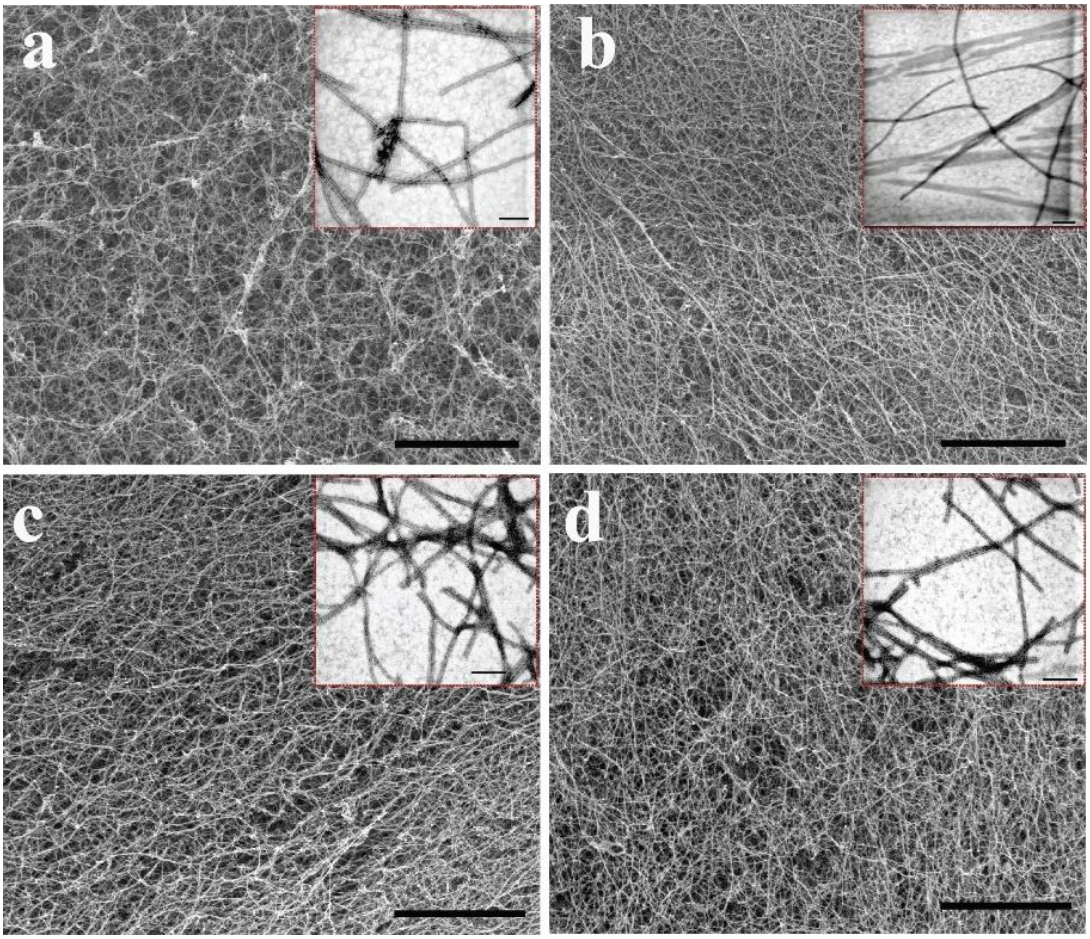

Figure 2. 3 SEM images of LN-PA/GAG-PA (a), LN-PA/E-PA (b), K-PA/GAG-PA (c) and K-PA/E-PA (d) show nanofiber networks resembling the fibrous ECM structure. Scale bars are 3 μm in length. STEM images of all PA nanofibers formed at pH 7.4 are given in inner frames of panels a, b, c and d. Scale bars are 100 nm in length.

We employed a CD spectrophotometer and observed predominant β-sheet structures with a chiral absorbance maximum at around 200 nm and minimum at around 220 nm (Figure 2.4). Besides biological cues, physical properties are also important to enhance the efficacy of the PA nanofibers used in this study. PA scaffolds used in this study are similar to ECM of neural tissues in terms of physical appearance of fibrous

networks. When designing a scaffold for nervous tissue, the mechanical characteristics of the scaffold should be similar to that of brain tissue, which is about 1 kPa [35]. To study the mechanical properties of PA gels, we used oscillatory rheology. Rheology results showed all PA combinations had higher storage modulus (G′) than loss modulus (G″), verifying the gel formation at physiological pH (Figure 2.5). Rheological measurements confirmed that all PA combinations formed gels and displayed similar properties to nervous tissue.

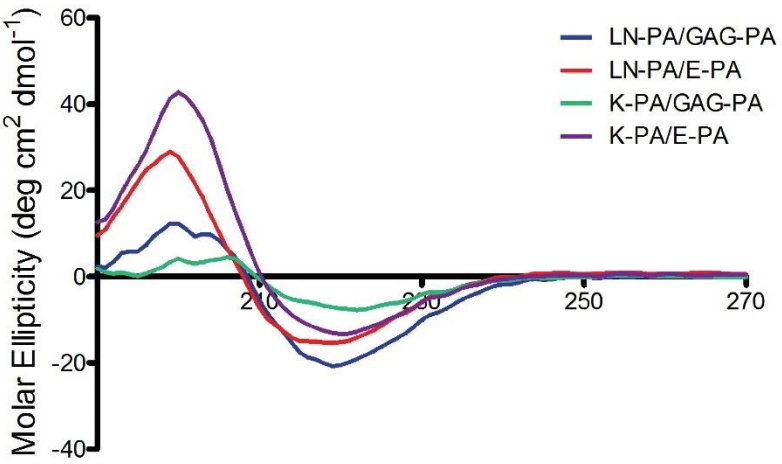

Figure 2. 4 Characterization of secondary structure of peptide nanostructures by CD.

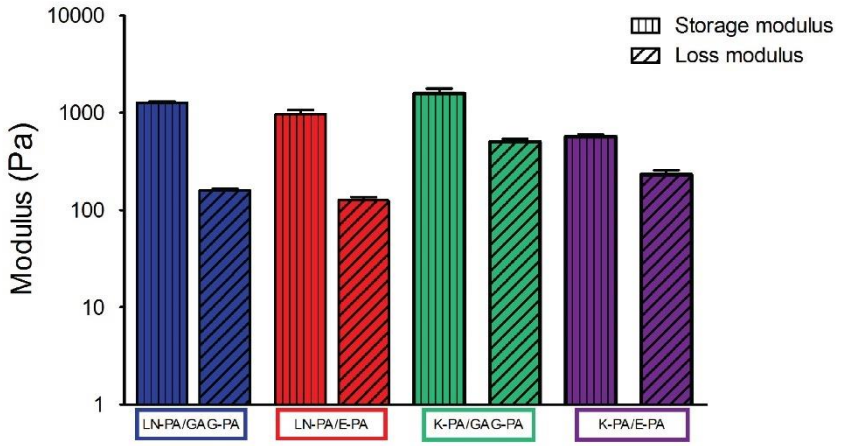

Figure 2. 5 Mechanical properties of PA gels measured by oscillatory rheology. Rheology results showed gelation as a result of nanofibrous network formation by all combinations at pH 7.4.

2.3.2 *In vitro* Studies

The dose response study was crucial to determine the IC_{50} value of the 6-OHDA concentration. Different concentrations of 6-OHDA (0–750 μM) were applied to SH-SY5Y cells and 6-OHDA-induced cytotoxicity was evaluated using Alamar blue assay. Viability of SH-SY5Y cells markedly decreased following 24 h incubation with an increasing concentration of 6-OHDA (Figure 2.6). A concentration of 50 μM for 6-OHDA was chosen for subsequent experiments since this concentration adequately decreased cell viability to about 50% ($p<0.001$).

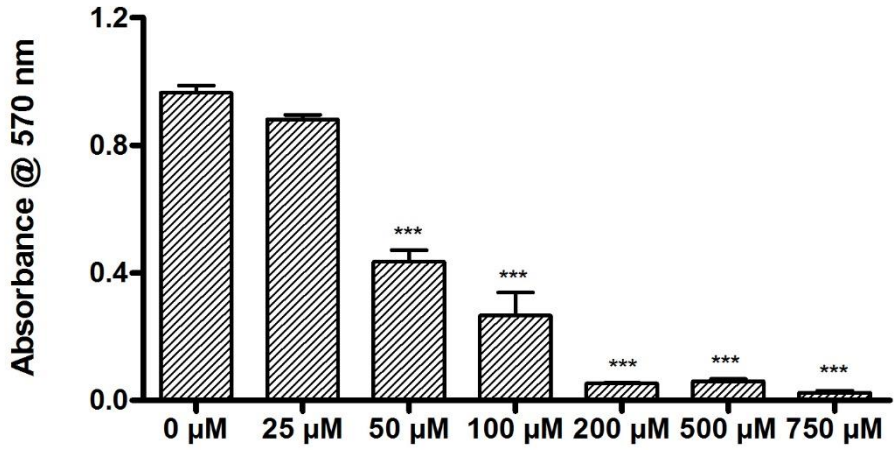

Figure 2. 6 Concentration-dependent toxicity of 6-OHDA in SH-SY5Y cells determined by Alamar blue assay. Values represent mean ± sem (***$p < 0.001$).

Cellular viability of SH-SY5Y cells treated with either 6-OHDA or vehicle was assessed by calcein-AM/ethidium homodimer 1 staining, by comparison to cells that were cultured on different PA nanofibers. Results demonstrated that the cell viability on LN-PA/GAG-PA nanofibers was the highest and significantly greater than other PA combinations (Figure 2.7).

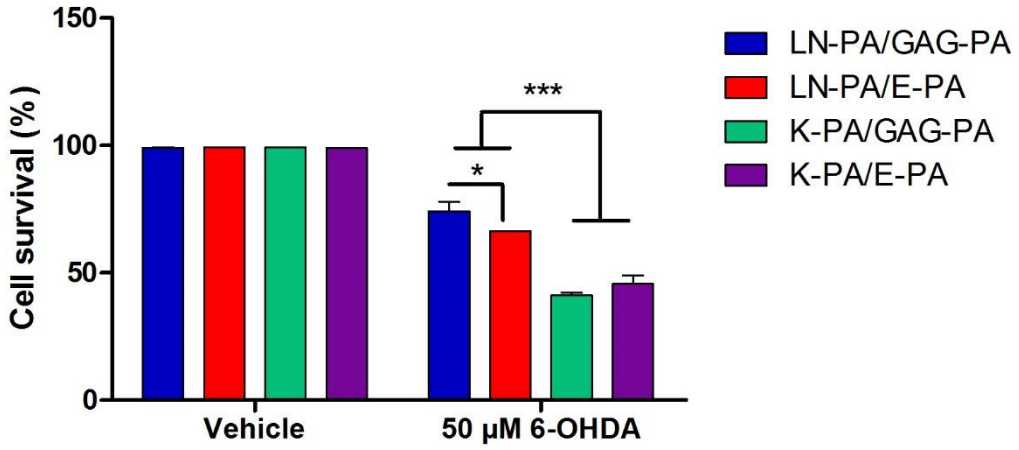

Figure 2. 7 Viability of SH-SY5Y cells when cultured on peptide nanofibers in the presence or absence of 50 µM 6-OHDA for 24 h analyzed by calcein/ethidium homodimer live-dead assay. Values represent mean ± sem (*$p < 0.05$, ***$p < 0.001$).

Using Annexin V and the propidium iodide double-staining system, the Annexin V^-/propidium $iodide^-$ population was considered as normal healthy cells, while Annexin V^+/propidium $iodide^-$ cells were taken as a measurement of early apoptosis and Annexin V^+/propidium $iodide^+$ as late apoptosis. After 24 h of incubation of cells seeded on different PA combinations and TCP with 6-OHDA, results showed that the percentage of live cells in LN-PA/GAG-PA group was significantly higher than other groups ($p<0.001$) (Figure 2.8). Also, percentage of late apoptotic cells was lowest in LN-PA/GAG-PA group compared to other groups ($p<0.001$), which showed that LN-PA/GAG-PA combination indicates a potentially favorable outcome for *in vivo* studies.

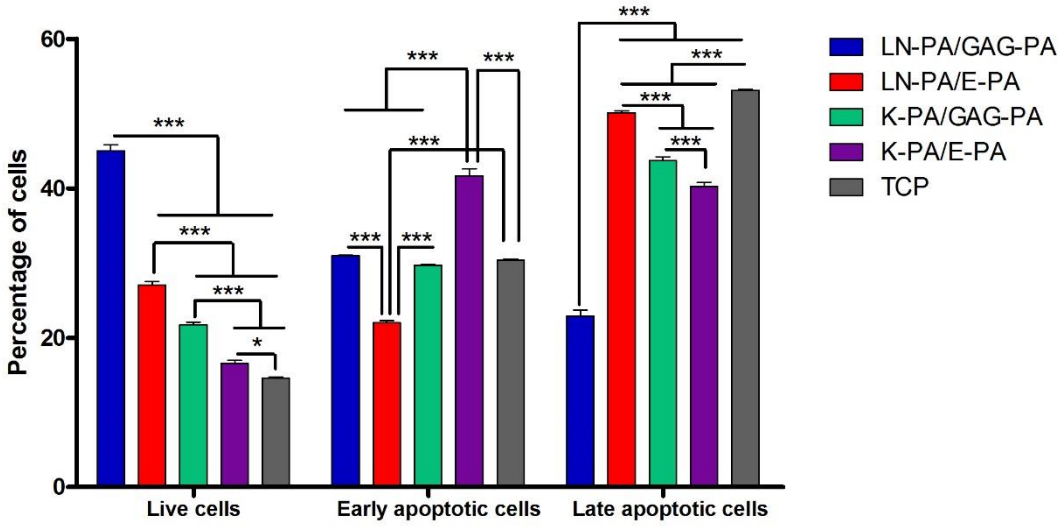

Figure 2. 8 Cell apoptosis on different PA combinations and TCP after 24 h of culture was tested by flow cytometry analysis. Values represent mean ± sem (*p < 0.05, ***p < 0.001).

2.3.3 Effect of Peptide Nanofibers on Behavioral Functions

The 6-OHDA model of nigral injury has been utilized for decades as a clinical experimental model of PD [87]. Intrastriatal injection of 6-OHDA leads to retrograde and progressive degeneration, thus providing a useful approach to study neuroprotective and neuroregenerative effects of experimental studies. We used this model for *in vivo* studies and injury was verified with amphetamine-induced rotational test. Rotational behavior was tested initially in 6-OHDA-lesioned rats in order to randomize rats to 6-OHDA + Sucrose and 6-OHDA + PA groups by ensuring similar number of ipsilateral rotations (275±11 and 275±6, respectively) (Figure 2.9a). Six weeks after treatment, rats in 6-OHDA + Sucrose group displayed almost identical number of ipsilateral rotations (273±7) to that observed before treatment onset while,

on the contrary, number of ipsilateral rotations were reduced significantly to 226±2 ($p<0.001$) in rats in the 6-OHDA + PA group after 6 weeks of treatment (Figure 2.9b).

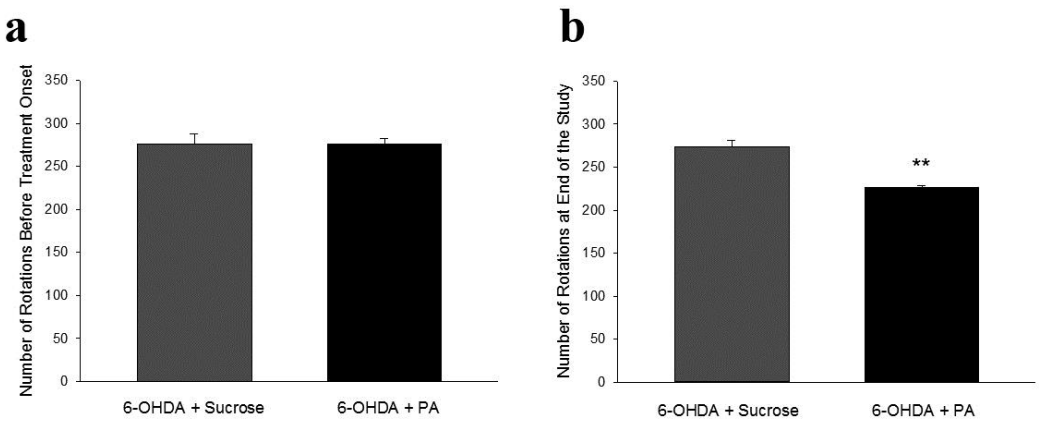

Figure 2. 9 Changes in rotational behavior evaluated by rotameter. Rats were injected i.p. with d-amphetamine (5 mg/kg), and ipsilateral rotations between 15 and 45 min were recorded using an automated Rotameter system. Initial behavioral task (a) was performed in order to ensure that the unilateral striatal 6-OHDA lesion was established and the data were used to randomize the 6-OHDA-lesioned rats into two treatment groups while the test was repeated 6 weeks after administration of PA nanofibers (b). Data are expressed as mean ± sem. (*$p < 0.05$ vs. 6-OHDA + Sucrose group).

In cylinder test, rats in Sham, L-Ascorbic Acid + PA, 6-OHDA + Sucrose and 6-OHDA + PA groups made 8.5±2, 8.3±1, 7.8±1 and 7.8±1 touches with only the ipsilateral forelimb, respectively (Figure 2.10a), and 45.5±8, 45.3±10, 30.8±6 and 36.5±6 touches with both forelimbs at the same time, respectively (Figure 2.10c). The number of touches with only the ipsilateral forelimb and both forelimbs did not differ significantly among groups. On the other hand, compared to sham group (7.36±0.5), number of contralateral touches was reduced significantly in 6-OHDA + Sucrose

(1.8±0.3; p<0.001) group while it was increased significantly in 6-OHDA + PA group to 4±0.8 (Figure 2.10b).

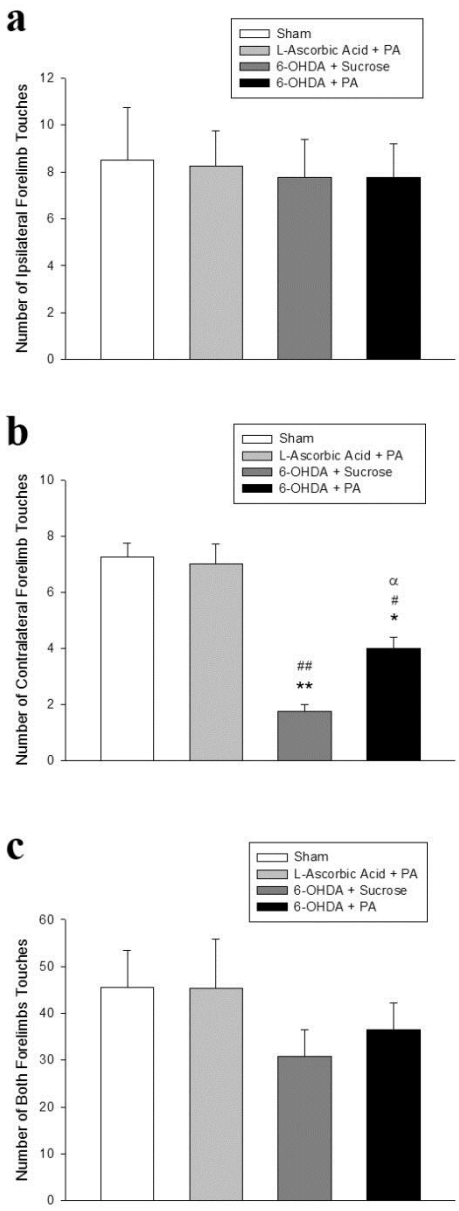

Figure 2. 10 Changes in forelimb asymmetry evaluated by cylinder test. Number of forelimb touches to the surface of a cylinder with the rats' ipsilateral (a), contralateral (b) and both forelimbs (c) was counted. Data are expressed as mean ± sem. *p < 0.05

and **$p < 0.01$ vs. sham group; $^{\#}p < 0.05$ and $^{\#\#}p < 0.01$ vs. L-ascorbic acid + PA group; and $^{\alpha}p < 0.05$ vs. 6-OHDA + sucrose group.

Number of adjusting steps that the rats made did not differ significantly among groups when rats were moved sideways on their ipsilateral forelimb both in the ipsilateral and contralateral directions (Figure 2.11a, b). On the contrary, number of adjusting steps was reduced significantly in rats in the 6-OHDA + Sucrose group when rats were moved sideways on their contralateral forelimb in the ipsilateral (9.7±1; $p<0.05$) (Figure 2.11c) and contralateral (3.5±0.2; $p<0.001$) (Figure 2.11d) directions compared to those in Sham group (14.4±0.4 in the ipsilateral and 10.4±0.5 in the contralateral direction). Compared to the 6-OHDA + Sucrose group, number of contralateral touches tended to increase (11.2±1) and did significantly increase (6.2±0.1; $p<0.05$) in rats in the 6-OHDA + PA group when rats in this group were moved sideways on their contralateral forelimb in the ipsilateral (Figure 2.11c) and contralateral (Figure 2.11d) direction, respectively.

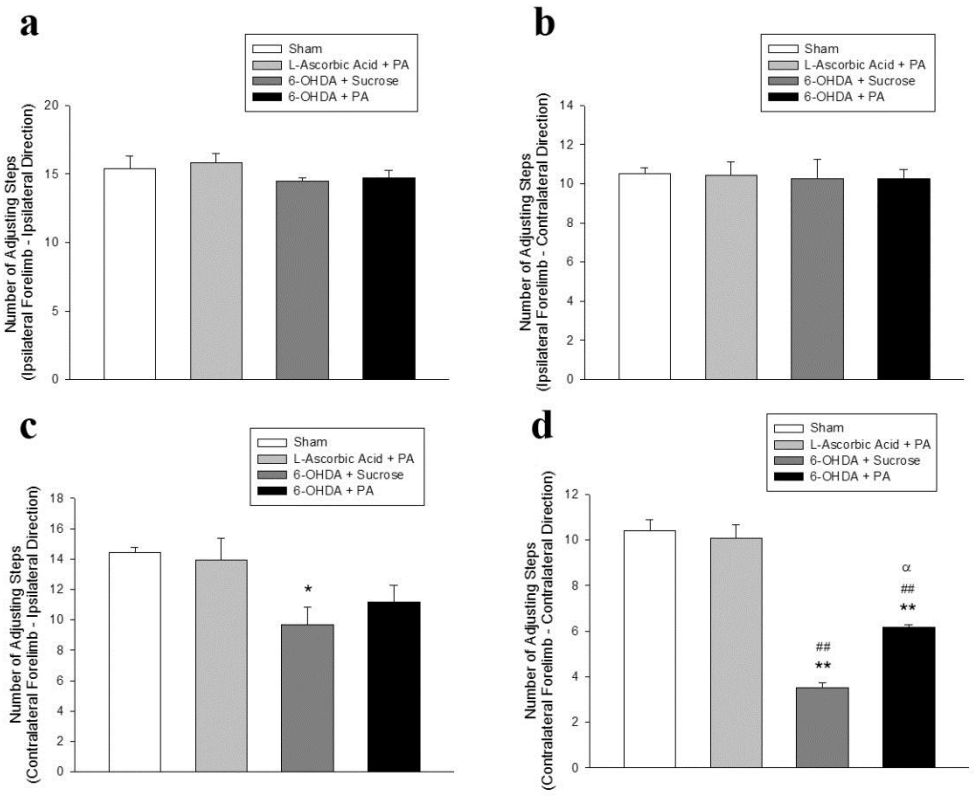

Figure 2. 11 Changes in forelimb akinesia evaluated by stepping test. Number of adjusting steps that the rats made were counted when rats were moved sideways with one paw touching the table at a speed of 100 cm/5 s first in the forehand and then in the backhand direction. Figure shows mean number of adjusting steps made by the rat on its ipsilateral forelimb towards ipsilateral direction (a), ipsilateral forelimb towards contralateral direction (b), contralateral forelimb towards ipsilateral direction (c) and contralateral forelimb towards contralateral direction (d). Data were expressed as mean ± sem of three tests performed with 30 min intervals on the same day. $^{**}p < 0.01$ vs. Sham group; $^{\#\#}p < 0.01$ vs. L-Ascorbic Acid + PA group; and $^{\alpha}p < 0.05$ vs. 6-OHDA + Sucrose group.

2.3.4 Histological Assessments

In order to monitor morphology of striatum, H&E staining was carried out on brain sections taken from the rat brains at the end of 6 weeks. H&E staining revealed that there was tissue loss due to injection of 6-OHDA in 6-OHDA + Sucrose sections. Entry of the cannula can be observed clearly and there was almost no cell accumulation towards the damaged area. In contrast, PA injection to the striatum provided better tissue integrity compared to sucrose control. The gel was degraded at the end of 6 weeks, and cells accumulated towards the injury site and covered this region (Figure 2.12). This result shows that the PA gel helps to maintain tissue integrity in 6-OHDA injected striata.

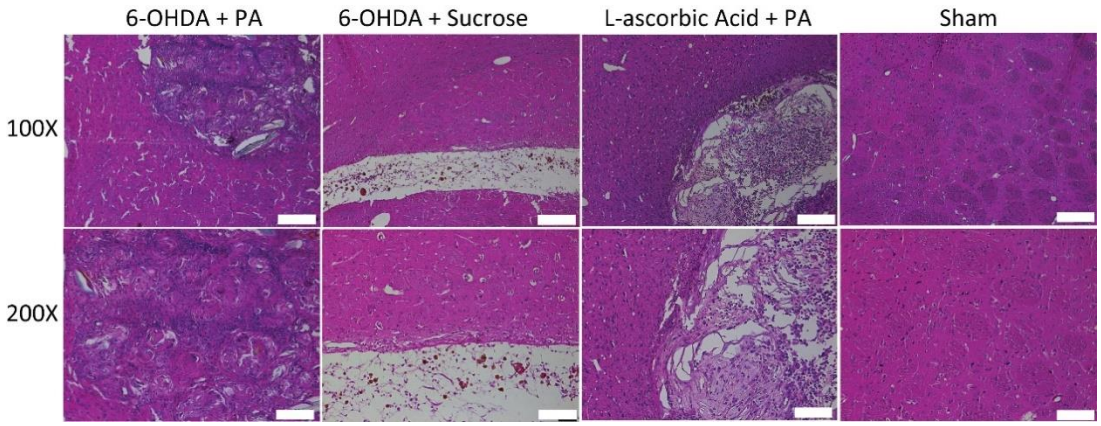

Figure 2. 12 H&E staining of striata of rat brain sections at postoperative week 6. The sections of 6-OHDA + PA group were compared with that of sham, L-Ascorbic Acid + PA and 6-OHDA + Sucrose groups. Images were taken with 100X (Scale bars 200 µm in length) and 200X magnifications (Scale bars 100 µm in length).

For characterization of cells within the injury site, immunohistochemistry against Iba-1 was performed, and cells that accumulated towards the injection site in gel in 6-OHDA + PA groups were characterized as microglia when staining positively for Iba-1, which is a calcium-binding protein and plays a role in regulation of microglial function (Figure 2.13). Microglial activation occurs in CNS as a result of several pathological situations including inflammation and degeneration [88, 89]. Microglia can serve for removal of deleterious debris by phagocytic activity after brain injury or neurodegeneration and contribute to neuroprotection by releasing neurotrophic factors [90, 91]. In addition, properly-activated microglia have been shown to restrict the lesion area and provide protection in an experimental model of PD [92]. Therefore, we suggest that PA nanofibers behaved as a scaffold mimicking the ECM which enabled cell accumulation to alleviate the extent of the injury created by 6-OHDA injection.

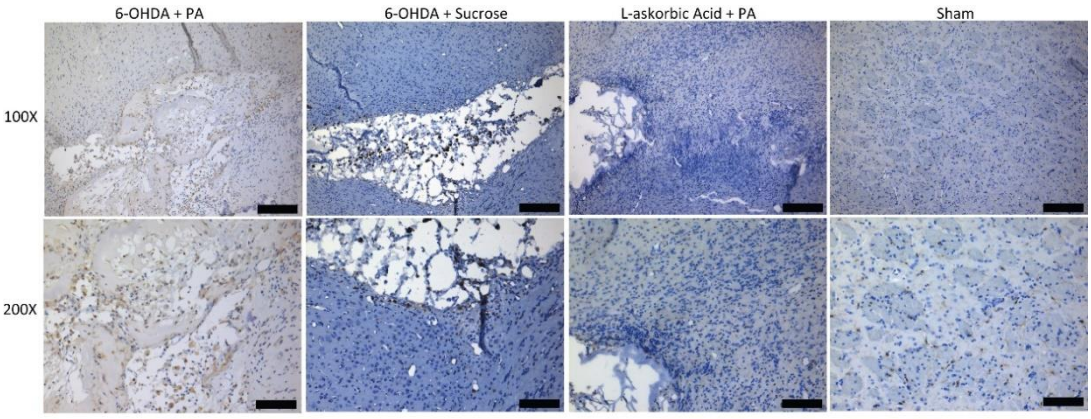

Figure 2. 13 Immunohistochemistry against Iba-1 protein for rat brain sections at postoperative week 6. The sections of 6-OHDA + PA group were compared with that of Sham, L-Ascorbic acid + PA and 6-OHDA + Sucrose groups. Images were taken with 100X (Scale bars 200 μm in length) and 200X magnifications (Scale bars 100 μm in length).

Intrastriatal 6-OHDA lesioning reduced the dopamine content in the ipsilateral striatum from 0.94±0.05 pmol/µg protein in Sham group to 0.44±0.02 pmol/µg protein ($p<0.001$) in 6-OHDA + Sucrose group (Figure 2.14). PA treatment enhanced this reduced dopamine content significantly to 0.75±0.01 pmol/µg protein ($p<0.05$) (Figure 2.14). Dopamine content of ipsilateral striatum did not differ in L-Ascorbic Acid + PA group (0.92±0.05 pmol/µg protein) compared with that in Sham group.

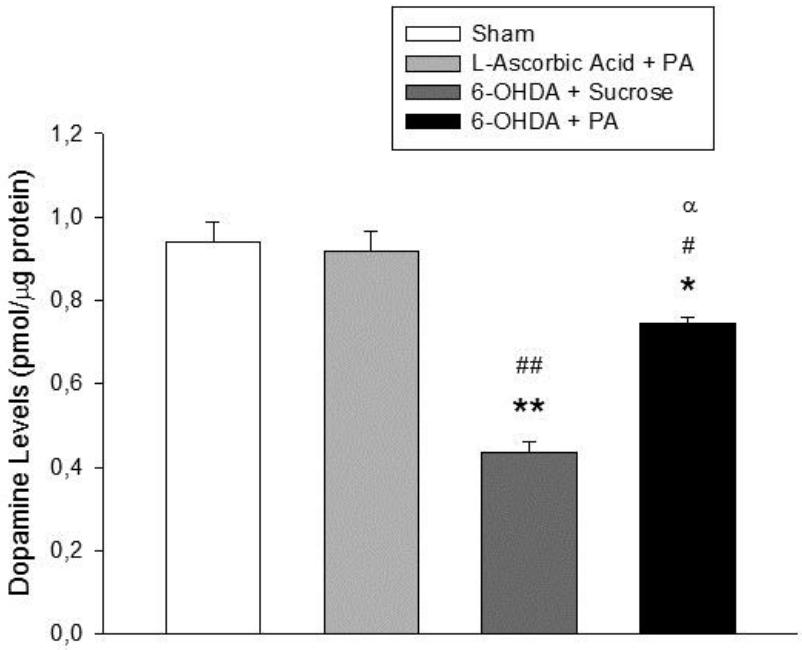

Figure 2. 14 Levels of dopamine in lesioned striatum. Data are expressed as mean ± sem. *$p < 0.05$ and **$p < 0.01$ vs. Sham group; $^{\#}p < 0.05$ and $^{\#\#}p < 0.01$ vs. L-Ascorbic Acid + PA group; and $^{\alpha}p < 0.05$ vs. 6-OHDA + Sucrose group.

Similarly to dopamine levels, TH levels were reduced significantly in rats in 6-OHDA + Sucrose group by 79% ($p<0.001$) compared with the Sham group (Figure 2.15). The fall in striatal TH was less pronounced, although significant, in 6-OHDA + PA group (by 49%; $p<0.001$) compared with Sham. On the other hand, TH levels were

significantly greater in 6-OHDA-lesioned rats treated with PA compared with those receiving Sucrose ($p<0.05$) (Figure 2.15).

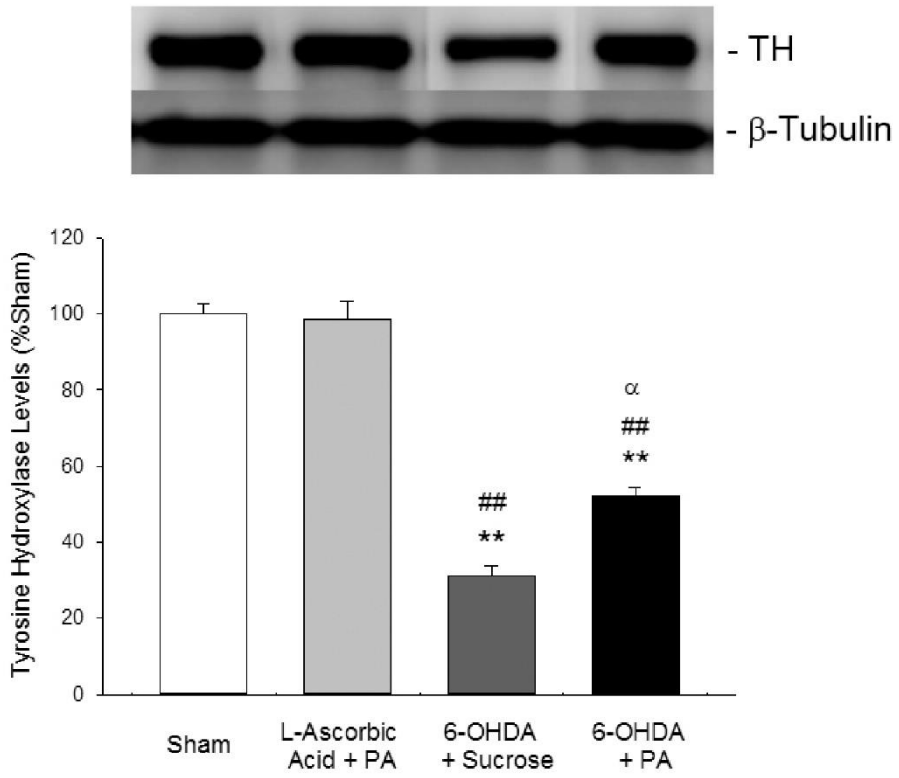

Figure 2. 15 Levels of TH analyzed by Western blot in lesioned striatum. Data are expressed as mean ± sem. **$p < 0.001$ vs. Sham group; $^{\#\#}p < 0.01$ vs. L-Ascorbic Acid + PA group; and $^{\alpha}p < 0.05$ vs. 6-OHDA + Sucrose group.

Immunohistochemistry against TH also showed that TH-immunoreactivity almost disappeared in striatal sections, and 6-OHDA injection caused progressive dopaminergic cell loss in 6-OHDA + Sucrose group both in injury site and around this region. However, this progressive cell loss was inhibited by PA gel in 6-OHDA + PA group. (Figure 2.16).

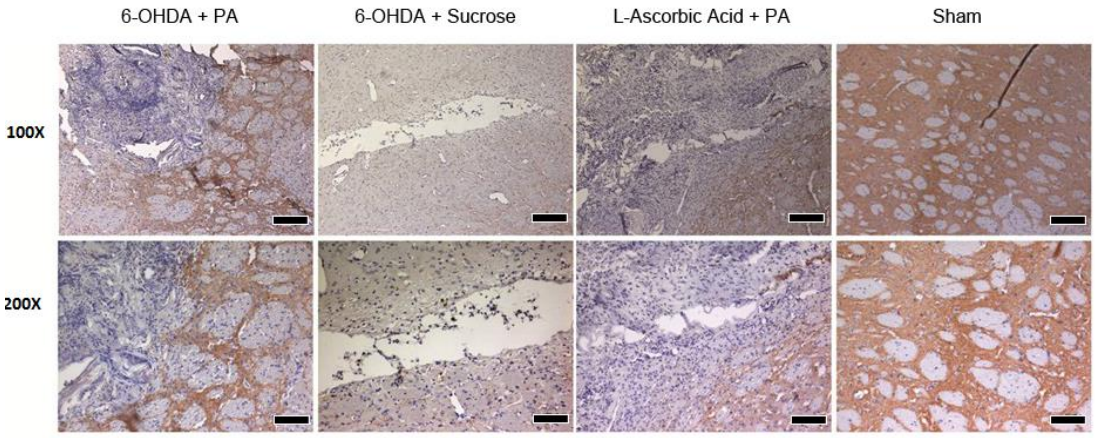

Figure 2. 16 Levels of TH analyzed by and immunohistochemistry. No staining against TH was observed in 6-OHDA + Sucrose group, while TH protein immunostaining was detected in the lesion area in 6-OHDA + PA group at an extent similar with that observed in L-Ascorbic Acid + PA group (B). Images were taken with 100X (Scale bars 200 μm in length) and 200X magnifications (Scale bars 100 μm in length).

Besides recruiting microglia, another mechanism by which PA nanofibers provide protection in the 6-OHDA rat model of PD might be represented by their anti-apoptotic activity. We investigated the extent of apoptosis by analyzing cleaved-Caspase-3 levels in the lesioned striatum. Compared with sham group, levels of cleaved-Caspase-3 almost doubled in rats with 6-OHDA lesion which received Sucrose intrastriatally (196±9%; $p<0.01$) while the increase in cleaved-Caspase-3 was less pronounced in parkinsonian rats which received PA (156±8%; $p<0.01$) (Figure 2.17). Strikingly, the reduction of cleaved-Caspase-3 levels in PA group was significant compared to Sucrose group ($p<0.01$). In good accord, a recent study showed that silencing of Caspase-3 by RNA interference reduced striatal dopaminergic cell loss and increased locomotor activity in a rat model of PD [61], suggesting a role for apoptosis in the

pathogenesis of PD. The reduction in cleaved-Caspase-3 levels observed in our study therefore contributes to our understanding of how PA nanofibers provide protection in a rat model of PD, as has been shown previously for IKVAV-carrying epitopes in spinal cord injury [30].

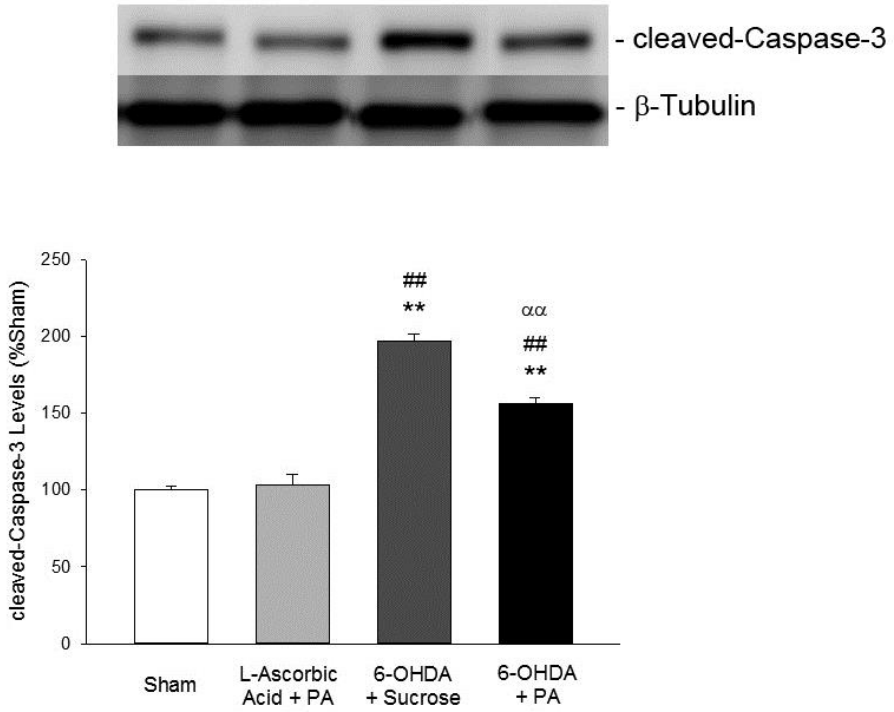

Figure 2. 17 Levels of cleaved-Caspase-3 analyzed by Western blot. Data were expressed as mean ± sem. **p < 0.01 vs. Sham group; $^{\#\#}$p < 0.01 vs. L-Ascorbic Acid + PA group; and $^{\alpha\alpha}$p < 0.001 vs. 6-OHDA + Sucrose group.

2.4 Conclusion

In summary, we utilized a bioactive PA nanofiber gel system for therapeutic effect in both for SH-SY5Y cell culture and experimental PD model. *In vitro* results revealed that laminin-derived peptide signals along with heparan-sulfate-mimicking epitope were found to provide better viability through decreasing the apoptosis after 6-OHDA

treatment. Furthermore, *in vivo* results showed that this scaffold is effective on reducing striatal injury and enhancing functional recovery after unilateral striatal injection of 6-OHDA. Also, histological analyses demonstrated that PA gel helped to maintain tissue integrity in 6-OHDA injected striata and prevented progressive dopaminergic cell loss around the damaged area. Overall, incorporation of heparan sulfate and laminin mimetic epitopes into PA nanofiber system decreased the toxic effect of 6-OHDA and provided better functional outcomes. This is the first study that reports the protective effects of PA nanofibers in a neurodegenerative disease model, which makes this system a promising therapeutic approach against degeneration in PD, but there still is a need for further studies to see the effects of these PA nanofibers on genetic model before the clinical trials since genetic models may better simulate the mechanisms underlying the genetic forms of PD. In addition, further studies on reducing the invasiveness of this technique would be beneficial prior to testing it in clinical settings.

Chapter 3

3. Effect of Schwann Cell Activity in Sciatic Nerve Regeneration by Glycosaminoglycan and Laminin Mimetic Peptide Nanofibers

This chapter of thesis was published in the following article [93]; Reproduced from "Sciatic nerve regeneration induced by glycosaminoglycan and laminin mimetic peptide nanofiber gels"; Mammadov, B.; Sever, M.; Gecer, M.; Zor, F.; Ozturk, S.; Akgun, H.; Ulas, U. H.; Orhan, Z.; Guler, M. O.; Tekinay, A. B., *RSC Advances*, 2016, 6(112), 110535-110547, with permission from the Royal Society of Chemistry.

3.1 Introduction

Peripheral nerve injuries which occur due to trauma [94], bone fractures or joint dislocations may lead to loss of sense or motor function in the distal segment of the injured axon [95]. The ability to achieve functional recovery after the injury mainly depends on the severity of peripheral nerve damage, surgical techniques and rehabilitation process after the surgery [96, 97]. Standard treatment strategies generally involve end-to-end suture of the damaged peripheral nerves if the damage is minor. However, autologous nerve grafts are usually required for larger gaps [98]. Although there have been good advances in surgical procedures, functional recovery after the treatment is mostly poor. At this point, tissue engineering and regenerative medicine studies may enhance the response to peripheral nerve injuries and increase functional outcomes as an alternative option.

Schwann cells are the glial cells in peripheral nervous system and they wrap around the axons for myelination. In case of injury, Schwann cells are activated in order to produce several neurotrophic factors and cell adhesion molecules, thereby, providing pathfinding for axonal regeneration. They are important in peripheral nerve regeneration through the reconstruction of myelin, which is essential for proper cell function in peripheral nervous system [99-101]. For all these reasons, Schwann cells are the most studied cell type in peripheral nerve regeneration studies. While designing peripheral nerve constructs, there are some important points that should be taken into consideration such as support for viability and proliferation of Schwann cells, proper storage of growth factors and presenting multiple cues to mimic native ECM [102].

In this study, ECM mimetic bioactive peptide nanofiber hydrogels with heparan sulfate and laminin derived epitopes were used as guidance cues for Schwann cells *in vitro*. Schwann cells displayed their characteristic morphology with better spreading pattern on bioactive peptide nanofibers. Also, these peptide nanofibers were found to promote Schwann cell viability and significantly enhance nerve growth factor (NGF) release. As a result, these findings propose an alternative choice for the treatment of nerve injuries in peripheral nerve system.

3.2 Experimental Section

3.2.1 Materials

Fmoc and tert-butoxycarbonyl (Boc) protected amino acids, [4-[α-(2′,4′-dimethoxyphenyl)Fmoc-aminomethyl]enoxy]acetamidonorleucyl-MBHA resin (Rink amide MBHA resin), Fmoc-Asp(OtBu)-Wang resin and HBTU were purchased from NovaBiochem and ABCR. The other chemicals were purchased from Thermo Fisher Scientific, USA, Merck Millipore, USA, or Sigma-Aldrich, USA. Live/Dead Assay

(L3224) was purchased from Thermo Fisher Scientific, USA. Antibodies and reagents for ELISA assay and poly-L-lysine (PLL) were purchased from R&D Systems, USA. Dulbecco's modified Eagle's medium (DMEM)-D-valine was purchased from Pan-Biotech, Germany. All other materials used in this study were purchased from Thermo Fisher Scientific, USA, and/or Sigma-Aldrich, USA.

3.2.2 Synthesis of PA Molecules

All PAs (Figure 3.1) were synthesized on Rink Amide MBHA resin or Fmoc-Glu(OtBu)-Wang resin with Fmoc solid phase peptide synthesis method. Amino acid couplings were performed with 2 equivalents of Fmoc protected amino acid, 1.95 equivalents HBTU and 3 equivalents of DIEA for 3 h. Fmoc removal was performed with 20% piperidine/DMF for 20 min. 10% acetic anhydride solution in DMF was used to block the remaining free amine groups after amino acid coupling. After each step, resin was washed 3 times with DMF, 3 times with DCM and 3 times with DMF, respectively. Sulfobenzoic acid was added to the side chain of lysine to synthesize sulfonated GAG-PA. A lysine residue with Mtt side chain protection was used for selective deprotection of amine groups in GAG-PA. Mtt removal was performed by shaking resins for 5 min with TFA:TIS:H_2O:DCM in the ratio of 5:2.5:2.5:90. Cleavage of the PAs from the resin was carried out with a mixture of TFA:TIS:H_2O in the ratio of 95:2.5:2.5 for 2 h. Excess TFA was removed by rotary evaporation. The remaining viscous PA solution was triturated with ice-cold ether and the resulting white precipitate was dried under vacuum.

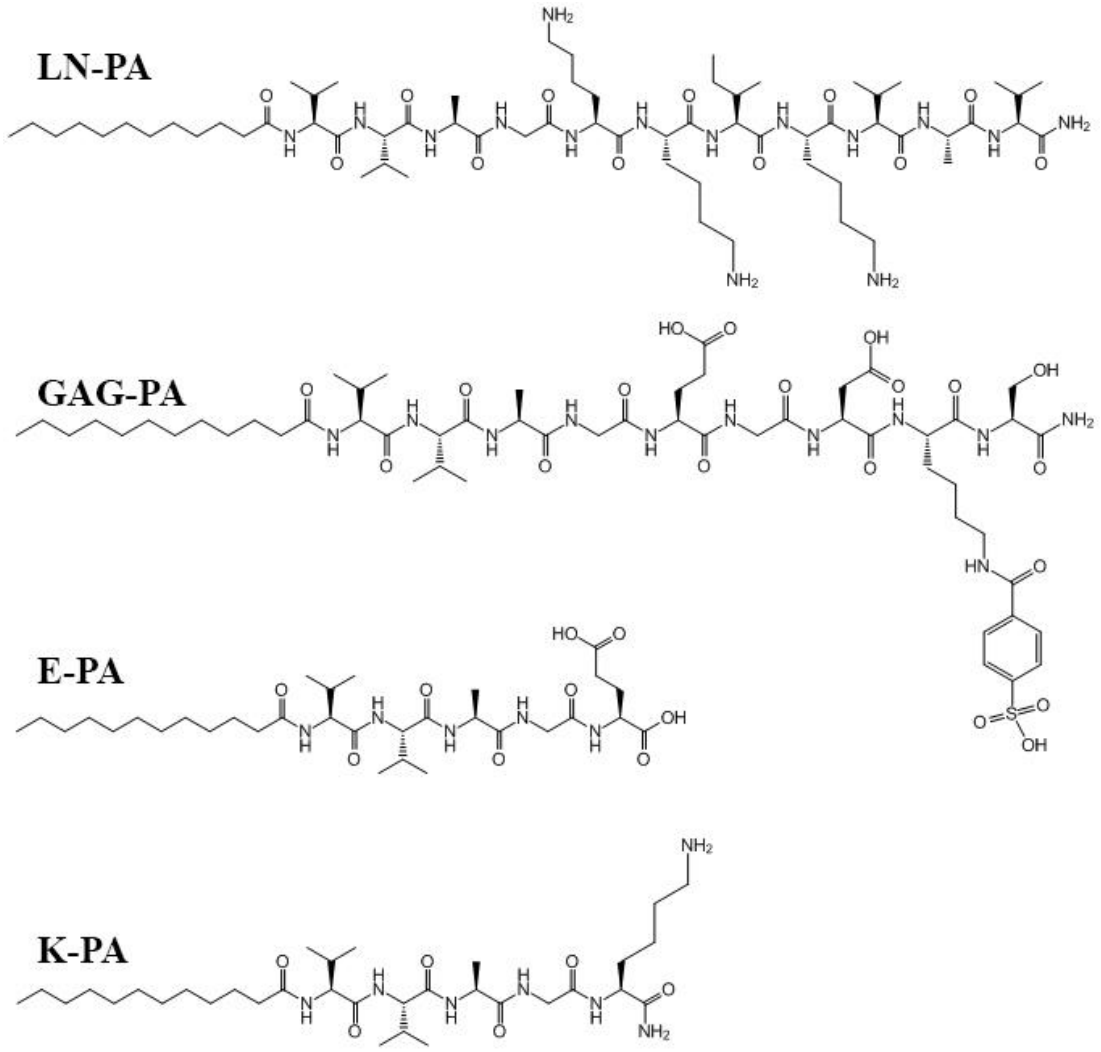

Figure 3. 1 Chemical structures of PA molecules used in the study.

Characterization of PA molecules was performed with LC-MS (Figure 3.2). Mass spectrum was obtained with Agilent LC-MS equipped with Agilent 6530 Q-TOF with an ESI source and Zorbax Extend-C18 2.1 x 50 mm column for basic conditions and Zorbax SB-C8 4.6 mm x 100 mm column for acidic conditions. A gradient of water (0.1% formic acid or 0.1% NH_4OH) and acetonitrile (0.1% formic acid or 0.1% NH_4OH) was used as a mobile phase. In order to purify the peptides, Agilent preparative reverse-phase HPLC system equipped with Zorbax Extend-C18 21.2 x 150 mm column was used for basic conditions and Zorbax SB-C8 21.2 x 150 mm column

was used for acidic conditions. A gradient of water (0.1% TFA or 0.1% NH_4OH) and acetonitrile (0.1% TFA or 0.1% NH_4OH) was used as a mobile phase. After the synthesis and purification of PA molecules, mixture of oppositely charged PAs in aqueous environment led to self-assembly resulting in nanofiber formation. As a result of encapsulation of water by the network, gelation took place instantly, depending on the initial concentration of the PA solutions. These nanofibers formed nanofiber networks which can encapsulate water to form hydrogels.

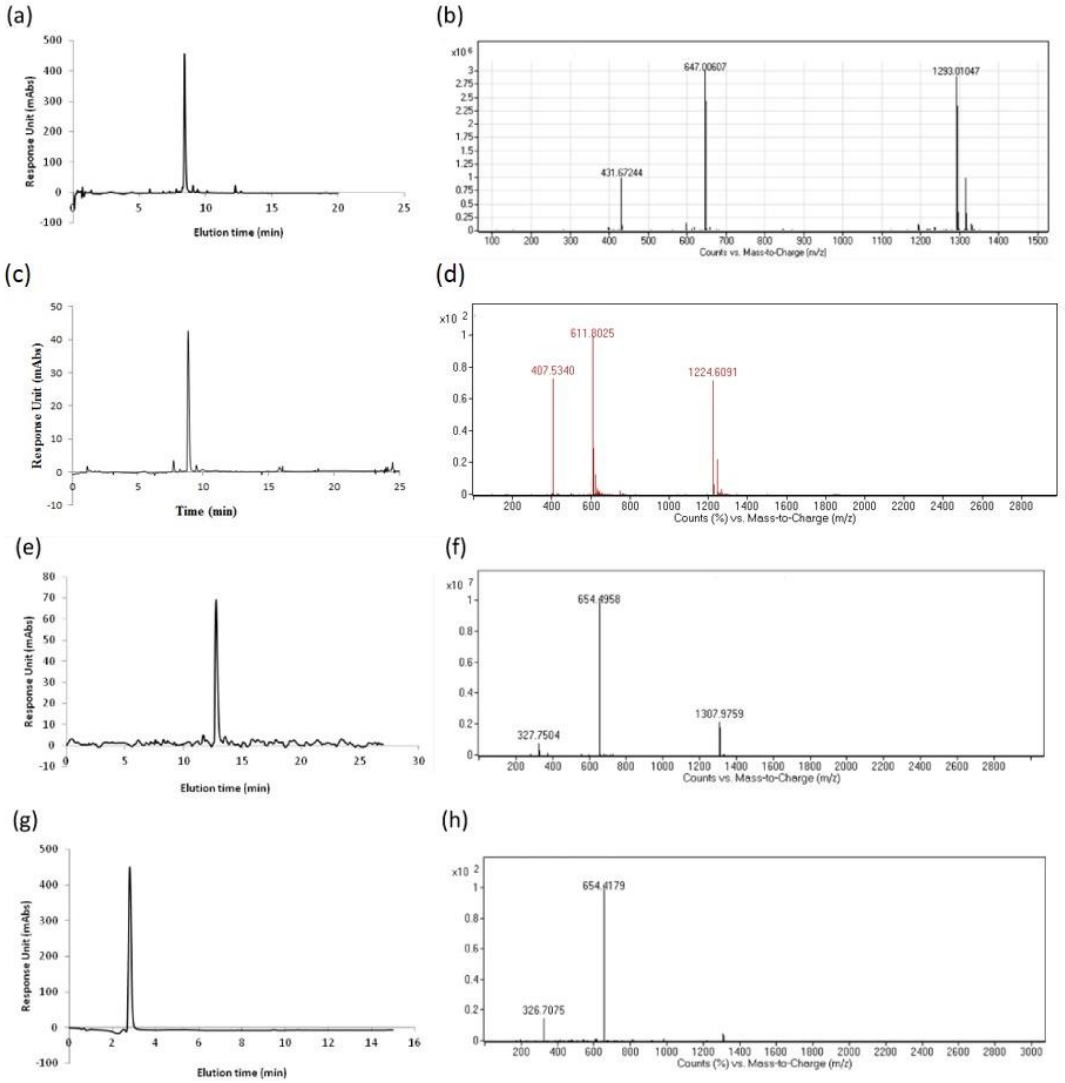

Figure 3. 2 LC-MS of LN-PA (a,b), GAG-PA (c,d), K-PA (e,f) and E-PA (g,h). Mass spectrometry of LN-PA; $[M+H]^{+}$ (calculated): 1292.93, $[M+H]^{+}$ (observed): 1293.01, $[M+2H]^{+2}/2$ (calculated): 646.96, $[M+2H]^{+2}/2$ (observed): 647.01, $[M+3H]^{+3}/3$ (calculated): 431.64, $[M+3H]^{+3}/3$ (observed): 431.67. Mass spectrometry of GAG-PA; $[M-H]^{-}$ (calculated): 1225.59, $[M-H]^{-}$ (observed):1224.61, $[M-2H]^{-2}/2$ (calculated): 612.29, $[M-2H]^{-2}/2$ (observed): 611.80, $[M-3H]^{-3}/3$ (calculated): 407.86, $[M-3H]^{-3}/3$ (observed): 407.53. Mass spectrometry of K-PA; $[2M+H]^{+}$ (calculated): 1307.96, $[2M+H]^{+}$ (observed): 1307.98, $[M+H]^{+}$ (calculated): 654.48, $[M+H]^{+}$ (observed):

654.50, $[M+2H]^{+2}/2$ (calculated): 327.74, $[M+2H]^{+2}/2$ (observed): 327.75. Mass spectrometry of E-PA; $[M-H]^{-}$ (calculated): 654.42, $[M-H]^{-}$ (observed): 654.42, $[M-2H]^{-2}/2$ (calculated): 326.71, $[M-2H]^{-2}/2$ (observed): 326.71.

3.2.3 Schwann Cell Isolation

Schwann cells were isolated from sciatic nerves of male Sprague-Dawley rats according to a previously published protocol [103]. Ten weeks old male Sprague-Dawley rats were used for Schwann cell isolation under the approval of Animal Ethics Committee of Gulhane Military Medical Academy. Briefly, 15 mm sciatic nerve segments were excised, teased and cut into 2-3 mm fragments after removing epineurium (Figure 3.3). Enzymatic dissociation in 0.05% collagenase was carried out at 37 °C for 60 min and tissue debris was removed by passing the suspension through a 40 μm cell strainer. Cells were cultured on PLL coated surfaces in DMEM-D-valine (4.5 mg/mL glucose) with 2 mM glutamine, 10% (v/v) fetal calf serum, 1% (v/v) N_2 supplement, 20 μg mL^{-1} bovine pituitary extract, 5 μM forskolin, 1% P/S, 0.25 μg mL^{-1} amphotericin B. Cells were observed at different time points (Figure 3.4) and used 19 days after isolation and within 9 passages.

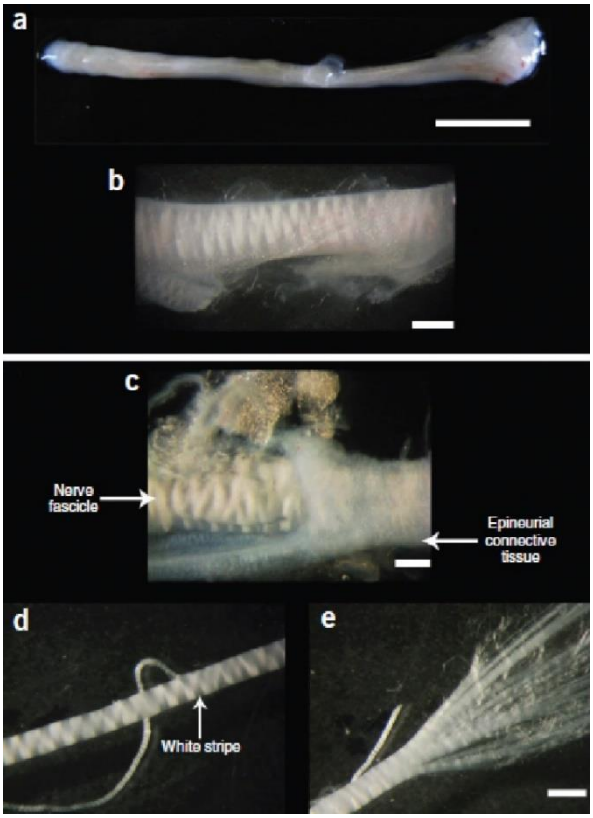

Figure 3. 3 Images of rat sciatic nerve (a), white stripes of nerve trunk under the epineurial connective tissue (b), stripped epineurial connective tissue and nerve fascicles (c), white stripes of nerve fascicle after the removal of connective tissue (d) and a number of nerve fibers after being teased (e). (Adapted from Ref. 103 with permission from Nature Publishing Group)

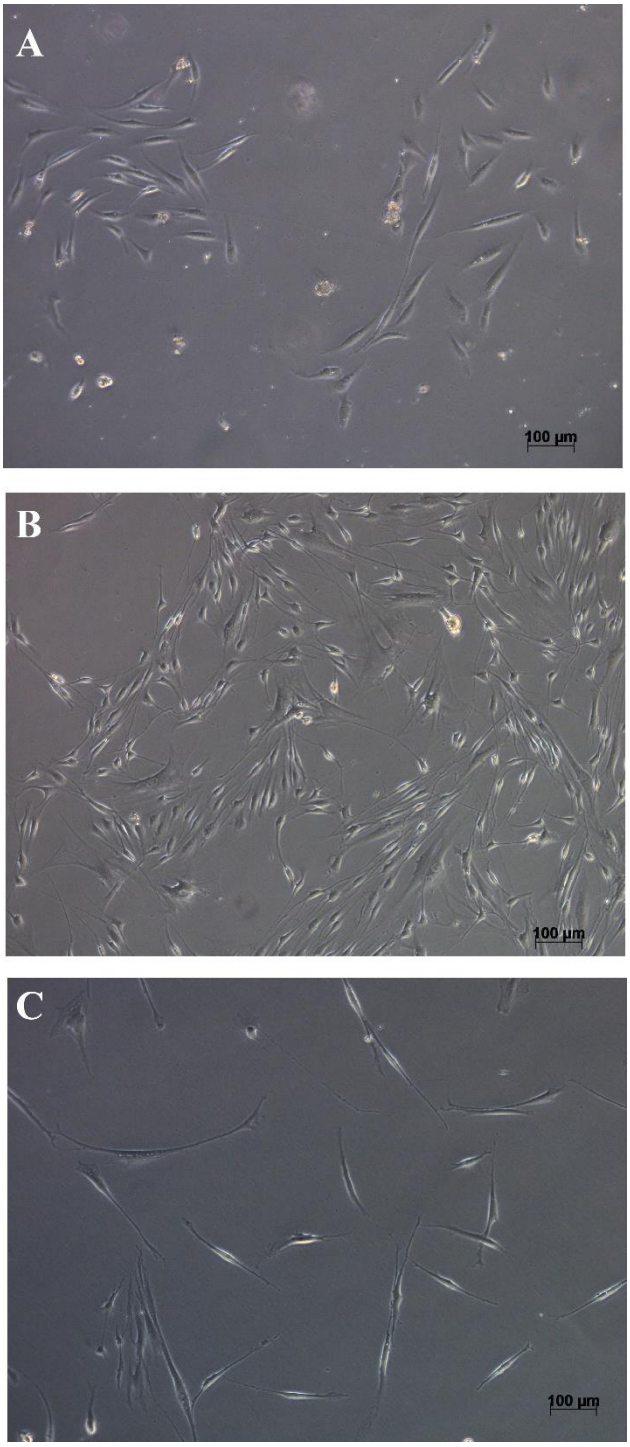

Figure 3. 4 Light microscopy images illustrating Schwann cell cultures at day 10 (A) and day 20 (B) and after the first passage (C).

3.2.4 Viability Assay

Equal volumes of 2 mM LN-PA and GAG-PA and appropriate concentrations of E-PA (1 mM) and K-PA (2 mM) were used to form gels with neutral charge in 96-well plates. After coating the plates with peptide nanofibers, the plates were incubated at 37 °C for 30 min. Then, they were placed into the laminar flow hood and incubated at room temperature overnight to evaporate the solvent. The plates coated with peptide nanofibers were treated with ultraviolet (UV) for sterilization before use. Since Schwann cells are not able to attach to TCP, PLL-coated surfaces were used as a control group for cell adhesion and growth. PLL coating was done on the day of the experiment, and the surface was dried for 2 h before cell seeding. Viability analysis was performed after 48 h of culture by calcein-AM and ethidium homodimer 1 (EthD-1) staining. Cells were cultured on PA nanofibers and PLL coated TCP at a density of 1×10^4 cells/well. After 48 h of incubation, cell medium was discarded; cells were washed with 1X PBS and incubated with 2 μM calcein-AM and 2 μM EthD-1 in PBS for 30 min at room temperature. Five random images were taken at 100× magnification from each well for both qualitative and quantitative analysis by using a fluorescence microscope. Cells were counted from images obtained with NIH ImageJ software.

3.2.5 SEM imaging of Schwann cells on PA nanofiber and PLL coated surfaces

The morphology and spreading of Schwann cells were examined by SEM imaging 13 mm glass coverslips placed in 24-well plates were coated with PA nanofibers and PLL solutions as described above. Cells were seeded on top of the coated surfaces at a density of 2.5×10^4 cells/well. After 48 h of incubation, cells were rinsed with PBS and fixed with 2% gluteraldehyde/PBS and 1 wt% OsO_4 for 1 h each, respectively. Fixed cells were washed with water and dehydrated sequentially in 20%, 40%, 60%,

80%, and 100% ethanol. Samples were critical point dried with Autosamdri-815B (Tousimis). Dried samples were coated with 6 nm Au/Pd and SEM (FEI Quanta 200 FEG) images were taken by using an ETD detector at high vacuum mode with 15 keV beam energy.

3.2.6 Immunocytochemistry

13 mm glass coverslips placed in 24-well plates were coated with PA nanofibers and PLL as described above. Schwann cells were seeded on top of the coated surfaces at a density of 2.5×10^4 cells/well. After 48 h of incubation, cells were fixed with 4% paraformaldehyde in PBS for 15 min at room temperature and treated with 0.3% Triton X/PBS (PBS-Tx 0.3%) for 15 min. After washing with PBS, blocking was carried out with 10% goat serum and 1% bovine serum albumin (BSA) in PBS with 0.3% Triton-X for 30 min. Cells were then treated with primary antibody against S100 (Millipore, 04-1054) at 1:100 dilution and incubated overnight at 4 °C. After washing with PBS several times, cells were incubated with goat anti-rabbit IgG H&L (DyLight® 488) preadsorbed (Abcam, ab96899) secondary antibody for 1 h at room temperature and they were washed with PBS several times. Coverslips were then mounted with Prolong Gold Antifade Reagent (Invitrogen) and sealed with nail polish. Samples were imaged with confocal microscopy (Zeiss LSM510).

3.2.7 Analysis of NGF secretion by Schwann cells

MaxiSorp plates for ELISA were coated with primary antibody specific to NGF. 1:125 antibody dilution was performed with assay buffer. After coating with primary antibody, plates were incubated overnight at 4 °C. Solutions were discarded next day and the wells were washed with washing buffer (Tween 20 in 0.9% (w/v) NaCl solution). After drying by tapping, blocking was carried out with 1X assay buffer for

2 h. Blocking was followed by addition of NGF (500 ng/mL) and culture medium to compare the NGF release from Schwann cells seeded on PA nanofiber and PLL coated surfaces after 48 h. The plate was incubated overnight at 4 °C. The next day, solutions were removed and the wells were washed with washing buffer 5 times. After drying by tapping, biotinylated antibody against NGF (1:500 dilution) was added and incubated for 2 h. After incubation, the wells were washed with washing buffer 5 times and dried by tapping. Streptavidin-linked HRP was added and incubated for 1 h. Then, solutions were removed and the wells were washed with washing buffer 5 times. After drying, 3, 3', 5, 5' tetramethylbenzidine was added and incubated until obtaining a bright blue color. The reaction was stopped with stop solution, and absorbances were measured by using a Spectramax M5 microplate reader at 450 nm wavelength. This value was subtracted from the reference value (650 nm).

3.2.8 Statistical Analysis

Statistical analyses were performed using one-way ANOVA with Bonferonni multiple comparison test. p-value of less than 0.05 was considered statistically significant. (*$p < 0.05$; **$p < 0.01$; ***$p < 0.001$). Error bars indicate sem.

3.3 Results and Discussion

3.3.1 Cell Behavior and Viability of Schwann Cells on Peptide Nanofibers

Since Schwann cells are crucial for peripheral neural regeneration, viability of Schwann cells cultured on peptide nanofibers or PLL coated surfaces was assessed by calcein-AM and ethidium homodimer staining after 48 h of culture. Cell viability was comparable on both surfaces, with no statistically significant difference. This indicates that peptide nanofibers are biocompatible with these cells (Figure 3.5).

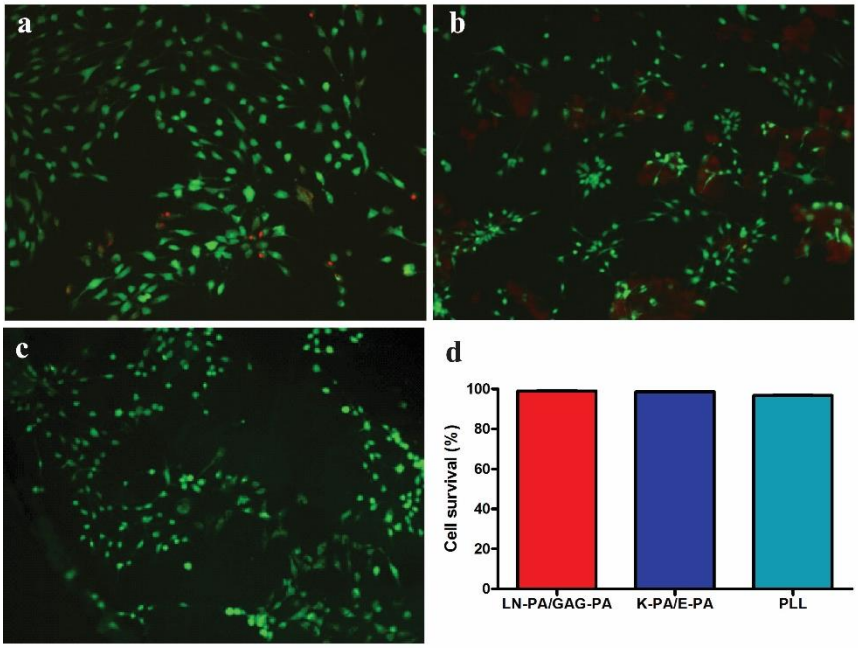

Figure 3. 5 Viability of Schwann cells on PLL coated surface (a), K-PA/E-PA scaffold (b) and LN-PA/GAG-PA scaffold (c) analyzed by live–dead assay after 48 h of incubation. Relative cell viability (d) showed that Schwann cells adapted to PA scaffolds and have comparable viability with PLL-coated surface at the end of 48 h. Scale bars are 100 μm.

Interaction of Schwann cells with the surrounding microenvironment was assessed by SEM imaging (Figure 3.6). SEM images revealed that Schwann cells on LN-PA/GAG-PA scaffold displayed a characteristic morphology that is different from that of the cells cultured on control peptide nanofibers and PLL coated surfaces. Cells spread better on the bioactive scaffold and interaction between cells was also at a higher level compared with control groups.

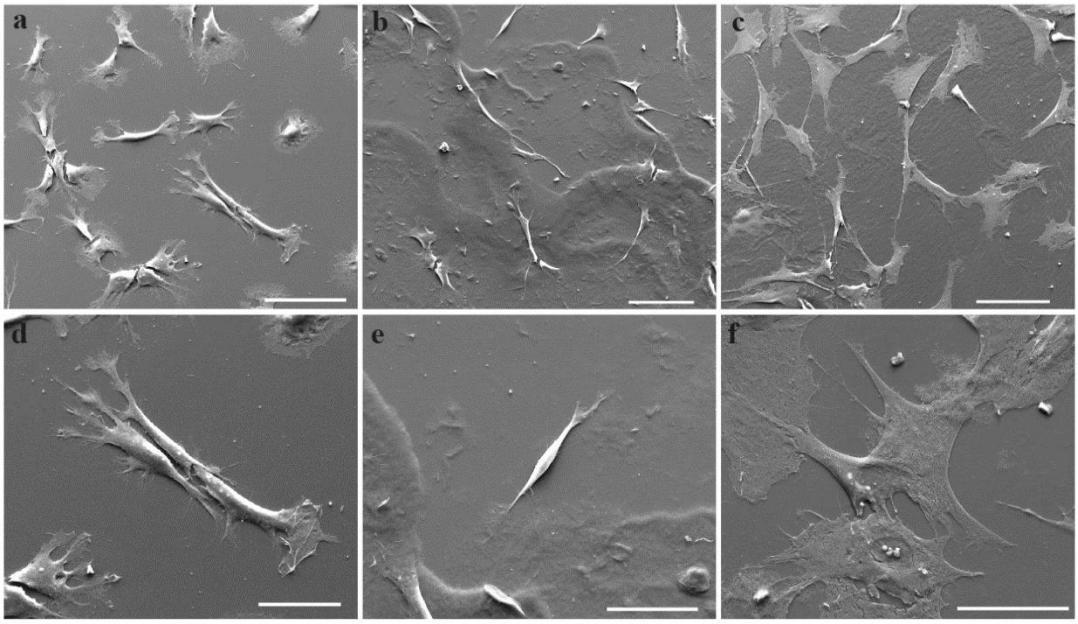

Figure 3. 6 PA substrates are biocompatible and support adhesion of Schwann cells. SEM images of Schwann cells cultured on PLL (a,d), K-PA/E-PA (b,e) and LN-PA/GAG-PA (c,f) gels. Scale bars are 100 μm (a, b, c) and 50 μm (d, e, f).

The effect of PA nanofibers on cells was further analyzed through immunofluorescence staining against S100 protein (Figure 3.7). Confocal images also showed that bioactive nanofibers (LN-PA/GAG-PA) induced more interactions between cells and cells adhered firmly onto the scaffold.

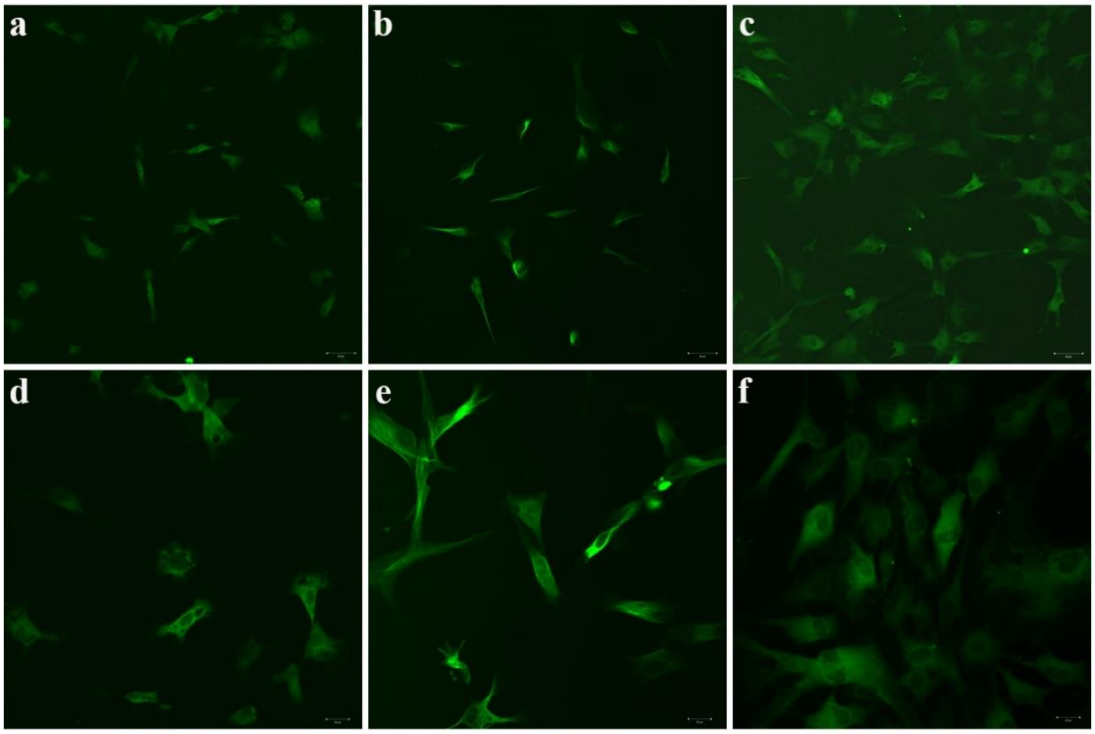

Figure 3. 7 Immunostaining against S100. Schwann cells cultured on cultured on PLL (a,d), K-PA/E-PA (b,e) and LN-PA/GAG-PA (c,f) gels. Confocal images were obtained after 48 h of incubation. Images were taken at 200x (a, b, c) and 400x (d, e, f) magnification.

3.3.2 NGF Secretion from Schwann Cells on Peptide Nanofibers

NGF plays a crucial role in nerve injury repair. NGF was also found to prevent cell loss, protect neurons after sciatic nerve transection [104] and increase the number of myelinated axons in the regenerating nerve [105]. To increase the local concentration of NGF at the injury site, NGF solution might be delivered to the injury site, but this is not feasible due to rapid diffusion in extracellular fluids. In addition, sustained delivery of NGF is not favorable in terms of cost and surgical risks. Instead, induction of NGF release from Schwann cells at the injury site would be more effective. In order to analyze the effect of peptide nanofibers on functionality of Schwann cells, ELISA

test was performed to determine the extracellular accumulation of NGF released by Schwann cells incubated on peptide nanofibers and PLL coated surfaces for 48 h. The NGF level secreted by Schwann cells was increased in the LN-PA/GAG-PA group by almost 2.0-fold compared to both K-PA/E-PA and PLL coated surfaces (Figure 3.8). The results showed that bioactive LN-PA/GAG-PA scaffold promotes secretion of NGF compared to the control surfaces. Thus, LN-PA/GAG-PA scaffold can provide a prolonged delivery of NGF and enhance the efficacy of nerve regeneration, which makes this scaffold a promising approach for peripheral nerve injury treatments.

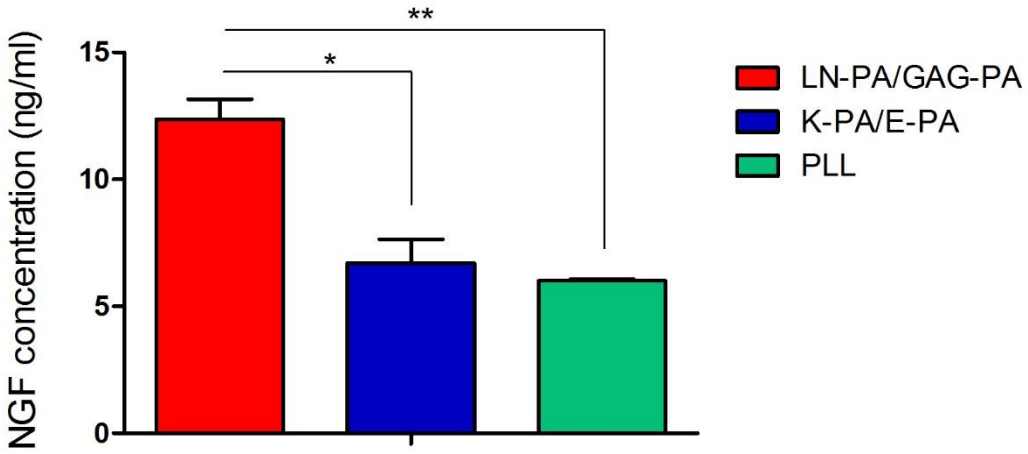

Figure 3. 8 NGF concentration in culture medium of Schwann cells cultured on LN-PA/GAG-PA, K-PA/E-PA and PLL coated surfaces after 48 h of incubation. Values represent mean ± sem (**$p < 0.01$, *$p < 0.05$).

3.4 Conclusion

Guidance cues for regenerating axons to provide healthy pathfinding is crucial in peripheral nerve regeneration studies, especially if there is a full transection. Transected nerves spanning large gaps between the proximal and distal ends of the axons display poor regeneration due to the lack of guidance cues. This usually leads

to loss of function after injury. Although Schwann cell-based therapies seem to be efficient and promising treatment options for peripheral nerve injuries, technical difficulties such as the time required for harvesting and culture of Schwann cells, immunological problems and morbidity may limit the efficacy of this approach. Therefore, supporting the viability of Schwann cells and inducing more neurotrophic factor release from these cells may be an alternative strategy for regeneration studies. In this study, we used peptide nanofibers mimicking the healthy ECM around neural cells and tested the effects of these bioactive peptide nanofibers on Schwann cells *in vitro*. These bioactive peptide nanofibers demonstrated increase in viability of Schwann cells, and they were also found to stimulate NGF release from Schwann cells significantly. As a result, these findings propose an alternative choice for the treatment of nerve injuries in peripheral nerve system.

Chapter 4

4. Tenascin-C Derived Signaling for Neural Differentiation in Three-Dimensional Nanofiber System

4.1 Introduction

Neural tissue engineering is a promising research field in regenerative medicine and aims to enhance the nerve regeneration process by understanding and mimicking the natural environment of neural cells through the use of bioactive scaffolds. The physical parameters of scaffolds are important in this context, as materials to be used in tissue engineering efforts must be able to support cells and allow the diffusion of oxygen, nutrients and growth factors. Physical properties of the microenvironment is one of the most important aspects of regenerative materials, and should be considered along with chemical and biological properties of the system when designing biomaterials for tissue engineering applications [106]. For *in vitro* studies, two-dimensional (2D) cell culture techniques are commonly used to study cell function and behavior, including cell attachment, proliferation, migration and differentiation, before the *in vivo* evaluation of regenerative potential. However, while it is easy to control and manipulate the environment in 2D cell cultures, they are less compatible with *in vivo* systems and fail to mimic the native three-dimensional (3D) tissues. In contrast, 3D cultures are more accurate in representing the *in vivo* architecture of tissue environments, since the cells within 3D culture systems can interact with each other in all dimensions [107].

Bioactive nanomaterials are particularly promising for the induction of neural differentiation and regeneration of nervous tissue, as they are able to provide

biological, chemical and physical guidance to cells [108, 109]. ECM is the non-cellular material that surrounds cells in tissue microenvironments and contains a wide range of proteins, proteoglycans, polysaccharides and signaling molecules, as well as water. Besides providing physical support to cells, ECM is fundamental in mediating the biochemical and biomechanical signaling mechanisms that occur between cells [9]. The development of bioactive materials that emulate the ECM of cells can therefore allow the precise manipulation of cellular behavior. Several short peptide sequences derived from ECM proteins have been used for neural cultures and were demonstrated to induce neural differentiation. Among these, the laminin-derived Ile-Lys-Val-Ala-Val (IKVAV) and Tyr-Ile-Gly-Ser-Arg (YIGSR), and the fibronectin-derived Arg-Gly-Asp (RGD) are the most commonly used sequences to promote neural cell adhesion, migration and differentiation [25, 26, 78]. Biomaterials functionalized with these sequences were previously shown to be effective in promoting neural adhesion, proliferation and/or differentiation in *in vitro* studies [23, 29, 110-112]. TN-C is a multifunctional ECM glycoprotein that affects cell migration and neurite outgrowth when introduced into neuronal cell cultures *in vitro* [113, 114]. It is expressed during the development of CNS by glial cells and some neurons [115]. TN-C was also shown to be involved in motor axon outgrowth [116] and plays a role in spinal cord regeneration [117]. Meiners *et al*. showed that TN-C contains an eight-amino acid domain (VFDNFVLK) crucial for neurite extension [118], and self-assembled scaffolds containing this sequence were recently shown to induce neurite outgrowth and migration in neural progenitor cells [24], as well as to promote osteogenic differentiation in MSCs [119].

In this study, we investigated the stimulation of neural differentiation by a 3D PA nanofiber gel functionalized with a TN-C derived epitope (VFDNFVLK) and explored the influence of culture microenvironment on this signal. The 3D cell culture system was found to provide both the biochemical and physical aspects of the native environment of neural cells, thereby filling the gap between 2D cell culture models and *in vivo* environments. Overall, we showed that 3D TN-C mimetic self-assembling nanofibers induced 3D neurite outgrowth and significantly increased the expressions of neural markers compared to 2D nanofiber and 3D epitope-free gel controls. This study features the cooperative effect of culture dimensionality and bioactive signals for the induction of neural differentiation, which is critical for the design of neuroregenerative scaffolds.

4.2 Experimental Section

4.2.1 Materials

All protected amino acids, lauric acid, 4-(2′,4′-dimethoxyphenyl-Fmoc-aminomethyl)-phenoxyacetamido-norleucyl-MBHA resin (Rink amide MBHA resin), HBTU, and DIEA were purchased from Nova-Biochem, ABCR, or Sigma-Aldrich. Cell culture materials were purchased from Invitrogen. All other chemicals and materials used in this study were purchased from Thermo Scientific or Sigma-Aldrich.

4.2.2 Synthesis and Characterization of PA Molecules

PA molecules were synthesized on Rink Amide MBHA resin by using Fmoc-protected solid phase peptide synthesis method. Amino acid couplings were performed with 2 equivalents of amino acids, which were activated with 1.95 equivalents of HBTU and 3 equivalents of DIEA for 2 h. Fmoc removal was performed with 20% piperidine–DMF solution for 20 min. 10% acetic anhydride–DMF solution was used to

permanently acetylate the unreacted amine groups after each coupling step. DMF and DCM were used as washing solvents after each step. Cleavage of the PAs and protection groups from the resin was carried out with a mixture of TFA:TIS:H_2O in the ratio of 95:2.5:2.5 for 3 h. Excess TFA removal was carried out by rotary evaporation. PAs in the remaining solution were precipitated in ice-cold diethyl ether overnight. The precipitate was collected by centrifugation next day and dissolved in ultrapure water. This solution was frozen at -80 °C for 4 h and then lyophilized for 4-5 days. PAs were characterized by LC–MS. Mass spectra were obtained with an Agilent LC-MS equipped with an Agilent 6530 Q-TOF with an ESI source, using a Zorbax Extend-C18 2.1x50 mm column for basic conditions and a Zorbax SB-C8 4.6x100 mm column for acidic conditions. A gradient of water (0.1% formic acid or 0.1% NH_4OH) and acetonitrile (0.1% formic acid or 0.1% NH_4OH) was used for elution. In order to remove residual TFA, positively-charged PAs were treated with 0.1 M HCl solution and lyophilized. To purify the peptides, an Agilent preparative reverse-phase HPLC system equipped with a Zorbax Extend-C18 21.2x150 mm column was used for basic conditions, and a Zorbax SB-C8 21.2x150 mm column was used for acidic conditions. A gradient of water (0.1% TFA or 0.1% NH_4OH) and acetonitrile (0.1% TFA or 0.1% NH_4OH) was used for elution. All peptide batches were freeze-dried and reconstituted in ultrapure water at pH 7.4 before use.

4.2.3 SEM Imaging of PA Nanofibers

PA nanofiber networks were observed by SEM imaging. Oppositely charged PA solutions were mixed in equal volumes with a final volume of 30 μL to produce gels with neutral charges (12 mM TC-PA solution was mixed with 6 mM EE-PA solution, or 10 mM KK-PA solution was mixed with 10 mM EE-PA solution). Gels were formed

on silicon wafer and dehydrated by sequential transfer to 20%, 40%, 60%, 80% and 100% v/v ethanol. Dehydrated gels were critical point-dried using a Tousimis Autosamdri 815B system. Dried PA gels were coated with 4 nm Au/Pd and SEM (FEI Quanta 200 FEG) images were taken using an ETD at high vacuum mode and 5 keV beam energy.

4.2.4 Secondary Structure Analysis

A JASCO J815 CD spectrometer was used at room temperature for CD measurements. Oppositely charged 2.5 x 10^{-4} M PA solutions were mixed at appropriate volume ratios to a final volume of 300 μL (200 μL TC-PA solution was mixed with 100 μL EE-PA solution, or 150 μL KK-PA solution was mixed with 150 μL EE-PA solution) to produce nanofibers with net neutral charge. Measurements were carried out from 300 nm to 190 nm; data interval and data pitch were 0.1 nm, and scanning speed was 100 nm min^{-1}. All measurements were performed with three accumulations. DIT was selected as 1 s, band width as 1 nm, and the sensitivity was standard.

4.2.5 Oscillatory Rheology

Oscillatory rheology measurements were performed with an Anton Paar Physica RM301 Rheometer operating with a 25 mm parallel plate configuration at 25 °C. Oppositely charged PA solutions with different concentrations were tested in order to optimize the stiffness of hydrogels according to the elastic properties of brain tissue. Different concentrations of each PA component, chosen to obtain neutral charges at a final volume of 250 μL, were carefully loaded onto the center of the lower plate and incubated for 10 min for gelation before measurement. After equilibration, the upper plate was lowered to a gap distance of 0.5 mm. Storage moduli (G′) and loss moduli

(G″) values were scanned from 100 rad s^{-1} to 0.1 rad s^{-1} of angular frequency, with a 0.5% shear strain. Three samples were measured for each PA gel.

4.2.6 Cell Culture and Maintenance

PC-12 cells were used in all cell culture experiments. Cells were cultured in 25 cm^2 flasks at 37 °C in a humidified incubator and supplied with 5% CO_2. PC-12 cells were maintained in Roswell Park Memorial Institute medium (RPMI) with 10% horse serum (HS), 5% FBS, 2 mM L-Glutamine and 1% P/S. The culture medium was changed every 3 days.

4.2.7 3D Cell Cultures

For 3D gel formation, positively charged PA dissolved in 30 µL of 0.25 M sucrose and negatively charged PA dissolved in 30 µL of culture medium were placed into the wells to form the base layer (12 mM TC-PA solution was mixed with 6 mM EE-PA solution, or 10 mM KK-PA solution was mixed with 10 mM EE-PA solution). This gel was stabilized in a 37 °C incubator for 1 h. Then, positively charged PA solution was placed onto this layer, and negatively charged PA solution containing PC-12 cells ($5x10^5$ cells/well) was added slowly with spiral motions. Gels were then placed into the incubator for 1 h for further stabilization (Figure 4.1). After 1 h, medium was added to each well. The day after gel formation, differentiation was induced with 20 ng/mL NGF treatment for induction groups. The experiment was finished after 7 days of induction.

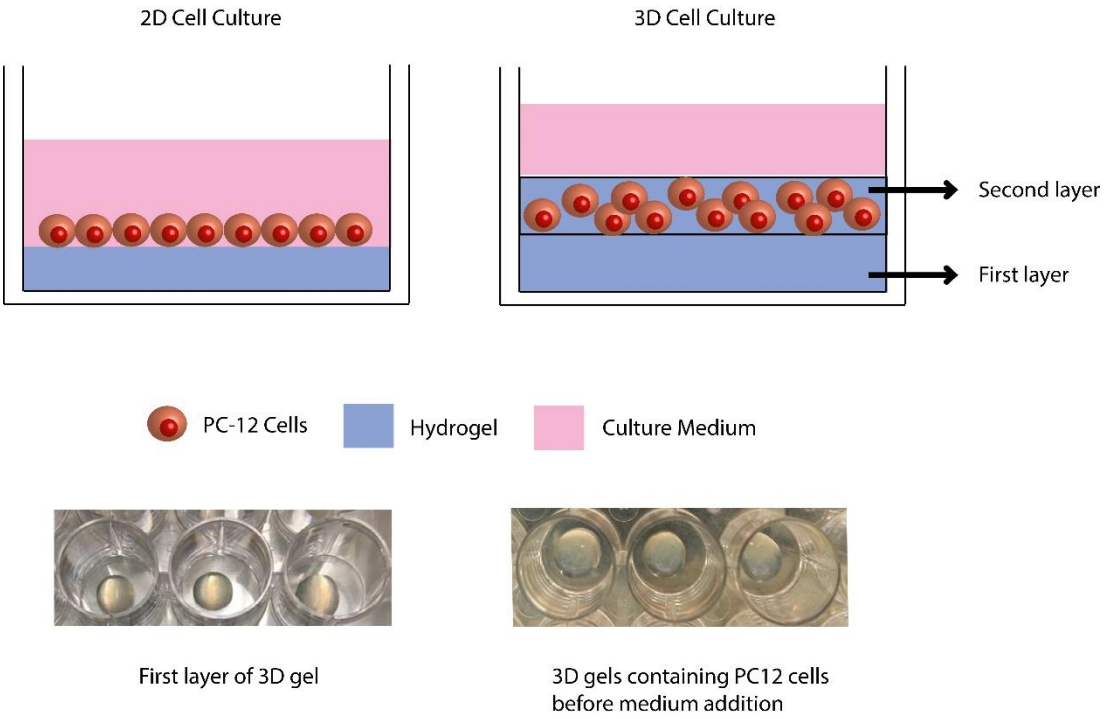

Figure 4. 1 *In vitro* experimental design.

Table 4. 1 Experimental Groups

3D		2D	
+NGF	**-NGF**	**+NGF**	**-NGF**
TC-PA/EE-PA (12 mM/6 mM)	TC-PA/EE-PA (12 mM/6 mM)	TC-PA/EE-PA (4 mM/2 mM)	TC-PA/EE-PA (4 mM/2 mM)
KK-PA/EE-PA (10 mM/10 mM)	KK-PA/EE-PA (10 mM/10 mM)	KK-PA/EE-PA (3 mM/3 mM)	KK-PA/EE-PA (3 mM/3 mM)

4.2.8 Flow Cytometry Analysis of Viability

Viability of PC-12 cells seeded on 2D or within 3D PA nanofibers was measured using the Annexin V-FITC Apoptosis Detection kit. After 24 h and 48 h of incubation, flow cytometry protocol for Annexin V and propidium iodide was performed according to

the manufacturer's instructions. Briefly; medium was discarded, cells were washed with cold PBS and resuspended in 100 µL of 1X annexin-binding buffer, 5 µL Alexa Fluor® 488 Annexin V and 1 µL of 100 µg/mL propidium iodide were added to each well. Cells were incubated at room temperature for 15 min and analyzed by flow cytometry, measuring the fluorescence emission at 530 nm (FL1 channel) and >575 nm (FL3 channel).

4.2.9 PC-12 Neurite Extension Assay

Equal volumes of 4 mM TC-PA and 2 mM EE-PA were used to form gels with neutral charges in 6-well plates, while equal volumes of 3 mM KK-PA and EE-PA were mixed to form the epitope-free control PA group. PA-coated plates were incubated at 37 °C for 30 min prior to overnight incubation in laminar flow hood at room temperature for solvent evaporation. The next day, PA matrices formed on 6-well plates were UV sterilized, and PC-12 cells (1.5×10^5 cells/well) were cultured on these matrices. Following the addition of cells in culture media to PA-coated surfaces, the PA matrix was rehydrated and formed a thin gel adhered to the plate surface. RPMI with 10% HS, 5% FBS, 2 mM L-Glutamine and 1% P/S was used as culture medium. The day after seeding cells, media were changed with neural induction medium consisting of minimum essential medium (MEM) with 2% HS, 1% FBS, 2 mM L-Glutamine, 1% P/S and 20 ng mL^{-1} NGF. At the end of 7 days of NGF induction, six random images of the cells from each well were obtained under light microscope at 200× magnification. Image J program was used in order to quantify the neurite length of the cells, and total neurite length was normalized using cell number/image. Also, neurite bearing cells were counted by using Image J, and percentage of neurite bearing cells

was calculated for further analysis of potential of peptide nanofibers in neurite extension.

4.2.10 SEM Imaging of PC-12 Cells on 2D or within 3D PA Nanofibers

The morphology and neurite extension pattern of PC-12 cells were examined by SEM imaging using an ETD detector at high vacuum mode at 5 keV beam energy. Seven days after incubation of PC-12 cells on 2D or within 3D PA nanofibers, cells were rinsed with PBS and fixed with 2% gluteraldehyde/PBS and 1 wt% OsO_4 for 1 h each. Fixed cells were washed with water, and then dehydrated sequentially in 20%, 40%, 60%, 80%, and 100% ethanol. Samples were critical point-dried with a Tousimis Autosamdri-815B system and coated with 6 nm Au−Pd before imaging.

4.2.11 Gene Expression Analysis

Gene expression profiles were assessed by quantitative RT-PCR analysis. Seven days after incubation of PC-12 cells on 2D or within 3D PA nanofibers, RNA isolation was performed with TRIzol (Invitrogen) reagent by considering the instructions of the manufacturer. After RNA extraction, amount and purity of the RNA samples were verified with Nanodrop 2000 (Thermo Scientific). Primer sequences to be used in qRT-PCR were designed with NCBI database. SuperScript III Platinum SYBR Green one-step qRT-PCR kit was used for qRT-PCR analysis with instructions of the manufacturer. Reaction conditions were briefly as follows: 55 °C for 5 min, 95 °C for 5 min, 40 cycles of 95 °C for 15 s, X °C for 30 s (varies according to primer sets), and 40 °C for 1 min, followed by a melting curve analysis to confirm product specificity. The reaction efficiencies for each primer set were evaluated by plotting a standard curve using 5-fold serial dilutions of total RNA. For analysis of the expression data, primary gene expression data were normalized by the expression level of

glyceraldehyde 3-phosphate dehydrogenase (GAPDH). A comparative Ct method (Pfaffl method) was used to analyze results.

Table 4. 2 Primers Used for qRT-PCR Expression Analysis

Gene	**Primer Sequence (Forward/Reverse)**	**Product size (bp)**
Neural Markers		
β-III-Tubulin	CCTGCCTCTTCGTCTCTAGC AACTTGGCCCCTATCTGGTT	222
Synaptophysin I (SYN1)	CCAGCTCAACAAATCCCAGT TGGTCTCAGCTTTCACCTCA	307
Reference Gene		
GAPDH	GTGCCAGCCTCGTCTCATA AACTTGCCGTGGGTAGAGTC	186

4.2.12 Western Blot Analysis

Total protein content of PC-12 cells cultured in different conditions (2D or 3D culture, in the presence or absence of NGF) was isolated using TRIzol (Invitrogen) according to the manufacturer's instructions. Protein concentrations were determined using a BCA Protein Assay Kit (Thermo Scientific). Equal amounts of proteins (50 μg, 15 μL) were separated on 12% SDS-PAGE gels under denaturing and nonreducing conditions and then transferred to a PVDF membrane. The membrane was blocked with 5% nonfat milk in TBST at room temperature for 1 h and then incubated with βIII tubulin antibody (Abcam, ab78078, 1:1000), synaptophysin (Abcam, ab32127, 1:10000), ERK 1/2 (Abcam, ab130004, 1:1000) and pERK (Abcam, ab50011, 1:1000) at 4 °C overnight. After washing in TBST, the blots were incubated with a HRP-conjugated

secondary antibody (Millipore, 12−349 Goat Anti Mouse IgG, 1:1000 or Abcam, ab6721 Goat Anti-Rabbit IgG 1:2000). Signals were visualized using a chemiluminescent signal enhancement system (Invitrogen, Novex ECL). GAPDH was used as the internal control and treated with the same protocol (Millipore, MAB374, 1:1000). Gels were visualized by enhanced chemiluminescence (Bio-Rad) according to the manufacturer's protocol on a Bio-Rad ChemiDoc™ Imaging System with Image Lab™ Software, and protein concentrations in gel slabs were quantified using ImageJ. Intensities of the bands were normalized by GAPDH.

4.2.13 Statistical Analysis

All quantitative values are presented as mean ± sem, and all the groups in experiments were performed with at least three replicates. One-way ANOVA was used for statistical analysis, and p-values less than 0.05 were considered statistically significant.

4.3 Results and Discussion

4.3.1 Design and Characterization of Peptide Nanofibers

Three-dimensional (3D) biomimetic nanofiber scaffolds have been used in biomedical tissue engineering due to their nanoscale architecture that is similar to the native ECM. These scaffolds are crucial for cellular organization and intercellular communication for regenerative purposes. However, use of any such scaffold in the closed microenvironment of nerve tissue presents a critical challenge. Therefore, it is important to consider the required parameters carefully while designing a material for neural differentiation. In this work, we developed a 3D self-assembled nanofiber gel carrying a bioactive epitope derived from the natural ECM protein TN-C (lauryl-VFDNFVLKK-Am, TC-PA) and utilized it in order to fill the gap between 2D cell culture systems and *in vivo* tissue architectures. The potential of the TN-C mimetic

peptide nanofiber system for promoting neurite outgrowth was also studied. The control PAs, negatively charged EE-PA (lauryl-VVAGEE-Am) and positively charged KK-PA (lauryl-VVAGK-Am), lacked this epitope (Figure 4.2). All PA molecules were synthesized by solid phase peptide synthesis, purified by preparative HPLC and characterized by LC−MS before use (Figure 4.3). Two nanofiber gels were used in this study: TC-PA/EE-PA gel contained TN-C derived bioactive epitopes while the KK-PA/EE-PA gel was used as an epitope-free negative control. When positively charged PA molecules were mixed with negatively charged PA molecules, they formed ECM-mimetic nanofibers through self-assembly mediated by β-sheet driving motifs and electrostatic and hydrophobic interactions [120].

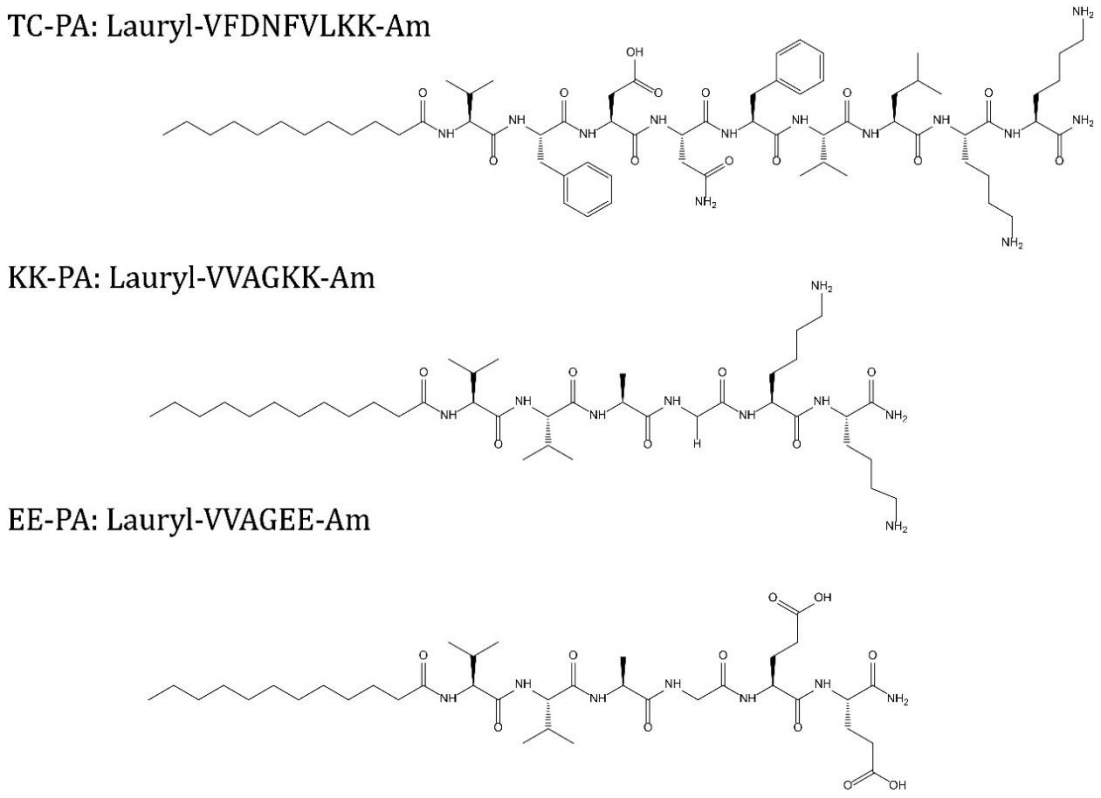

Figure 4. 2 Chemical structures of PA molecules.

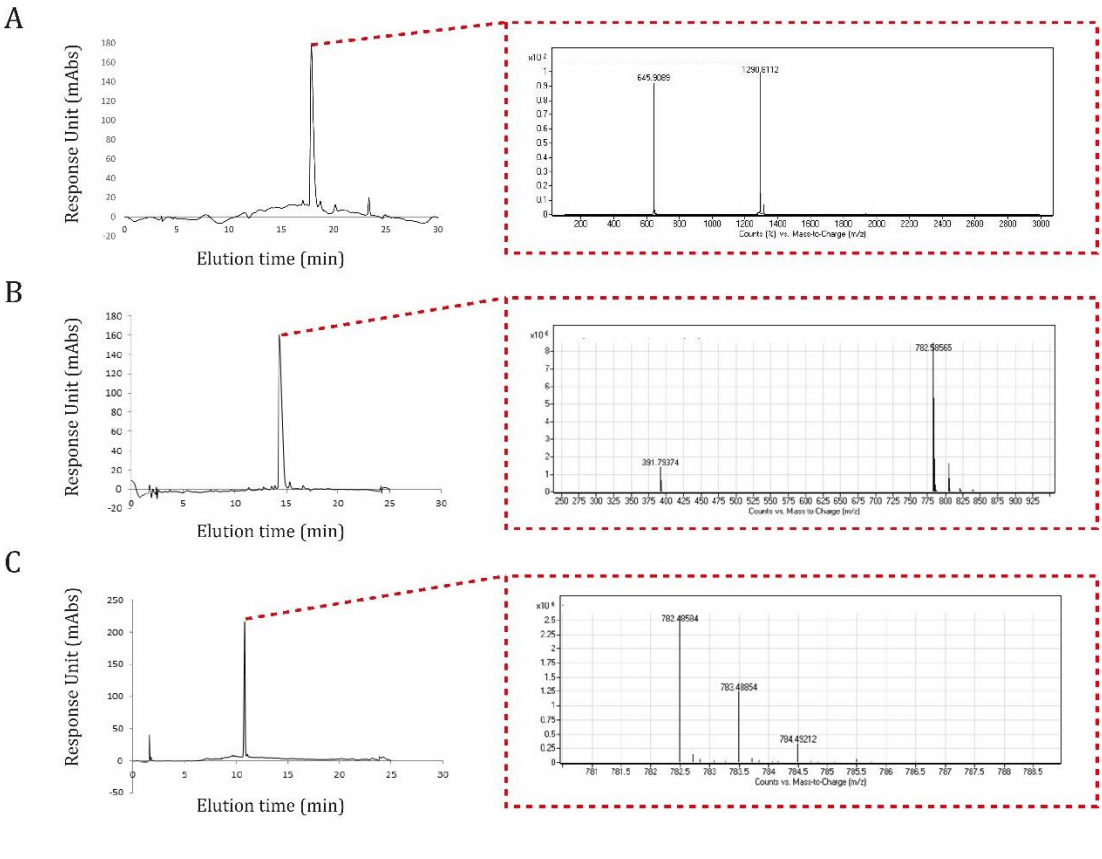

Figure 4. 3 LC-MS of TC-PA (A), KK-PA (B) and EE-PA (C). Mass spectrometry of TC-PA (A) $[M+H]^{+}$ (calculated): 1290.81, $[M+H]^{+}$ (observed): 1290.81, $[M+2H]^{+2}/2$ (calculated): 645.91, $[M+2H]^{+2}/2$ (observed): 645.91. Mass spectrometry of KK-PA (B); $[M+H]^{+}$ (calculated): 782.58, $[M+H]^{+}$ (observed): 782.59, $[M+2H]^{+2}/2$ (calculated): 391.79, $[M+2H]^{+2}/2$ (observed): 391.79. Mass spectrometry of EE-PA (C); $[M-H]^{-}$ (calculated): 782.47, $[M-H]^{-}$ (observed): 782.48.

SEM images revealed the nanofibrous and porous structure of peptide nanofiber gels, which resemble the networks formed by the natural ECM of cells at physiological pH (Figure 4.4). The secondary structures of the nanofibers were characterized with CD spectroscopy. Upon mixing negative and positively charged PA molecules, both bioactive and control nanofiber systems demonstrated predominantly β-sheet structure

with a chiral absorbance maximum at around 200 nm and minimum at around 220 nm (Figure 4.5).

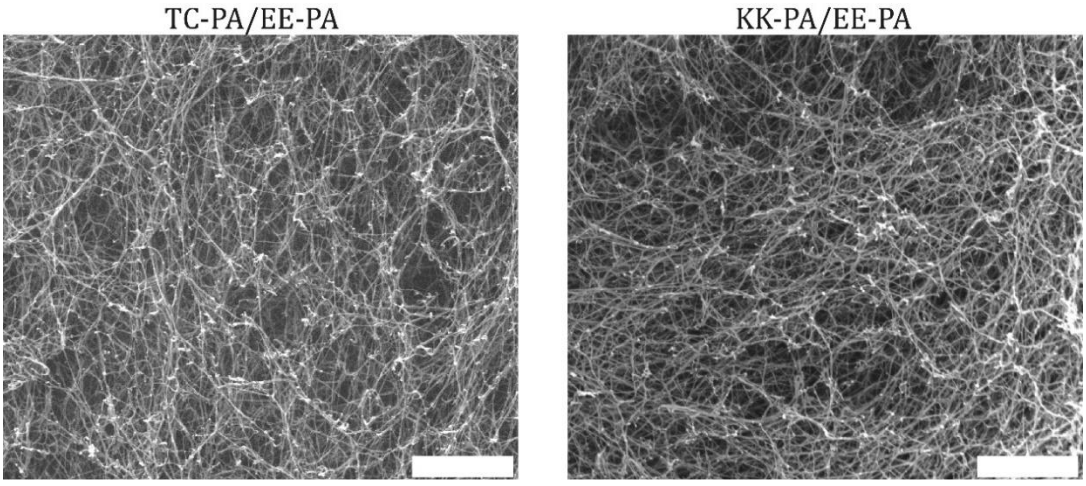

Figure 4. 4 SEM images of TC-PA/EE-PA and KK-PA/EE-PA, scale bars: 1μm.

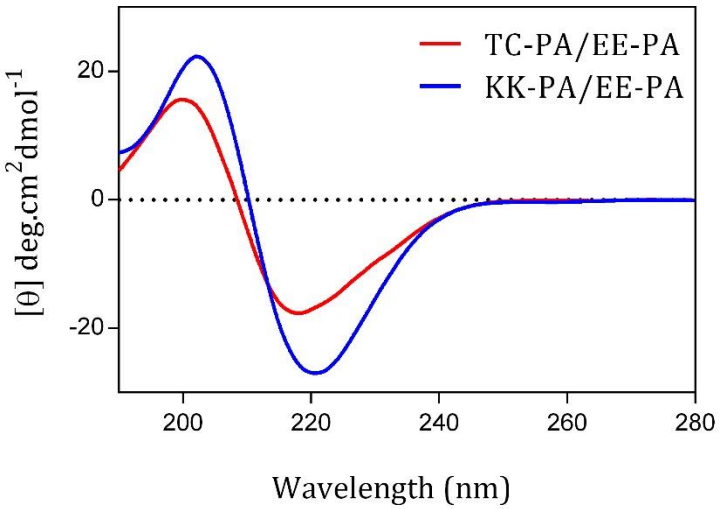

Figure 4. 5 CD spectra of TC-PA/EE-PA and KK-PA/EE-PA nanofibers.

Physical characteristics of the matrix are known to serve as potent cues for determining cell fates. When designing an artificial scaffold for neural cell culture, the mechanical

properties of the scaffold should be optimized to resemble these of brain tissue, which has an elastic modulus of about 1 kPa [35]. Different concentrations of PA solutions were used to form neutral gels with mechanical properties close to the nervous system. Using frequency sweep rheology measurements at constant strain, we performed oscillatory rheology analyses to assess the mechanical properties of peptide nanofiber gels. 12 mM TC-PA solution and 6 mM EE-PA solution (for the TC-PA/EE-PA combination) or 10 mM KK-PA solution and 10 mM EE-PA solution (for the KK-PA/EE-PA combination) were used to form nanofiber gels with neutral charge at physiological pH. Both gel systems had higher storage moduli (G′) than loss moduli (G″), which indicates the gel-like structure of the system with approximately 1 kPa storage modulus at physiological pH (Figure 4.6).

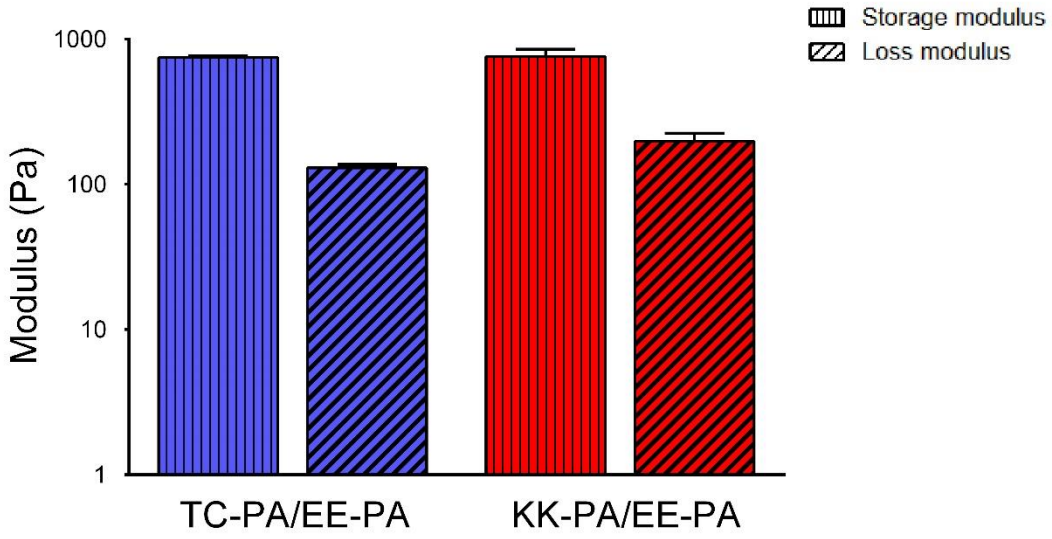

Figure 4. 6 Equilibrium storage and loss modulus of TC-PA/EE-PA and KK-PA/EE-PA in water.

4.3.2 Effect of TN-C Mimetic Peptide Nanofibers on Cell Viability

The cytotoxicity of regenerative materials under both *in vitro* and *in vivo* conditions is an important parameter that will determine their potential in clinical applications. Biomaterials used in tissue engineering applications should ideally not cause any toxic products or lead to any adverse reactions, which can be evaluated through *in vitro* cytotoxicity tests. In this study, cellular viability of PC-12 cells seeded on 2D or within 3D TN-C mimetic peptide nanofibers was assessed by flow cytometry analysis, by comparison to cells that were cultured on 2D or within 3D epitope-free peptide nanofibers at varying time points (24 h and 48 h). Annexin V and propidium iodide were used to evaluate cellular survival, with the Annexin V^-/propidium $iodide^-$ population being considered as healthy cells, the Annexin V^+/propidium $iodide^-$ population as cells under early stages of apoptosis, and the Annexin V^+/propidium $iodide^+$ population as cells in late apoptosis. After 24 h and 48 h of incubation, results showed that the percentages of live cells in all conditions were comparable with each other with no significant differences (Figure 4.7). It is important to emphasize that the 3D scaffolds had the appropriate stiffness and porosity to support cell viability without diffusional transport limitations, which can limit the transfer of O_2 and other essential nutrients and cause the accumulation of toxic waste products within the scaffold space.

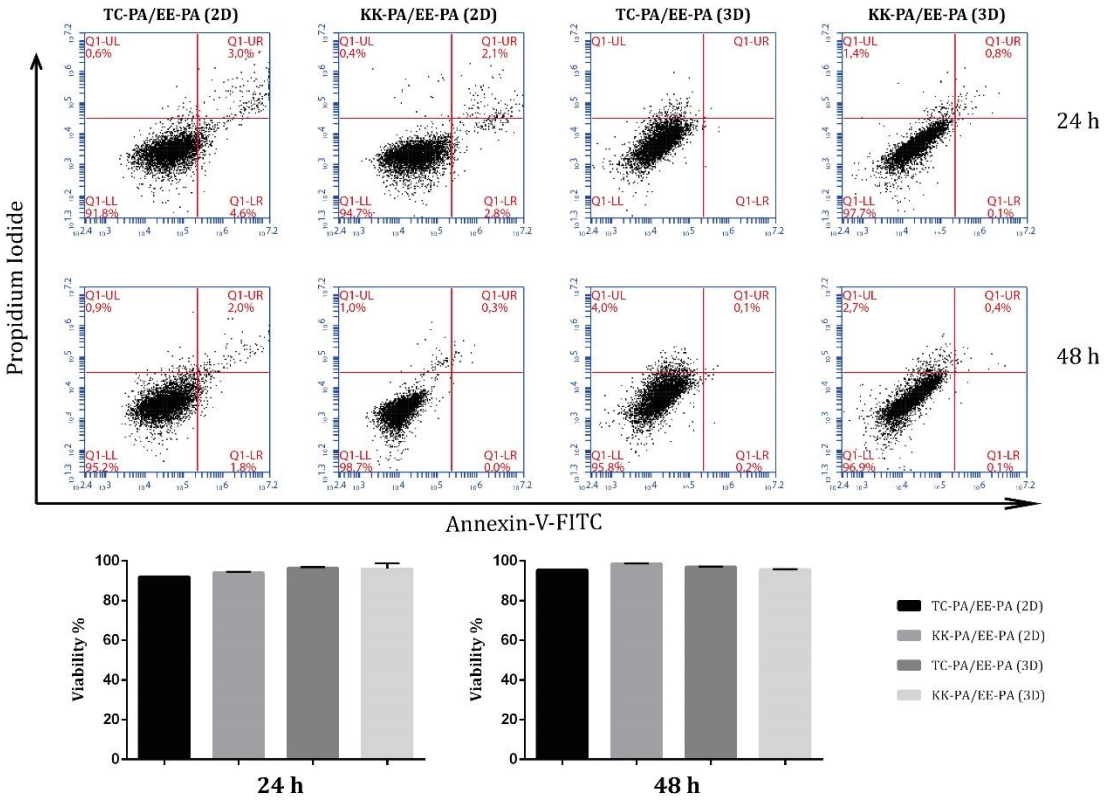

Figure 4. 7 Viability of PC-12 cells seeded on 2D or within 3D peptide nanofibers which was tested by flow cytometry analysis. Values represent mean ± standard deviation.

4.3.3 Effect of TN-C Mimetic Peptide Nanofibers on Neurite Outgrowth

The ability to promote neurite outgrowths is crucial for neuroregenerative biomaterials, since neurite development is required to generate functional synapses. PC-12 is a rat adrenal gland pheochromocytoma-derived cell line that is commonly used as a model system in *in vitro* studies for the induction of differentiation in the presence of NGF [121, 122]. Therefore, we used PC-12 cells to evaluate the potential of TN-C mimetic peptide nanofibers to promote neurite extension, and measured neurite lengths and the percentage of neurite-bearing cells on 2D TC-PA/EE-PA and KK-PA/EE-PA nanofibers. Neurite lengths measured at days 3 and 7 after neural

induction revealed that TC-PA/EE-PA scaffold is a potent neurite inducer. Neurite extension on this scaffold was found to be significantly greater at both time points compared to the epitope-free KK-PA/EE-PA scaffold. In addition, the percentage of neurite-bearing cells on TN-C mimetic scaffold was significantly higher compared to the control scaffold (Figure 4.8). Moreover, neurite extension was promoted on TC-PA/EE-PA scaffolds at as early as 3 days, which further underlines the neurite outgrowth-promoting potential of TN-C derived signals in combination with NGF.

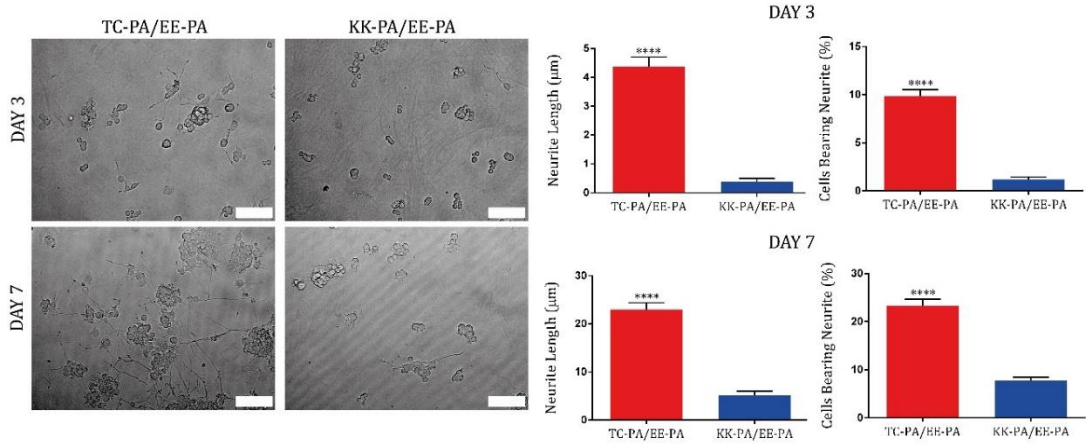

Figure 4. 8 PC-12 cells cultured on TC-PA/EE-PA and KK-PA/EE-PA nanofibers for 3 and 7 days, scale bars: 100 μm. Neurite length and percentage of neurite bearing cells was quantified for day 3 and day 7 by Image J. Values represent mean ± sem (***p<0.0001).

For 3D cell culture, we encapsulated PC-12 cells within PA nanofibers in order to introduce TN-C signaling in all dimensions. 3D gels used in this study were composed of two layers. The first layer comprised a mixture of positively and negatively charged PA solutions, and the second layer included cells encapsulated within the PA mixture. Therefore, cells encountered the first layer instead of the TCP when migrating

downwards, and interacted with TN-C derived epitope in three dimensions. SEM images revealed that encapsulation of PC-12 cells within 3D nanofibers bearing TN-C derived epitopes induced neurite outgrowth in three dimensions, unlike 2D cell culture conditions in which neurite extension was only in two dimensions (Figure 4.9).

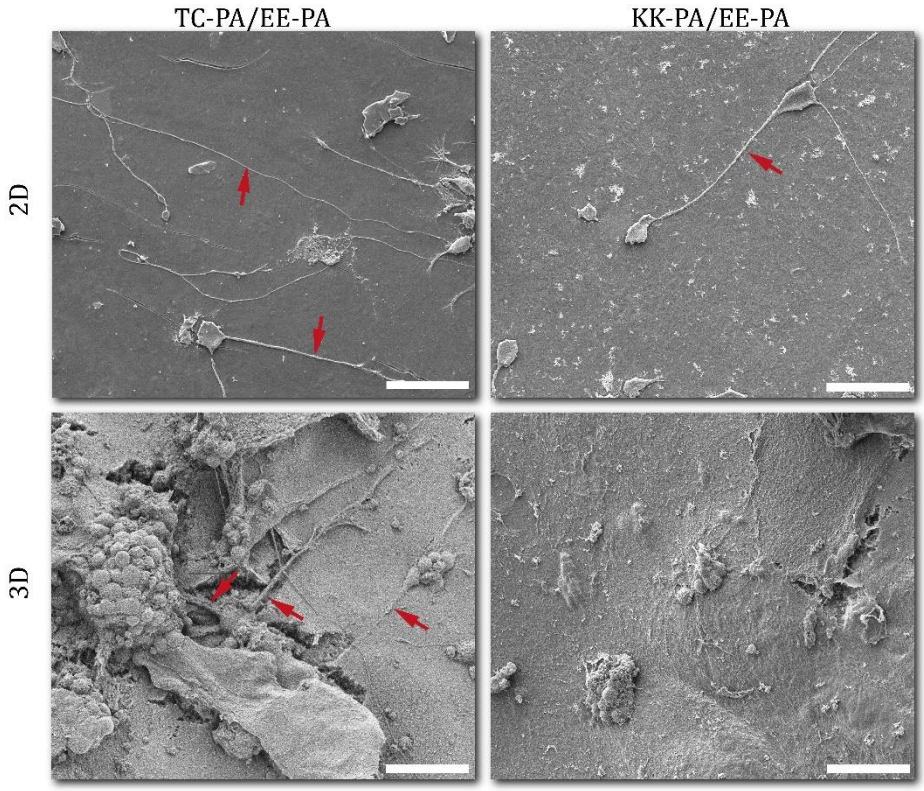

Figure 4. 9 SEM images of PC-12 cells cultured on 2D TC-PA/EE-PA, EE-PA/KK-PA nanofibers, and 3D TC-PA/EE-PA, EE-PA/KK-PA gels on day 7 after cell seeding. Scale bars are 50 μm.

4.3.4 Effect of TN-C Mimetic Peptide Nanofibers on Neural Gene Expressions

Gene expression profiles of PC-12 cells cultured on 2D or within 3D bioactive or non-bioactive nanofibers were analyzed to understand the effect of the TN-C derived epitope on neural differentiation. Gene expressions of β-III tubulin and SYN1 at different conditions were determined as indicators of neural differentiation. β-III

tubulin is a good marker for neural differentiation, since it is expressed in both mature and immature neurons [123, 124]. Encapsulation of PC-12 cells within 3D TN-C mimetic peptide nanofibers increased gene expression of βIII-tubulin in the presence of NGF when compared to other groups (Figure 4.10A).

Synaptophysin is a commonly used neural differentiation marker and presynaptic vesicle protein that is present in axons, expressed throughout the brain and responsible for synapse formation [125, 126]. Results of SYN1 expression in different experimental groups displayed a similar pattern with βIII-tubulin expression. In the presence of NGF, TN-C epitope significantly increased the gene expression of SYN1 when the cells were encapsulated within the 3D nanofiber gel. Strikingly, when the cells were encapsulated within 3D TN-C mimetic nanofibers in the absence of NGF, SYN1 expression was enhanced to a greater extent compared to 2D culture conditions, suggesting that the 3D introduction of TN-C signaling to cells is more effective for inducing SYN1 expression (Figure 6A). However, when the neural gene expressions of PC-12 cells cultured on 2D or within 3D epitope-free control of nanofiber gel were analyzed, presence or absence of NGF did not correlate with the microenvironment, suggesting that bioactivity and microenvironment cooperate for neural differentiation (Figure 4.10B). Overall, these results confirm the SEM results showing extensive neurite outgrowth in PC-12 cells encapsulated within 3D TN-C mimetic nanofibers.

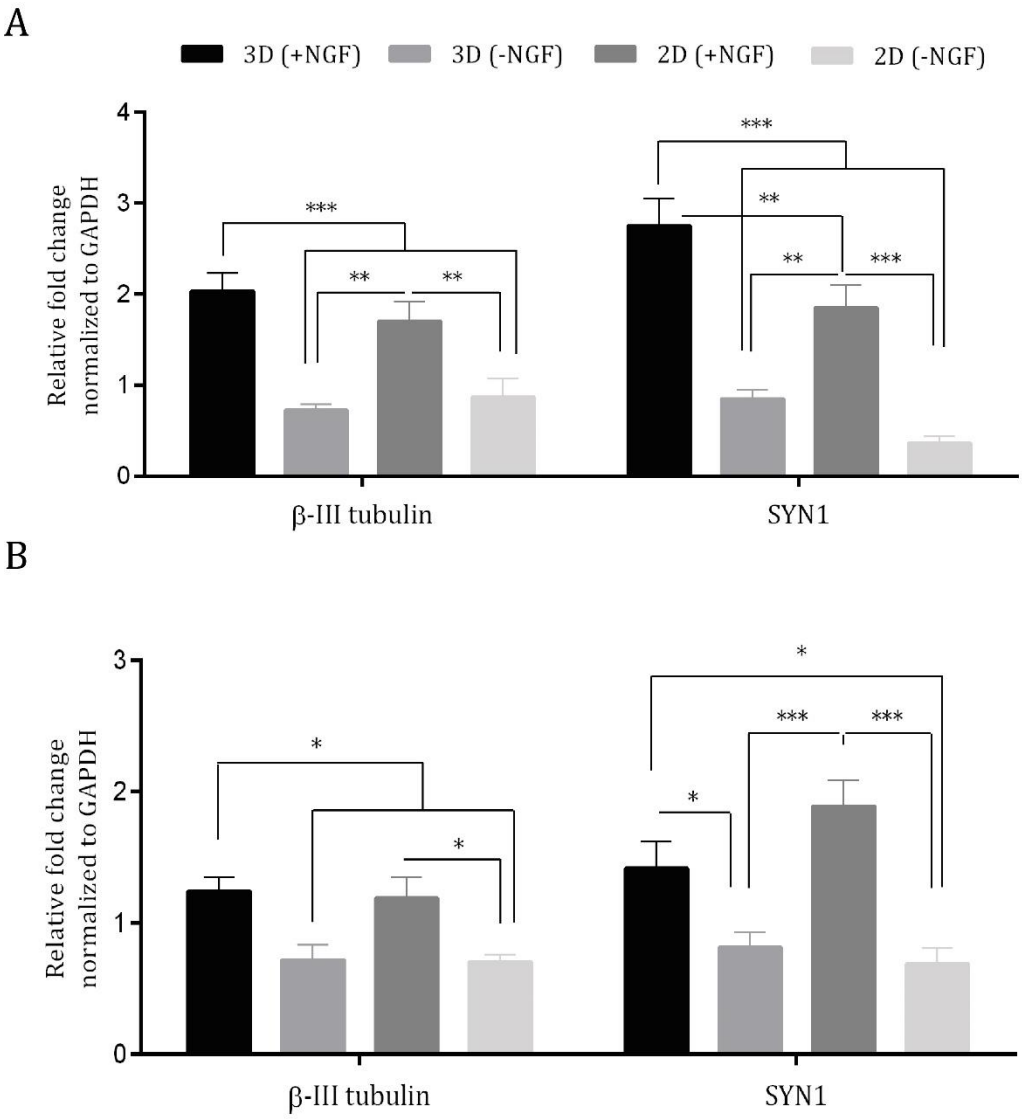

Figure 4. 10 Gene expression analyses of β-III tubulin and SYN1 on day 7 on 2D nanofibers and in 3D hydrogels with and without the addition of NGF. Gene expression levels of PC-12 cells cultured on TC-PA/EE-PA nanofibers and hydrogels (A). Gene expression levels of PC-12 cells on KK-PA/EE-PA nanofibers and hydrogels (B). Expression level of each gene was normalized to GAPDH. Values represent mean ± sem (***p<0.001, **p<0.01, *p<0.05).

4.3.5 Effect of TN-C Mimetic Peptide Nanofibers on Neural Protein Expressions

For further analysis of the neural differentiation potential of PC-12 cells with TN-C signaling and 3D cell culture, protein expression levels of neural markers were quantified with Western blotting. Protein-level analysis revealed increased expression of SYN1 and βIII-tubulin proteins in PC-12 cells concomitantly with enhanced neural differentiation induced by TN-C signaling in the 3D nanofiber system compared to epitope-free 3D nanofibers (Figure 4.11). Our results suggest that introducing TN-C signals in three dimensions not only increased the expression levels of neural markers at the gene level, but also maintained the translation of gene upregulation at the protein level.

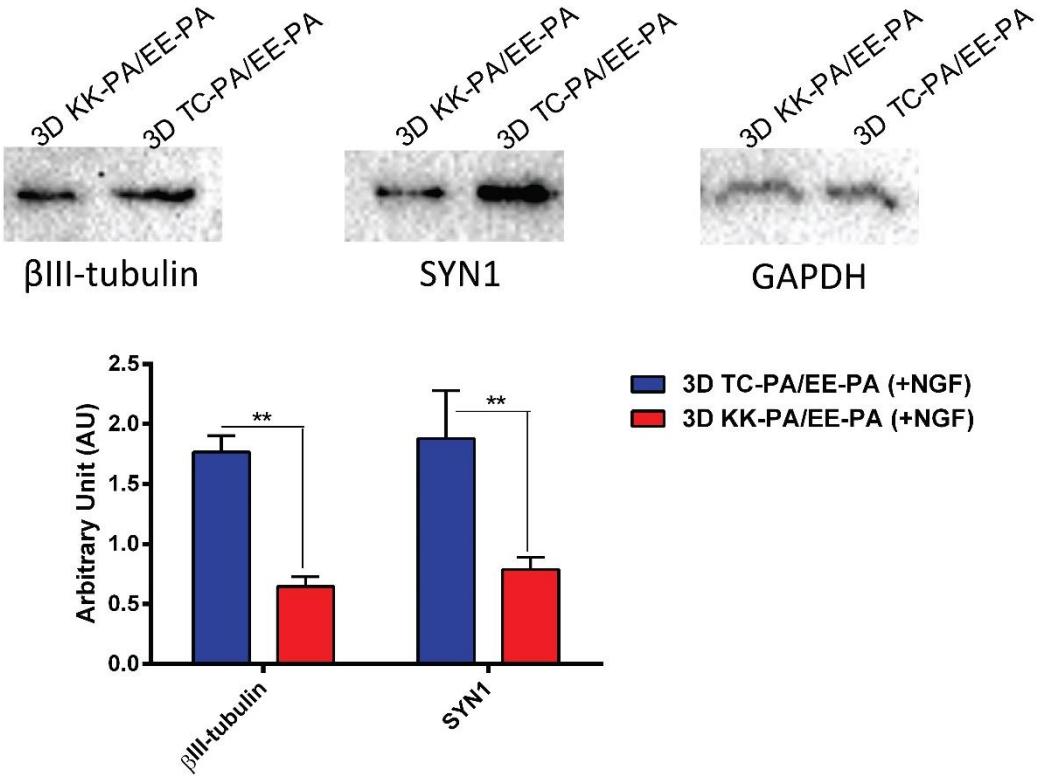

Figure 4. 11 Western blot analysis of βIII-tubulin and SYN1 protein expression of PC-12 cells seeded in 3D TC-PA/EE-PA or KK-PA/EE-PA hydrogels with NGF induction. Values represent mean ± sem (**$p<0.01$).

We further confirmed neural differentiation as a result of the synergy between TN-C signaling and 3D gel system by evaluating the activation of ERK 1/2 module, since ERK1/2 is strongly activated by growth factors such as NGF [127], which was used in our study. We found that there was no statistically significant difference between [phospho ERK 1/2]/[total ERK 1/2] ratio of cells seeded within 3D bioactive and non-bioactive gels (Figure 4.12). Consequently, the effect of NGF was the same for both 3D conditions (bioactive or non-bioactive), and neural differentiation induction effect in TN-C mimetic 3D gel only came from the action of TN-C signaling in the context of a 3D microenvironment.

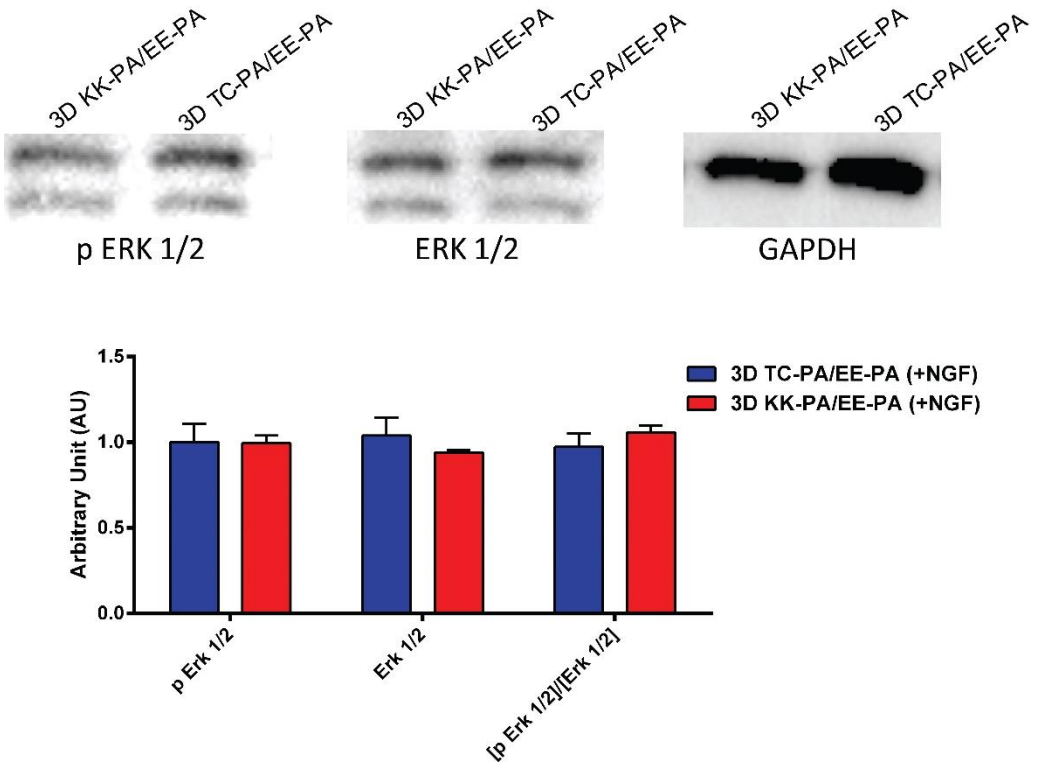

Figure 4. 12 Western blot analysis of ERK phosphorylation (p ERK) and total ERK expression. Values represent mean ± sem.

4.4 Conclusion

In this study, we investigated the potential of a TN-C derived signal-incorporated 3D nanofiber system in inducing neurite extension and neural differentiation of PC-12 cells. TN-C mimetic peptide nanofibers exhibited a neurite outgrowth promoting-effect and contributed to the differentiation of PC-12 cells through the regulation of neural markers. Since PC-12 cells are commonly used as a model for *in vitro* studies of neuroregeneration, enhancement of neurite extension and differentiation in this cell line is relevant for the future clinical applications of biomaterial scaffolds. In this study, we showed that 3D cell culture with favorable mechanical and biochemical properties was able to support the neural differentiation of PC-12 cells with extensive

neurite outgrowth. Nanofibers with TN-C derived signals promoted significant neurite extension, which was further stimulated by 3D nanofiber scaffolds presenting bioactive signals in all three dimensions. In addition, mechanical properties of the gel system were close to those of brain tissue, which might also have contributed to the ability of the scaffold to induce neural differentiation. By combining the physical and biochemical properties of PA nanofibers in one system, it is possible to direct the fate of the neural or neural progenitor cells for further neuroregenerative clinical applications.

Chapter 5

5. Tenascin-C mimetic peptide nanofibers for stem cell differentiation into osteogenic lineage

This chapter of the thesis was published in the following article [119]; Reproduced from "Tenascin-C mimetic peptide nanofibers direct stem cell differentiation to osteogenic lineage"; Sever, M.; Mammadov, M.; Guler, M. O.; Tekinay, A. B., *Biomacromolecules*, 15(12), 4480-4487, with permission from ACS Publications.

5.1 Introduction

Recent advances in stem cell biology have shown that MSCs are pluripotent progenitor cells with the ability to differentiate into cartilage, bone, muscle, tendon, ligament, and fat cells, and they play important roles in the repair of bone defects [128, 129]. *In vitro* MSC differentiation into specific and distinct phenotypes involves certain cellular transitions [129]. The differentiation of MSCs *in vitro* largely depends on the culture conditions. The interaction of external factors, such as nutrients, structural characteristics, and bioactivity of the environment, with internal factors (genetic and epigenetic characteristics) [130] is important for the transition from one differentiation stage to another. Osteogenic differentiation of MSCs *in vitro* is mostly induced by the presence of osteogenic supplements including dexamethasone, ascorbic acid, and β-glycerol phosphate [131]. Surface structure is also important for the behavior of the cells [132], and it directly affects the cell response [133-135] and new tissue formation process [130, 132]. Cell fate can be manipulated through altering the rigidity of the substrate, and it was reported that osteogenic differentiation of MSCs was maximized

on matrices with moduli between 10 and 40 kPa [34, 136, 137], which emphasizes the role of physical characteristics of the matrix as regulators of stem cell behavior to guide tissue development.

The components of the ECM are important for the regulation of cell behavior during tissue development and pathology, as well as for the maintenance of normal function. ECM not only acts as a scaffold for the cells; but it also functions as a store of growth factors and cytokines [138]. In bone, a large number of ECM components including collagens, proteoglycans and glycoproteins contribute to the structure of bone [139, 140]. TN is an ECM glycoprotein, which is also known as cytotactin or hexabrachion. TN family of glycoproteins (TN-C, TN-R, TN-W, TN-X, and TN-Y) show highly dynamic patterns of expression in the embryo, especially during neural development, skeletogenesis, and vasculogenesis. They are also expressed in adults during processes including wound healing, nerve regeneration, and tissue involution, and in pathogenesis such as vascular disease, tumorigenesis, and metastasis [141]. Within this family, TN-C is a hexamer of disulfide-linked subunits. Each subunit is composed of several domains of repeated structural units, which include epidermal growth factor-like repeats and fibronectin type III (FNIII) repeats [142]. TN-C interacts with a variety of ECM molecules such as fibronectin, as well as cell surface molecules including integrins, contactin/F11, annexin II, and heparan sulfated proteoglycans, and acts as a regulator of cell behavior including adhesion, spreading and proliferation [143]. TN-C is found in the condensing mesenchyme of developing bones, which is the primary center of ossification, and the periosteal and endosteal surfaces of mineralized bone [144, 145]. Since TN-C is found in the matrix on bone surfaces and is mostly absent in the connective tissues surrounding bone, this protein is thought to be important in

the regulation of osteoblast or osteoclast function [146]. It was previously shown that exogenous TN-C is able to affect the morphology and differentiation of osteoblast-like cells and that endogenous TN-C plays an important role in the maintenance of the morphology, differentiation, and proliferation in these cells [146]. In another study, a short linear amino acid sequence derived from human TN-C, VFDNFVLK, was found to be necessary and sufficient to maintain the function of full sequence TN-C for the formation of the neurite outgrowth [118].

The ability of self-assembled PA nanofibers to mimic natural ECM renders them attractive for regenerative medicine applications. PA nanofibers can be modified to meet the needs of a variety of tissues by varying the functional peptide sequences. Hydrophobic collapse of alkyl tails and β-sheet formation between PA molecules result in the formation of nanofibers in aqueous solution, where short biofunctional amino acid sequences can be presented on the surface of these nanofibers [77]. The supramolecular architecture of PA nanofibers enable ease of using a combination of several bioactive sequences for manipulating the cells in terms of adhesion, proliferation, and differentiation [21, 29, 147-151]. For instance, a combination of bioactive sequences inspired by ECM proteins was used to control cell behavior for biomineralization and bone regeneration when supplemented with osteogenic culture media [21].

A TN-C derived peptide sequence (VFDNFVLKK) was previously shown to sufficiently maintain the function of full length TN-C protein in inducing neurite outgrowth. In the present study, we investigated whether the same sequence is also capable of inducing osteogenic differentiation based on the fact that TN-C is a common protein in ECM of both neural and bone tissue (Figure 5.1). Overall, we

showed that TN-C mimetic self-assembled peptide nanofibers significantly enhanced the attachment, proliferation, and osteogenic differentiation of rat mesenchymal stem cells (rMSCs) even in the absence of any external bioactive factors and regardless of the suitable mechanical properties normally required for osteogenic differentiation. Since mechanical cues and external osteogenic supplements are known to be important requirements for osteogenic commitment of MSCs, this study presents a striking example for the ability of a single biological cue to override these requirements and makes TN-C mimetic peptide nanofibers a promising new platform for bone regeneration.

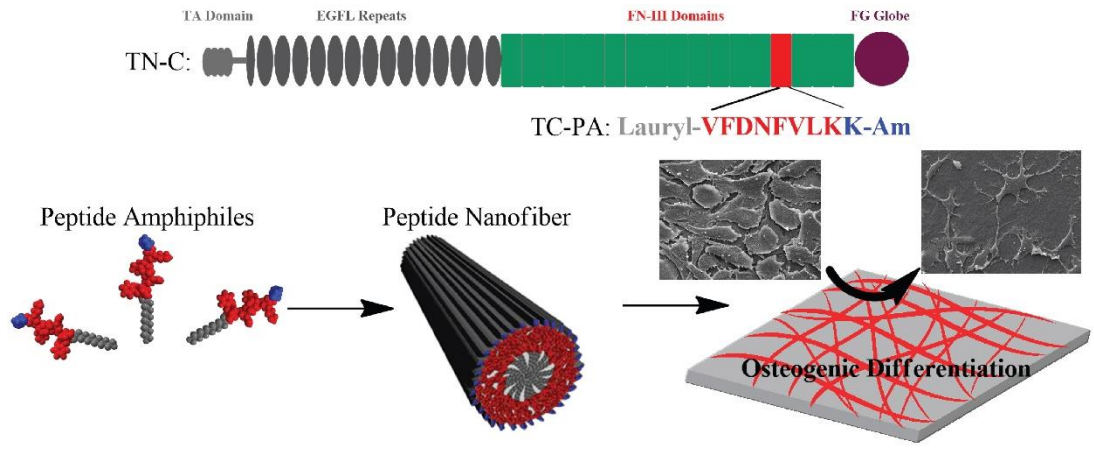

Figure 5. 1 Schematic diagram of the study.

5.2 Experimental Section

5.2.1 Materials

All protected amino acids, lauric acid, 4-(2′,4′-dimethoxyphenyl-Fmoc-aminomethyl)-phenoxyacetamido-norleucyl-MBHA resin (Rink amide MBHA resin), HBTU, and DIEA were purchased from Nova-Biochem, ABCR, or Sigma-Aldrich. Calcein-AM and other cell culture materials were purchased from Invitrogen. All other chemicals

and materials used in this study were purchased from Thermo Scientific or Sigma-Aldrich.

5.2.2 Synthesis of PA Molecules

PA molecules were synthesized on Rink amide MBHA resin or Fmoc-Glu(OtBu)-Wang resin using the Fmoc-protected solid phase peptide synthesis method. Amino acid couplings were performed with 2 equivalents of amino acids activated with 1.95 equivalents of HBTU and 3 equivalents of DIEA for 2 h. Fmoc removal was performed with 20% piperidine/DMF solution for 20 min. Acetic anhydride (10%)/DMF solution was used to permanently acetylate the unreacted amine groups after each coupling step. DMF and DCM were used as washing solvents after each step. Cleavage of the PAs and protection groups from the resin was carried out with a mixture of TFA/TIS/H_2O in the ratio of 95:2.5:2.5 for 3 h. Excess TFA removal was carried out by rotary evaporation. PAs in the remaining solution were precipitated in ice-cold diethyl ether overnight. The precipitate was collected by centrifugation next day and dissolved in ultrapure water. This solution was frozen at −80 °C for 4 h and then lyophilized for 4–5 days. PAs were characterized by LC–MS. Mass spectrum was obtained with Agilent LC-MS equipped with Agilent 6530 Q-TOF with an ESI source and Zorbax Extend-C18 2.1 mm × 50 mm column for basic conditions and Zorbax SB-C8 4.6 mm × 100 mm column for acidic conditions. A gradient of water (0.1% formic acid or 0.1% NH_4OH) and acetonitrile (0.1% formic acid or 0.1% NH_4OH) was used. In order to remove residual TFA, positively charged PAs were treated with 0.1 M HCl solution and lyophilized. To purify the peptides, an Agilent preparative reverse-phase HPLC system equipped with a Zorbax Extend-C18 21.2 mm × 150 mm column was used for basic conditions, and a Zorbax SB-C8 21.2 mm × 150 mm column was used

for acidic conditions. A gradient of water (0.1% TFA or 0.1% NH_4OH) and acetonitrile (0.1% TFA or 0.1% NH_4OH) was used. All peptide batches were freeze-dried and reconstituted in ultrapure water at pH 7.4 before use.

5.2.3 SEM Imaging of PA Nanofiber Network

PA nanofiber networks were observed by imaging with SEM. Negatively and positively charged PA solutions (8 mM) were mixed at 2:1 volume ratio (final volume being 50 μL) to produce gels with neutral charge. Gels were formed on silicon wafer and dehydrated by transferring to 20%, 40%, 60%, 80%, and 100% v/v ethanol sequentially. They were critical point-dried by using Autosamdri 815B equipment from Tousimis. Dried PA gels were coated with 4 nm Au/Pd, and SEM (FEI Quanta 200 FEG) images were taken using an ETD at high vacuum mode at 5 keV beam energy.

5.2.4 STEM Imaging of PA Nanofiber Matrices

Samples for STEM imaging were prepared by mixing 2 mM TC-PA or 2 mM K-PA and 1 mM E-PA in equal volumes and then diluting sample 10 times and placing them on a 200-mesh carbon TEM grid for 10 min followed by 2 wt % uranyl acetate staining for 2 min and drying. STEM images at HAADF mode were acquired with FEI Tecnai G2 F30 TEM at 300 kV.

5.2.5 Secondary Structure Analysis

A JASCO J815 CD spectrometer was used at room temperature. Negatively and positively charged 2.5×10^{-4} M PA solutions were mixed at 2:1 volume ratio (final volume being 500 μL) to produce nanofibers with net neutral charge. Measurements were carried out from 300 to 190 nm data interval, data pitch being 0.1 nm, and

scanning speed being 100 nm min^{-1}, all measurements with three accumulations. DIT was selected as 1 s, bandwidth as 1 nm, and the sensitivity was standard.

5.2.6 Oscillatory Rheology

Oscillatory rheology measurements were performed with Anton Paar Physica RM301 rheometer operated with a 25 mm parallel plate configuration at 25 °C. Total volume of 250 μL with 8 mM concentrations of each PA component was carefully loaded onto the center of the lower plate and incubated for 10 min for gelation before measurement. After equilibration, the upper plate was lowered to a gap distance of 0.5 mm. Storage moduli and loss moduli values were scanned from 100 to 0.1 rad s^{-1} of angular frequency, with a 0.5% shear strain. Three samples were measured for each PA gel.

5.2.7 Cell Culture and Maintenance

Rat mesenchymal stem cells (rMSCs, Invitrogen, passage number 7) were used in all cell culture experiments including viability, proliferation, gene expression analysis, alkaline phosphatase (ALP) activity, and calcium deposition. Cells were cultured in 75 cm^2 flasks at a density of 2×10^3 cells/cm^2 at 37 °C in a humidified incubator and supplied with 5% CO_2. Cells were maintained in DMEM supplemented with 10% FBS, 1% P/S, and 2 mM L-glutamine. All cell culture experiments were carried out after reaching 90% confluency. The culture medium was changed every 3–4 days. Cells were seeded with the same medium content. The day after seeding cells, cell medium was replaced with MEM with 3% FBS, 1% P/S, and 2 mM L-glutamine. For alizarin red staining, this medium was also supplemented with 10 mM β-glycerophosphate, differently from the other experiments. Medium was changed every 3 days.

5.2.8 Viability Assay

To form TC-PA/E-PA or K-PA/E-PA gel, equal volumes of 3 mM TC-PA or K-PA and 1.5 mM E-PA were used in order to neutralize the charges. PA-gel coated plates were incubated at 37 °C for 30 min, prior to overnight incubation in a laminar flow hood at room temperature for solvent evaporation. The next day, PA matrix formed on the plates was UV sterilized. By addition of cells in culture media to PA-coated surfaces, rehydration of the PA matrix formed a thin-gel on the surface. The viability tests of MSCs were performed at predetermined time intervals (24, 48, 72 h) by calcein-AM and EthD-1 staining and Alamar blue assay. Cells were incubated on PA-coated and uncoated TCP at a density of 2×10^3 cells/cm^2. After 24, 48, and 72 h of incubation, cell medium was discarded; cells were washed with PBS and then incubated with 2 μM calcein-AM and 2 μM EthD-1 in PBS for 30 min at room temperature. Finally, five random images were taken at 10× magnification from each well for both qualitative and quantitative analysis by using a fluorescence microscope. Cells were counted with NIH ImageJ software for proliferation. For Alamar blue assay, medium was discarded after 24, 48, and 72 h of incubation and replaced with medium containing 10% Alamar blue. Blank group contained only Alamar blue medium without cells. After 4 h incubation at 37 °C, absorbance measurement was performed by Spectramax M5 microplate reader at 570 and 600 nm as reference.

5.2.9 SEM Imaging of MSCs on PA Nanofiber Coated Surfaces

The morphology and spreading of MSCs were examined by SEM imaging by using an ETD detector at high vacuum mode at 5 keV beam energy. For this purpose, glass coverslips were coated with PAs, and cells were seeded on top of the coated and uncoated surfaces at a density of 2×10^3 cells/cm^2. Seven and twelve days after

incubation, cells were rinsed with PBS and fixed with 2% gluteraldehyde/PBS and 1 wt % OsO_4 for 1 h each, respectively. Fixed cells were washed with water and then dehydrated sequentially in 20%, 40%, 60%, 80%, and 100% ethanol. Samples were critical point dried with Autosamdri-815B Tousimis and coated with 6 nm Au–Pd before imaging.

5.2.10 Gene Expression Analysis

Gene expression profiles for differentiation were assessed by quantitative RT-PCR analysis. rMSCs were seeded at a density of 2×10^3 cells/cm^2 on peptide nanofiber coated surfaces and bare surface, and after 12 days of incubation of the cells on PA-coated surfaces and TCP, RNA isolation was performed with TRIzol (Invitrogen) reagent by considering the instructions of the manufacturer. After RNA extraction, amount and purity of the RNA samples were verified with Nanodrop 2000 (Thermo Scientific). Primer sequences to be used in qRT-PCR were designed with NCBI database. SuperScript III Platinum SYBR Green one-step qRT-PCR kit was used for qRT-PCR analysis with instructions of the manufacturer. Reaction conditions were briefly as follows: 55 °C for 5 min, 95 °C for 5 min, 40 cycles of 95 °C for 15 s, X °C for 30 s (varies according to primer sets), and 40 °C for 1 min, followed by a melting curve analysis to confirm product specificity. The reaction efficiencies for each primer set were evaluated by plotting a standard curve using 5-fold serial dilutions of total RNA. For analysis of the expression data, primary gene expression data was normalized by the expression level of GAPDH. A comparative Ct method (Pfaffl method) was used to analyze results.

Table 5. 1 Primers Used for qRT-PCR Expression Analysis

Gene	Primer Sequence (Forward/Reverse)	Product size (bp)
Neural Markers		
β-III-Tubulin	CCTGCCTCTTCGTCTCTAGC AACTTGGCCCCTATCTGGTT	222
NFL	CCATGCAGGACACAATCAAC CAATGTCCAATGCCATCTTG	281
SYN1	CCAGCTCAACAAATCCCAGT TGGTCTCAGCTTTCACCTCA	307
Astroglial Markers		
MBP	AAATCGGCTCACAAGGGATT CTGTCTCTTCCTCCCAGCTT	168
BLBP	ACTGTAAGTCTGTGATTCGGTTG ACGACATCCCCAAAGGTGAG	133
Pax6	TAGCCCAGTTTTCAGAGCCAC AATTCGGGAAATGTCGCACG	201
Chondrogenic Markers		
Collagen II	CGAGGTGACAAAGGAGAAGC AGGGCCAGAAGTACCCTGAT	126
Osteogenic Markers		
Sox9	CCACCCCGATTACAAGTACC GTCGGTGGACCCTGAGATT	204
Runx2	GGACGAGGCAAGAGTTTCACT CCCTAAATCACTGAGGCGGT	177
Osteopontin	AGTTTGGCAGCTCAGAGGAG TGCTTGGAAGAGTTTCTTGCTT	162
Collagen I	TGACTGGAAGAGCGGAGAGT GGTCATGCTCTCTCCAAACC	193
Fibroblast Markers		
FSP	CTTGGTCTGGTCTCAACGGT GCAGCTTCGTCTGTCCTTCT	185
Myogenic Markers		
Pax7	GTGCCCTCAGTGAGTTCGATT GGGAGGTCGGGTTCTGATTC	188
MSC Markers		
CD44	CAGAAGGGACAACTGCCTCA AATGGGTATTTGGAGCCGCA	198
CD90	ACCAAGGATGAGGGCGACTA CACTTGACCAGCTTGTCTCTGA	104
Reference Gene		
GAPDH	GTGCCAGCCTCGTCTCATA AACTTGCCGTGGGTAGAGTC	186

5.2.11 ALP Activity Assay

ALP activity of rMSCs was analyzed by measuring the colorimetric product of p-nitrophenol from endogenous ALP reaction after 3 and 7 days of culture in differentiation medium. Cells (3×10^3 cm^{-2}) were seeded on PA-coated and uncoated TCP surfaces. Medium change was done every 3 days. At predetermined time points, cells were rinsed with PBS, and protein extraction was performed by using M-PER protein extraction kit (Thermo)/5% protease inhibitor solution as 150 μL/well for 30 min on shaker. After centrifugation of samples at 14000g for 10 min at 4 °C, supernatants that contain proteins were taken, and BCA protein assay was performed to quantify protein amount as described in manufacturer's protocol. Absorbance was determined at 562 nm by using a microplate reader. For ALP activity, 50 μL of protein sample was incubated with 150 μL of p-nitrophenol phosphate substrate in 96-well plates for 30 min on shaker. Serial dilutions of p-nitrophenol in 0.25 M NaOH were used as standards. Finally, optical density was determined at 405 nm by using Spectramax M5 microplate reader. ALP results were normalized to total protein amount.

5.2.12 Imaging Mineral Deposition by Alizarin Red Staining

The ability of mineralized nodule formation and calcium deposition of MSCs on PA nanofiber-coated and uncoated TCPs were assessed by using alizarin red-S staining as described previously [152]. In brief, cells were incubated for 7 and 12 days at the densities of 4×10^3 cells/cm^2. Cells were washed with PBS and fixed with ice-cold ethanol for 1 h at room temperature. Then, fixed cells were washed with distilled water and stained with 40 mM alizarin red-S solution (pH 4.2) for 30 min at room temperature on shaker. After washing 4–5 times with distilled water to get rid of

nonspecific binding, PBS was added and the calcium nodules were imaged under a microscope. For quantification of calcium amount, PBS was discarded and 10% cetylpyridinium chloride was added and incubated for 30 min at room temperature. At the end of incubation, solution was transferred to 96-well plate and absorbance measurement was done at 562 nm. Cetylpyridinium chloride was used to release the remaining calcium-bound alizarin red S.

5.2.13 Statistical Analysis

All quantitative values are presented as mean ± sem, and all the groups in experiments were performed with at least three replicates. Two-way ANOVA was used for statistical analysis, and p-value of less than 0.05 was considered statistically significant.

5.3 Results and Discussion

5.3.1 Design and Characterization of Peptide Nanofibers

In this study, osteogenic scaffolds were generated through self-assembly of PA molecules that carry natural ECM protein TN-C derived epitope (lauryl-VFDNFVLKK-Am (TC-PA)) [118]. The control nanofibers did not display this epitope ((lauryl-VVAGE-OH (E-PA) and lauryl-VVAGK-Am (K-PA)) (Figure 5.2). The PA molecules were synthesized with solid phase peptide synthesis method and purified with LC-MS (Figure 5.3).

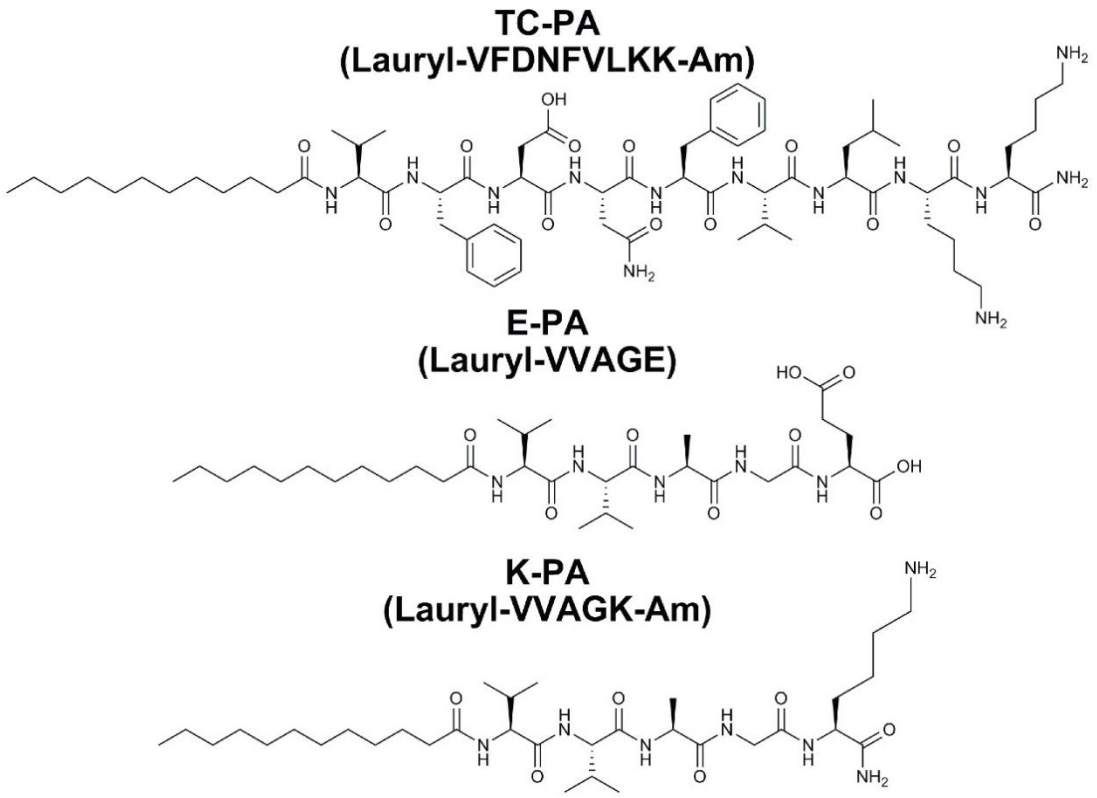

Figure 5. 2 Self-assembled PA nanofibers. All PA molecules had a hydrophobic alkyl tail consisting of lauric acid. While TC-PA had bioactive sequence, VFDNFVLK, epitope free PA molecules carried a β-sheet forming peptide sequence, VVAG. This sequence consists of four nonpolar amino acid residues, among which valine has a very high β sheet-forming propensity provided by its hydrophobic side chain, while glycine is used as a spacer between the hydrophobic part of the sequence and hydrophilic epitope region [153, 154].

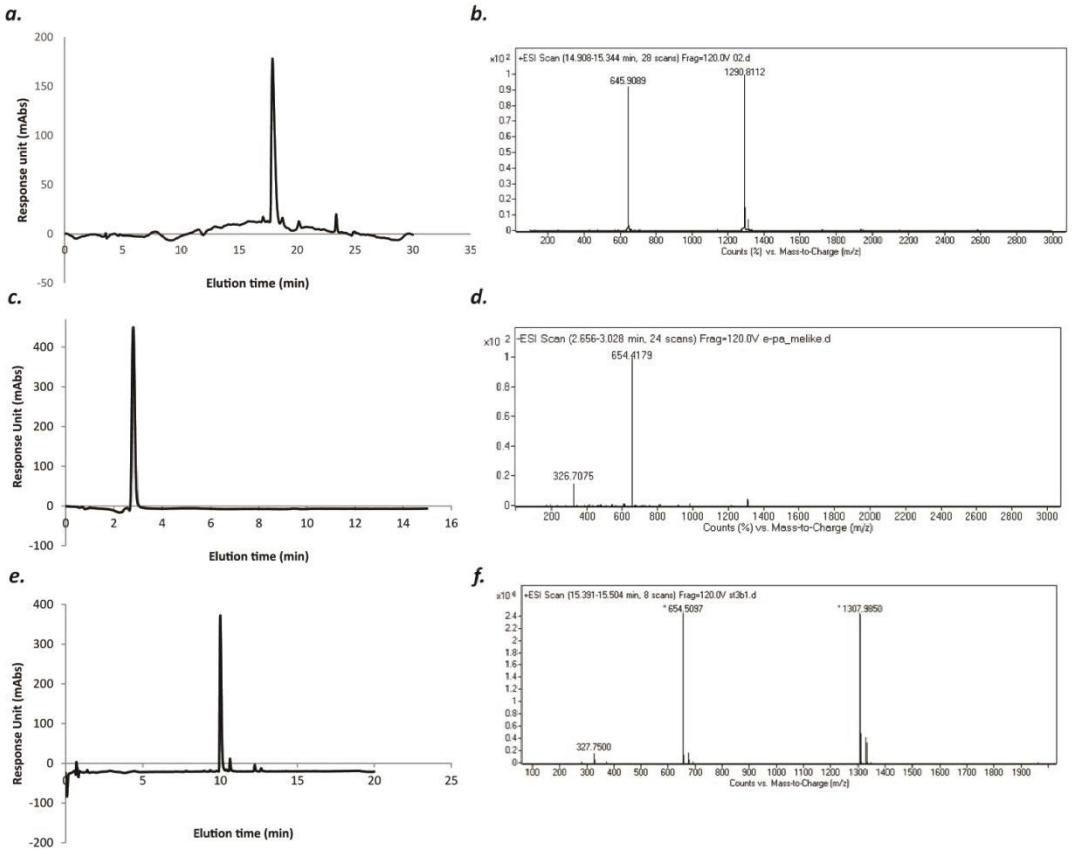

Figure 5. 3 LC and MS of PA molecules used. LC results verify the purity of TC-PA (a), E-PA (c) and K-PA (e). MS of PA-TC (b), $[M+H]^{+}$ (calculated): 1290.81 $[M+H]^{+}$ (observed): 1290.81 $[M+2H]^{+2}/2$ (calculated): 645.91 $[M+2H]^{+2}/2$ (observed): 645.91. MS of PA-E (d), $[M-H]^{-}$ (calculated): 654.42 $[M-H]^{-}$ (observed): 654.42, $[M-2H]^{-2}/2$ (calculated): 326.71 $[M-2H]^{-2}/2$ (observed): 326.71. MS of PA-K (f), $[2M+H]^{+}$ (calculated): 1307.96 $[2M+H]^{+}$ (observed): 1307.98 $[M+H]^{+}$ (calculated): 654.48 $[M+H]^{+}$ (observed): 654.51 $[M+2H]^{+2}/2$ (calculated): 327.74 $[M+2H]^{+2}/2$ (observed): 327.75

TC-PA molecules formed nanofibers through self-assembly when mixed with oppositely charged E-PA due to electrostatic interactions, hydrophobic collapse, and β-sheet driving units at physiological pH [120]. Positively charged K-PA and negatively charged E-PA molecules were mixed to induce formation of nanofibers as

an epitope-free control. STEM imaging showed that both TC-PA/E-PA and K-PA/E-PA nanofibers were uniform in diameter (10–20 nm) and several micrometers in length (Figure 5.4). These nanofibers formed bundles that formed nanofiber networks that can encapsulate water to form hydrogels. These nanofiber networks resembled the nanofibrous structure of natural ECM at physiological pH as evidenced by SEM imaging (Figure 5.5).

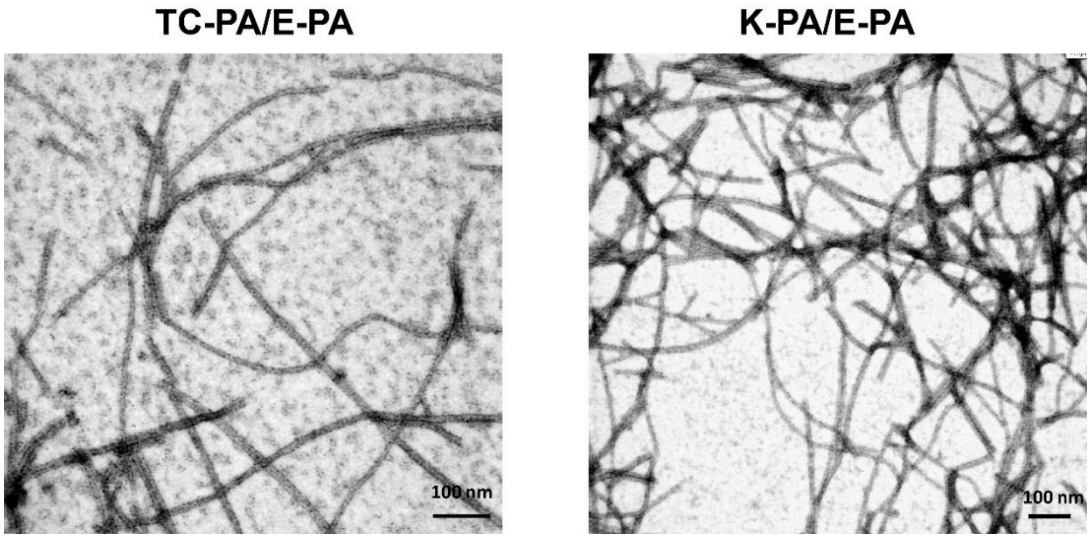

Figure 5. 4 STEM images of the TC-PA/E-PA and K-PA/E-PA nanofibers formed at pH 7.4. Scale bars are 100 nm in length.

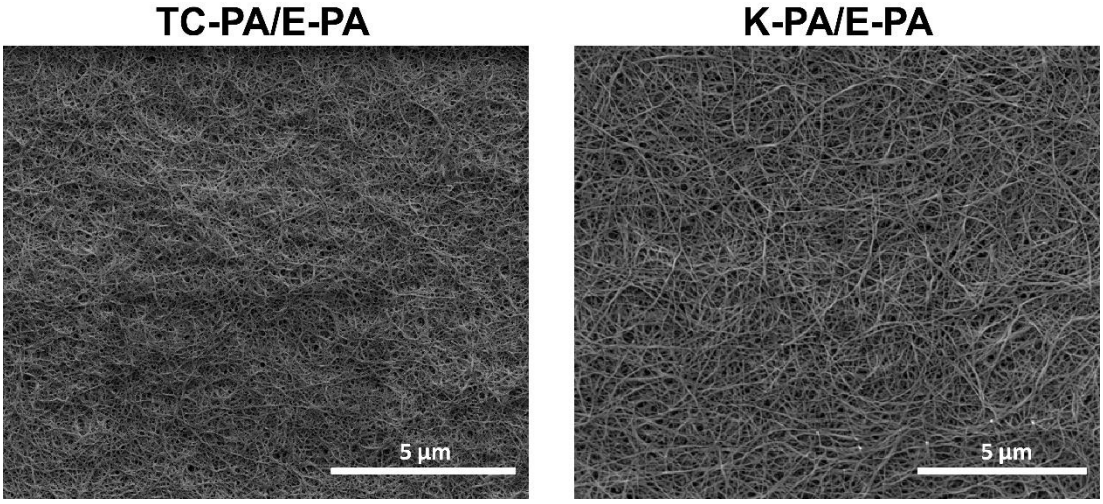

Figure 5. 5 SEM images of TC-PA/E-PA and K-PA/E-PA gels reveal the ECM-like morphology of PA scaffolds. Scale bars are 5 µm in length.

The secondary structures of the TN-C mimetic and control nanofibers were characterized using CD spectroscopy. Both nanofiber types demonstrated predominantly β-sheet structure with a chiral absorbance maximum at around 200 nm and minimum at around 220 nm (Figure 5.6).

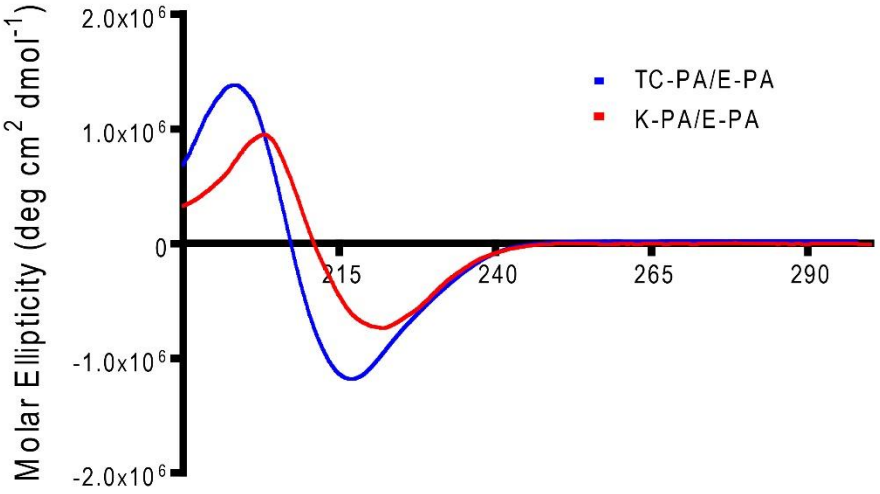

Figure 5. 6 Characterization of secondary structure of peptide nanostructures by CD spectroscopy.

Physical characteristics of the matrix are known to be a potent cue for stem cell differentiation. Mechanical properties of the gels were compared by using frequency sweep rheology measurements at constant strain. Each gel (TC-PA/E-PA gel and K-PA/E-PA gel) had higher storage modulus (G′) than loss modulus (G″), indicating gel formation at physiological pH (Figure 5.7). The elastic modulus of TN-C mimetic PA scaffold is around 270 Pa, which is lower than the elasticity of hard matrices used to induce osteogenic differentiation *in vitro* [34, 136, 137] and relatively lower than the elasticity modulus of epitope-free control scaffold, which was around 1000 Pa.

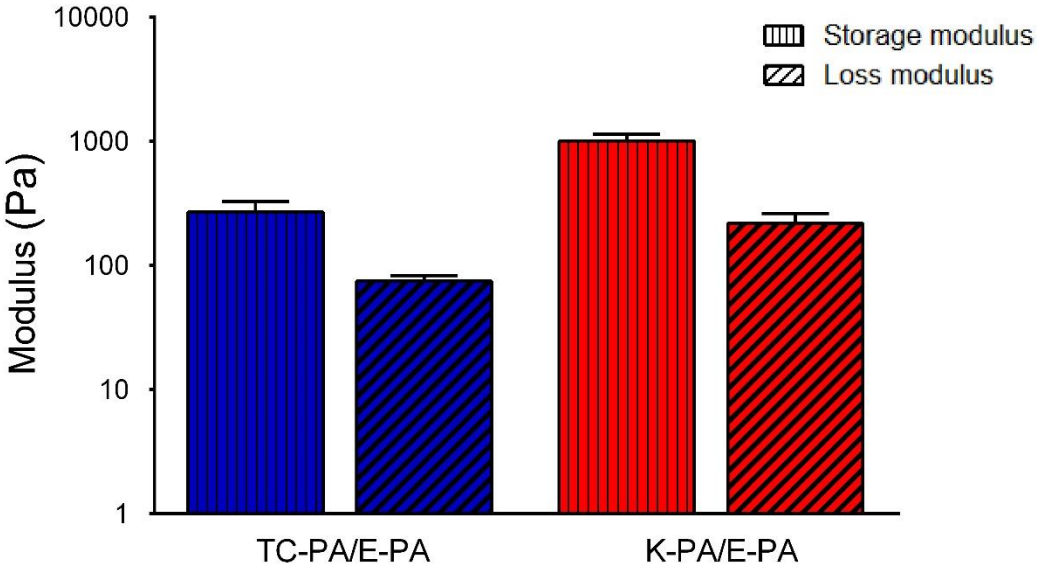

Figure 5. 7 Mechanical properties of PA gels characterized by oscillatory rheology.

5.3.2 Effect of TN-C Mimetic Nanofibers on Cell Adhesion and Spreading

Cellular viability of rMSCs seeded on TN-C mimetic peptide nanofibers was assessed by calcein AM staining, by comparison to cells that were cultured on a bare glass surface and epitope-free peptide nanofibers at varying time points (24, 48, and 72 h). Although a lower viability was observed on TN-C mimetic PA scaffold at early time

points, cells adapted to the surface after 48 h. MSCs are multipotent cells that are known to present a nonhomogeneous cell population. Although the cells that we used were previously selected to express certain MSC markers (Invitrogen), cultured MSCs display variable phenotypes like proliferation capacity and viability as well as giving different response to differentiation stimuli. The plastic properties of MSCs can also contribute to heterogeneity of MSC cultures [155]. Cellular heterogeneity within the population can be caused by persistent cell individuality coming from fluctuations of protein levels, which induce nongenetic cell individuality [156]. Heterogeneity of MSC cultures may be the reason for differences in viability of our cells on TN-C mimetic scaffold at different time points. Although a group of the cells died up to 48 h, viability of the cells on all surfaces was comparable at the end of 72 h with no significant differences between groups (Figure 5.8). This indicates that this bioactive material is causing differential effects on different cell groups.

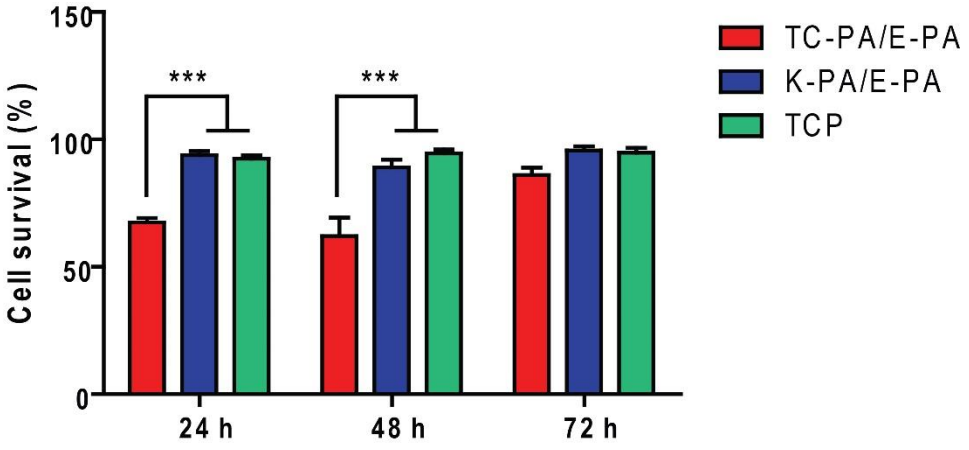

Figure 5. 8 Viability of rMSCs when cultured on peptide nanofibers and TCP analyzed by calcein ethidium homodimer live−dead assay. This assay showed that rMSCs adapted to PA scaffolds and have comparable viability with bare surface at the end of 72 h.

SEM images of cells seeded on the scaffold revealed that rMSCs spread and attained their different morphologies on all of the surfaces on day 7 and 12 (Figure 5.9). These results indicated that TN-C mimetic peptide nanofibers provide attachment and spreading of rMSCs. Also, SEM images indicated that rMSCs on TN-C mimetic scaffold display a characteristic morphology that is different from that of the cells seeded on control peptide nanofibers and bare surfaces, possibly due to the effect of 2D microenvironment on differentiation process.

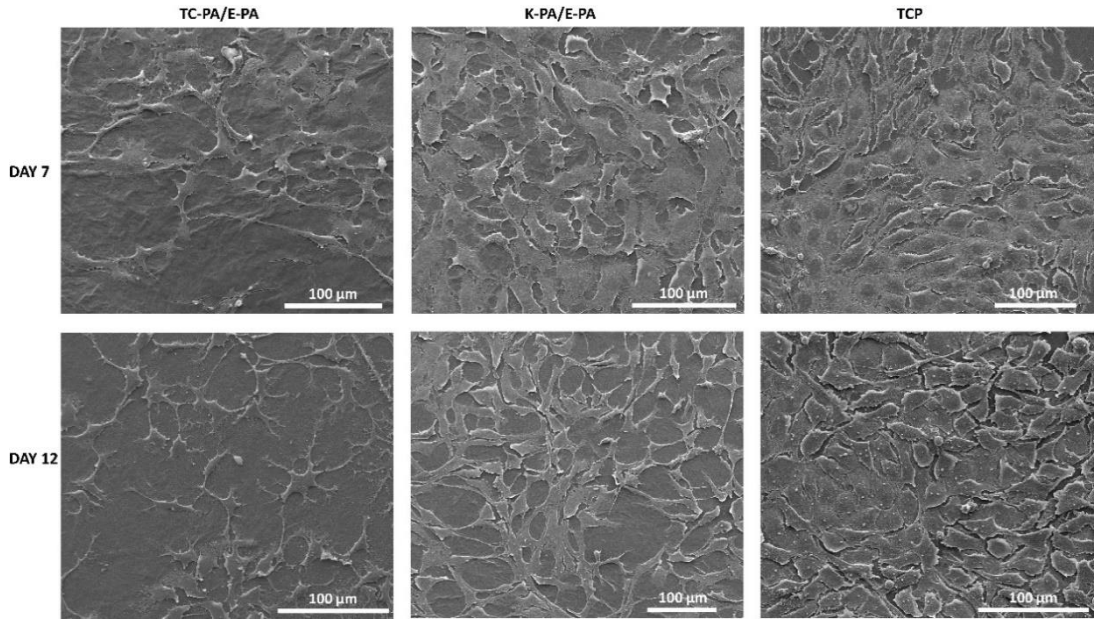

Figure 5. 9 PA substrates are biocompatible and support adhesion of rMSCs. SEM images of rMSCs cultured on TC-PA/E-PA, E-PA/K-PA gels, and TCP at 7 days and 12 days after cell seeding. Scale bars are 100 µm.

5.3.3 Effect of TN-C Mimetic Peptide Nanofibers on Gene Expressions of Osteogenic Markers

To understand whether the morphological change of rMSCs on TN-C mimetic scaffold is caused by osteogenic differentiation, gene expression profiles of cells cultured on

peptide network coated and bare surfaces were analyzed. First, expression of MSC markers including CD44 and CD90 were studied to verify the differentiation of MSCs. Although decrease in CD44 expression was not significant, decrease in CD90 was found to be statistically significant, confirming the loss of MSC characteristics of the cells (Figure 5.10a). In order to check the effect of biologically active peptide nanofiber systems on the progression of osteogenic differentiation of rMSCs at mRNA level, expression of osteogenic markers including Runx2, osteopontin, and collagen I was examined with Sox9 on day 12 (Figure 5.10b). Although Sox9 is the best-known master regulator for chondrocyte differentiation and cartilage formation [157], it is specifically expressed in the osteogenic cell compartments together with osteogenic markers such as Runx2, collagen I, and osteopontin [158]. Expressions of Sox9 and Runx2 genes, early markers of ostegenic differentiation, were upregulated by ~2.0- and 1.6-fold, respectively, when rMSCs were cultured on TC-PA/E-PA compared with cells on K-PA/E-PA and TCP surfaces. Osteopontin is a secreted adhesive glycoprotein detected within bone ECM. Osteopontin expression of the cells on TN-C mimetic scaffold was also increased, by about 3-folds. Collagen I is an important component of bone ECM, which interacts with cell surface integrins and other ECM proteins. This protein plays an important role in cell adhesion, proliferation, and differentiation of the osteoblast phenotype. In parallel to osteopontin expression, collagen I expression was also significantly upregulated in cells cultured on TC-PA/E-PA scaffold (4.5- and 1.9-fold increase when compared with K-PA/E-PA and TCP, respectively). These significant differences in the mRNA expression of ostegenic markers between the cells seeded on the TN-C mimetic peptide nanofiber scaffold and

epitope free scaffold, as well as bare surface, were considered as evidence of osteogenic differentiation.

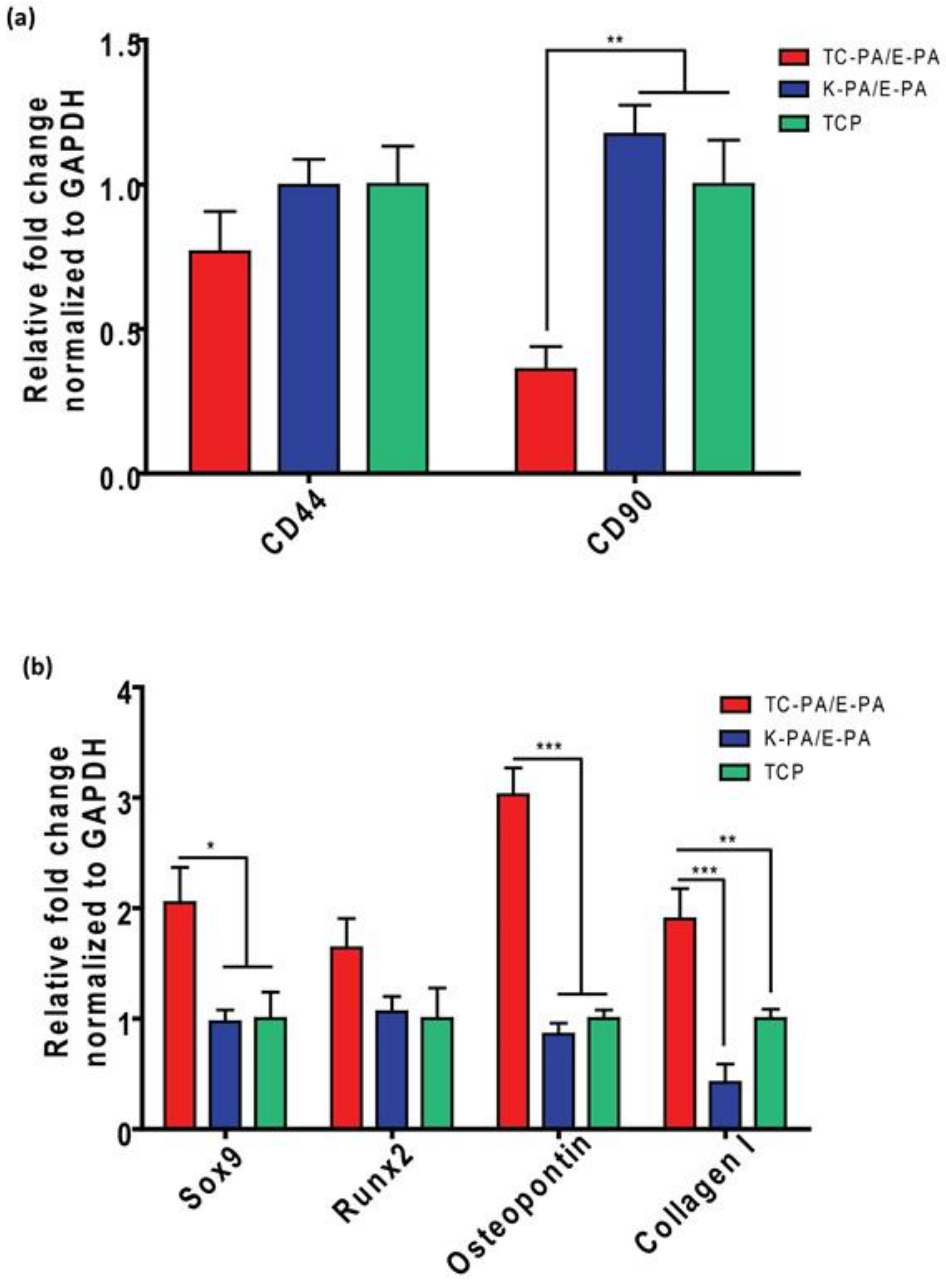

Figure 5. 10 Gene expression analyses of (a) MSC markers and (b) osteogenic markers. The expression level of each gene was normalized against TCP and GAPDH was used as the internal control. Values represent mean ± sem (***$p < 0.001$, **$p < 0.01$, *$p < 0.05$).

It is widely known that MSCs have capacity to differentiate into a variety of cell types. Therefore, to be sure that the differentiated cells we observed belong to osteogenic lineage and not other cell types, we analyzed expression of specific markers of other common cell types that MSCs can differentiate into. Collagen II expression was analyzed for chondrogenic differentiation along with Pax7 for myogenic differentiation, FSP for fibroblast differentiation, βIII-tubulin, NFL, and SYN1 for neural differentiation, and MBP, BLBP, and Pax6 for astroglial differentiation (Figure 5.11). There was no detectable up-regulation in the expression of these markers indicating that rMSCs underwent osteogenic lineage commitment.

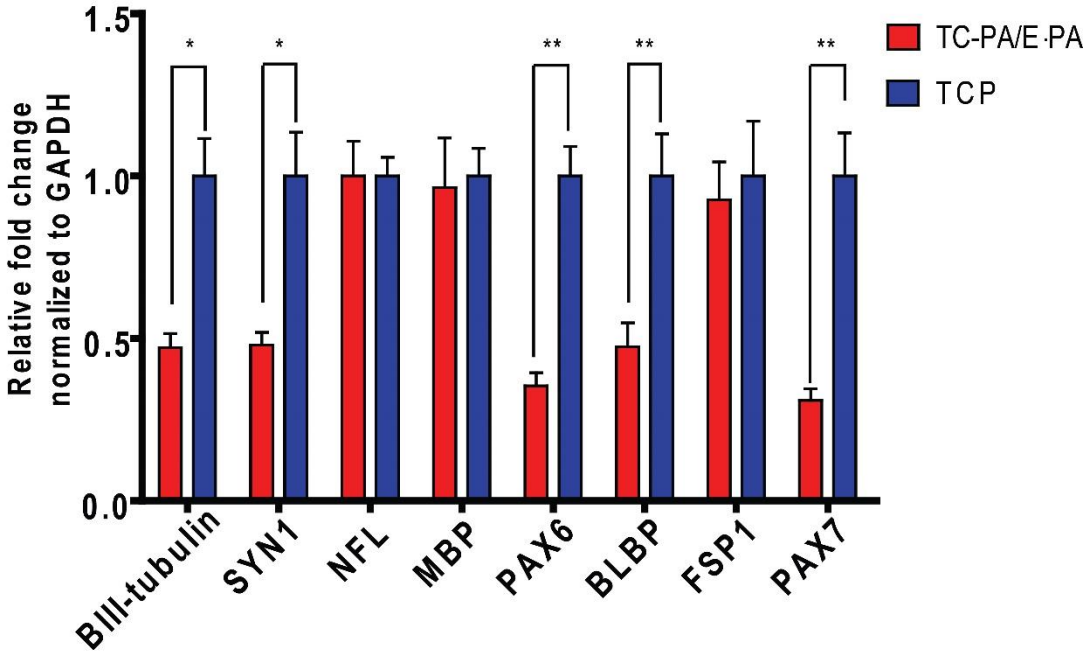

Figure 5. 11 Gene expression levels of different differentiation markers in rMSCs at week 2 on TC-PA/E-PA substrate and bare surface. (*$p<0.05$, ** $p<0.01$)

5.3.4 Effect of TN-C Mimetic Peptide Nanofibers on ALP Activity and Mineralization

The osteoblasts are the differentiated bone-forming cells responsible for secreting collagen–proteoglycan matrix and calcification of bone matrix. When MSCs undergo osteogenic differentiation, they express osteoblast markers. MSCs undergo osteogenic differentiation in a progressive manner [159]. The early phase of *in vitro* osteogenic differentiation can be characterized by the expression of ALP at mRNA and protein level [160]. After the initial peak of ALP expression, its level starts to decrease. Late stage of osteogenic differentiation results in elevated expression of osteopontin, followed by calcium and phosphate deposition [159, 161]. Thus, early phase of osteogenic differentiation was analyzed with ALP assay, and the amount of calcium deposition was assayed with alizarin red staining for detection of late phase differentiation. Compared with epitope free scaffold and bare surface, ALP activity of rMSCs on TN-C mimetic scaffold was increased significantly by about 2-folds on day 3. Although, ALP activity of rMSCs on biologically active scaffold displayed lower ALP activity on day 7 compared to that on day 3, ALP activity of cells on bioactive surface still remained higher than those on epitope free scaffold and TCP (Figure 5.12).

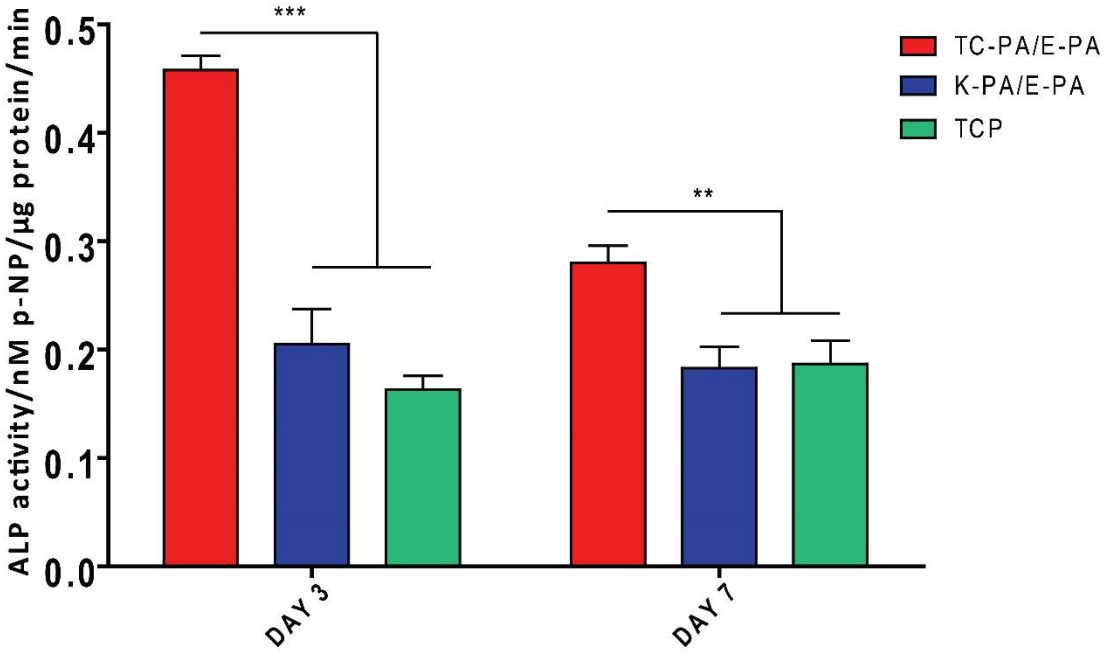

Figure 5. 12 ALP activity of rMSCs on days 3 and 7.

In order to test the mineral deposition of rMSCs as a late marker of osteogenic differention, alizarin red staining was performed on day 7 and day 12, and calcium deposition was quantified by extracting alizarin red bound calcium from the surface followed by a colorimetric measurement. The results indicated that calcium deposition on TC-PA/E-PA was significantly higher compared to that on K-PA/E-PA surface and bare surface on day 12. Similar mineral deposition pattern was also observed on day 7 (Figure 5.13 and Figure 5.14).

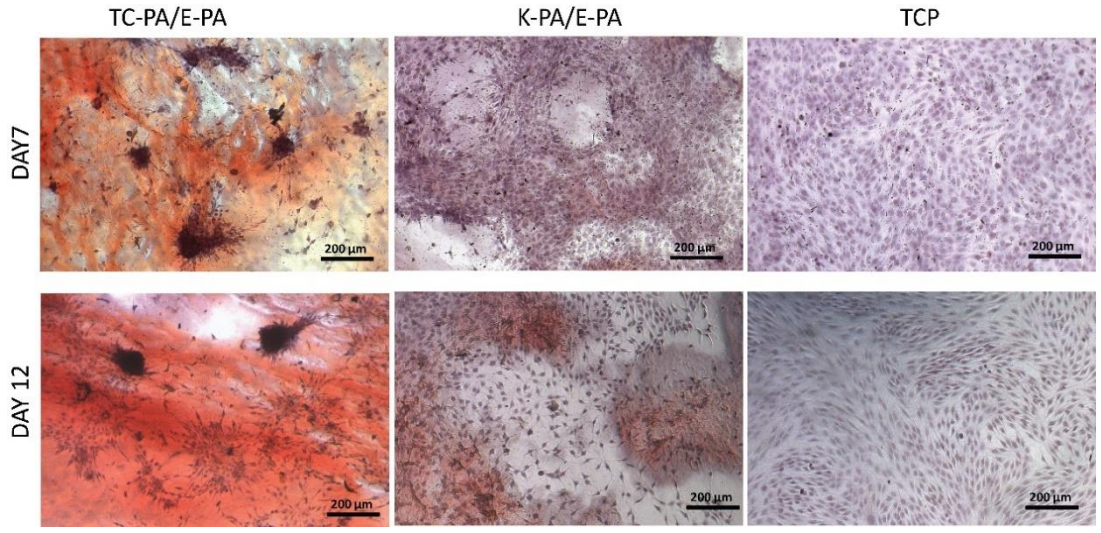

Figure 5. 13 Deposition of calcium on peptide coated substrates and TCP on days 7 and 12 as demonstrated by alizarin red staining.

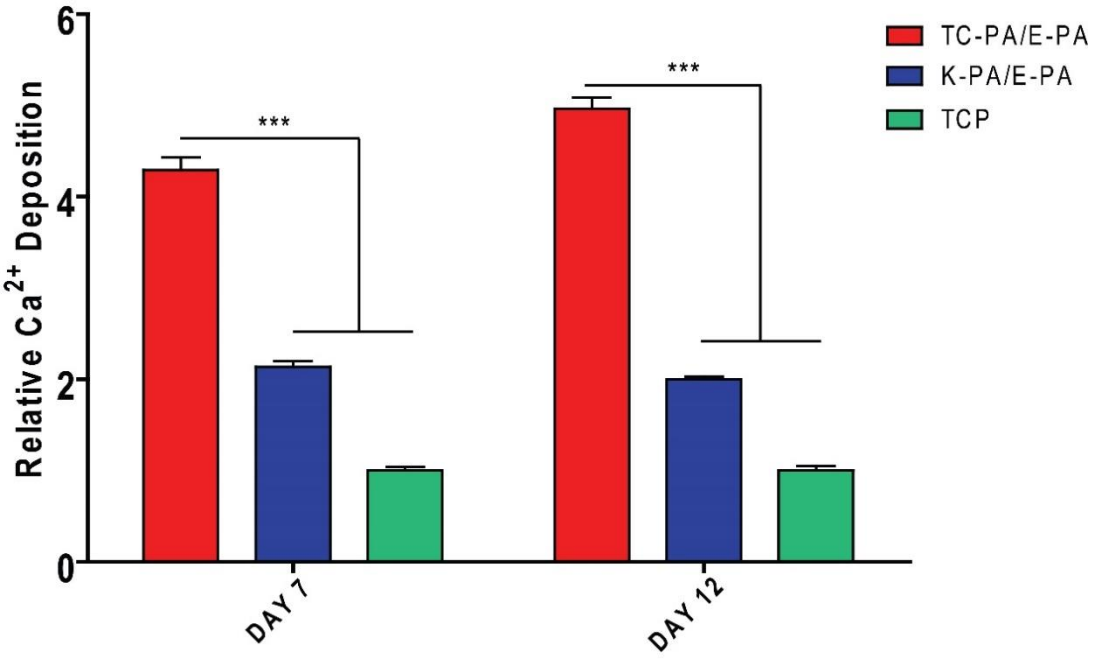

Figure 5. 14 Quantification of relative calcium deposition on days 7 and 12 (***p < 0.001, **p < 0.01).

The differentiation of MSCs *in vitro* largely depends on the culture conditions. Osteogenic differentiation of MSCs is generally induced by the presence of

dexamethasone, ascorbic acid, and β-glycerol phosphate [131]. However, TN-C mimetic peptide scaffold can induce osteogenic differentiation despite the absence of these constituents or supplemental osteogenic growth factors. TN-C derived bioactive epitope acted as the sole triggering factor for osteogenic commitment of MSCs, since ALP activity, calcium deposition, and expression of osteogenic marker genes were higher on TN-C mimetic peptide nanofibers compared to epitope free control peptide nanofibers and bare surface. Although the presence of a stiff environment is also known to be an important requirement for induction of osteogenic differentiation [34, 136, 137], bioactivity caused by TN-C derived peptide sequence is more effective than the requirement of high modulus to induce osteogenic differentiation. Therefore, bioactivity introduced by this TN-C mimetic PA scaffold is the only factor to induce osteogenic differentiation compensating for the lack of osteogenic supplements in the medium and rigidity of the substrate.

5.4 Conclusion

Bone tissue regeneration is essential for the treatment of large bone defects. Alternative to the current treatments, which have several drawbacks including infection, chronic pain, and stiffness, using biomaterial scaffolds that can mimic the microenvironment of osteogenic cells has become highly promising for clinical therapy in recent years since these biomaterials can provide key bioactive signals to create a synthetic microenvironment to control cell fate. In this study, we presented that a single bioactive epitope, TN-C mimetic peptide, enables MSCs to (1) attach and adapt to the bioactive gel, (2) go through a morphological change that is supported with a change in the gene expression profile as a sign of differentiation, (3) display increased ALP activity, and (4) deposit calcium and form a mineralized matrix. The

results show that the extracellular mimetic approach used here allows MSCs to undergo the osteogenic differentiation pathway without any additional factors including growth factor and medium supplements and regardless of suitable mechanical properties normally required for osteogenic differentiation. Overall, our results showed that incorporation of TN-C derived bioactive epitope into a self-assembled PA nanofiber system constitutes a promising platform for bone formation by providing a suitable microenvironment for osteogenic differentiation.

Chapter 6

6. Conclusion and Future Prospects

Tissue engineering and regenerative medicine have advanced with the opportunities provided by new biomaterials with various characteristics for therapeutic purposes. The self-assembled peptide nanostructures with bioactive signals have been widely utilized as synthetic ECM mimetic materials. The cell-material interactions have been improved through incorporation of soluble bioactive molecules such as growth factors, or surface modification of the materials such as introducing bioactivity via short bioactive peptide sequences derived from natural ECM proteins. As a result of these interactions, it is possible to regulate cell fate including viability, proliferation, migration and differentiation at a molecular level, and induce regeneration.

Biomaterials that are generated as a result of self-assembling process and include short peptides and peptide derivatives have significant potential in regenerative medicine applications. Mimicking native ECMs which have regulatory functions in tissue formation and regeneration is a novel strategy for the design of synthetic biomaterials. Synthetic materials are commonly used in tissue engineering applications because of their specific properties such as modifiable elasticity, high water content and ability for encapsulation of cells. These synthetic materials must also be multifunctional in order to mimic the natural ECM both biochemically and biophysically.

Biomimetic nanomaterials bearing natural bioactive signals which are derived from ECM components like laminin and heparan sulfates provide promising therapeutic strategies for the regeneration of the nervous system. However, no research has been reported exploring the use of biomimetic materials against degeneration in PD. In this

work, we investigated potential therapeutic effects of heparan sulfate and laminin mimetic PA nanofibers on reduction of striatal injury in experimental PD model. PA nanofibers enhanced functional recovery associated with enhanced striatal dopamine and TH content as well as reduced cleaved-Caspase-3 levels. Overall, this study shows the improvement in consequences of Parkinsonism in rats and provides a new platform for treatment of PD.

These peptide nanofibers having dual active epitopes (derived from laminin and GAG) also proved to be effective in supporting the viability of Schwann cells and NGF release from Schwann cells with better spreading and cellular interaction pattern *in vitro*. Thus, this scaffold can provide a prolonged delivery of NGF and enhance the efficacy of nerve regeneration, which makes it a promising approach for peripheral nerve injuries.

Effect of 3D PA nanofiber gel functionalized with a TN-C derived epitope on neural differentiation was also investigated. The 3D cell culture system was found to provide both the biochemical and physical aspects of the native environment of neural cells, thereby filling the gap between 2D cell culture models and *in vivo* environments. Overall, we showed that 3D TN-C mimetic self-assembling nanofibers induced 3D neurite outgrowth and significantly increased the expressions of neural markers compared to 2D nanofiber and 3D epitope-free gel controls. This study features the cooperative effect of culture dimensionality and bioactive signals for the induction of neural differentiation, which is critical for the design of neuroregenerative scaffolds. Also, advances in 3D cell culture technologies will enable to create tissue-like structures *in vitro*, and the ability of 3D cell culture systems to mimic tissue structures will facilitate the development of further organoid platforms.

Also, TN-C mimetic peptide nanofibers were also tested for osteogenic differentiation of MSCs. They were found to significantly enhance the attachment, proliferation, and osteogenic differentiation of MSCs even in the absence of any external bioactive factors and regardless of the suitable stiff mechanical properties normally required for osteogenic differentiation.

In conclusion, several applications of self-assembled peptide nanofibers were provided with differentiation and regeneration purposes here. These materials can be fabricated in a wide range in order to use in biomedical applications. Results obtained in this field have become inspiring for the scientists and helped them for the discovery of innovative tools at nano-scale for regenerative medicine.

However, despite the fact that there has been extensive progress in tissue engineering and regenerative medicine studies over the past decades, the nanomaterials used for regenerative purposes is a novel approach, and only some of them have been implemented into clinical trials. There are some safety concerns for human applications. Biocompatibility and biodegradability are important limitations for the development of new nanomaterials and their translation into the clinics. These concerns should be addressed sufficiently, and comprehensive studies will be necessary to ensure the use of these nanomaterials in a safe manner. Also, most of the cellular interactions are still unknown, and it limits our knowledge about the mechanisms of tissue degeneration and regeneration process. Therefore, lack of information about these mechanisms causes a challenge in the development of new materials for biological applications. Understanding the basic principles of interactions in biological systems and optimization of chemical, biological and physical parameters of the scaffolds are required for the improvement of bio-mimetic nanomaterials in

order to control some basic activities in cells including proliferation, adhesion and differentiation. In the future, development of the successfully engineered nanomaterials for biological applications will depend on the ability of studies to solve these problems in a comprehensive and detailed manner. This field will be further developed through focusing on the cell-materials interactions and their underlying mechanisms at molecular level.

Bibliography

[1] L. E. Hebert, P. A. Scherr, J. L. Bienias, D. A. Bennett, and D. A. Evans, "Alzheimer disease in the US population: prevalence estimates using the 2000 census", *Archives of Neurology,* vol. 60, no. 8, pp. 1119-1122, 2003.

[2] J. Wancata, M. Musalek, R. Alexandrowicz, and M. Krautgartner, "Number of dementia sufferers in Europe between the years 2000 and 2050", *European Psychiatry,* vol. 18, no. 6, pp. 306-313, 2003.

[3] P. L. Jones, C. Schmidhauser, and M. J. Bissell, "Regulation of gene expression and cell function by extracellular matrix", *Critical Reviews in Eukaryotic Gene Expression,* vol. 3, no. 2, pp. 137-154, 1993.

[4] R. L. Juliano and S. Haskill, "Signal transduction from the extracellular matrix", *Journal of Cell Biology,* vol. 120, no. 3, pp. 577-585, 1993.

[5] H. Birkedal-Hansen, "Proteolytic remodeling of extracellular matrix", *Current Opinion in Cell Biology,* vol. 7, no. 5, pp. 728-735, 1995.

[6] H. Jarvelainen, A. Sainio, M. Koulu, T. N. Wight, and R. Penttinen, "Extracellular matrix molecules: potential targets in pharmacotherapy", *Pharmacological Reviews,* vol. 61, no. 2, pp. 198-223, 2009.

[7] L. Schaefer and R. M. Schaefer, "Proteoglycans: from structural compounds to signaling molecules", *Cell and Tissue Research,* vol. 339, no. 1, pp. 237-246, 2010.

[8] T. Rozario and D. W. DeSimone, "The extracellular matrix in development and morphogenesis: a dynamic view", *Developmental Biology,* vol. 341, no. 1, pp. 126-140, 2010.

[9] C. Frantz, K. M. Stewart, and V. M. Weaver, "The extracellular matrix at a glance", *Journal of Cell Science,* vol. 123, no. 24, pp. 4195-4200, 2010.

[10] F. T. Bosman and I. Stamenkovic, "Functional structure and composition of the extracellular matrix", *The Journal of Pathology,* vol. 200, no. 4, pp. 423-428, 2003.

[11] J. D. Esko, K. Kimata, and U. Lindahl, "Proteoglycans and Sulfated Glycosaminoglycans", in *Essentials of Glycobiology*, A. Varki *et al.*, Eds. 2nd ed. Cold Spring Harbor (NY), 2009.

[12] A. D. Akintola *et al.,* "Promoter methylation is associated with the age-dependent loss of N-cadherin in the rat kidney", *American Journal of Physiology - Renal Physiology,* vol. 294, no. 1, pp. F170-F176, 2008.

[13] G. Stoll, J. W. Griffin, C. Y. Li, and B. D. Trapp, "Wallerian degeneration in the peripheral nervous system: participation of both Schwann cells and macrophages in myelin degradation", *Journal of Neurocytology,* vol. 18, no. 5, pp. 671-683, 1989.

[14] J. L. Platt *et al.*, "Transplantation of discordant xenografts: a review of progress", *Immunology Today,* vol. 11, no. 12, pp. 450-6; discussion 456-457, 1990.

[15] T. E. Trumble and F. G. Shon, "The physiology of nerve transplantation", *Hand Clinics,* vol. 16, no. 1, pp. 105-122, 2000.

[16] A. M. Avellino, D. Hart, A. T. Dailey, M. MacKinnon, D. Ellegala, and M. Kliot, "Differential macrophage responses in the peripheral and central nervous system during wallerian degeneration of axons", *Experimental Neurology,* vol. 136, no. 2, pp. 183-198, 1995.

[17] P. J. Horner and F. H. Gage, "Regenerating the damaged central nervous system", *Nature,* vol. 407, no. 6807, pp. 963-970, 2000.

[18] J. B. Matson and S. I. Stupp, "Self-assembling peptide scaffolds for regenerative medicine", *Chemical Communications*, vol. 48, no. 1, pp. 26-33, 2012.

[19] J. P. Fisher, M. D. Timmer, T. A. Holland, D. Dean, P. S. Engel, and A. G. Mikos, "Photoinitiated cross-linking of the biodegradable polyester poly(propylene fumarate). Part I. Determination of network structure", *Biomacromolecules*, vol. 4, no. 5, pp. 1327-1334, 2003.

[20] M. P. Lutolf *et al.*, "Synthetic matrix metalloproteinase-sensitive hydrogels for the conduction of tissue regeneration: engineering cell-invasion characteristics",

Proceedings of the National Academy of Sciences, vol. 100, no. 9, pp. 5413-5418, 2003.

[21] J. D. Hartgerink, E. Beniash, and S. I. Stupp, "Self-assembly and mineralization of peptide-amphiphile nanofibers", *Science,* vol. 294, no. 5547, pp. 1684-1688, 2001.

[22] S. E. Paramonov, H. W. Jun, and J. D. Hartgerink, "Self-assembly of peptide-amphiphile nanofibers: the roles of hydrogen bonding and amphiphilic packing", *Journal of the American Chemical Society,* vol. 128, no. 22, pp. 7291-7298, 2006.

[23] B. Mammadov, R. Mammadov, M. O. Guler, and A. B. Tekinay, "Cooperative effect of heparan sulfate and laminin mimetic peptide nanofibers on the promotion of neurite outgrowth", *Acta Biomaterialia,* vol. 8, no. 6, pp. 2077-2086, 2012.

[24] E. J. Berns *et al.*, "A tenascin-C mimetic peptide amphiphile nanofiber gel promotes neurite outgrowth and cell migration of neurosphere-derived cells", *Acta Biomaterialia,* vol. 37, pp. 50-58, 2016.

[25] J. Graf *et al.*, "A pentapeptide from the laminin B1 chain mediates cell adhesion and binds the 67,000 laminin receptor", *Biochemistry,* vol. 26, no. 22, pp. 6896-6900, 1987.

[26] M. D. Pierschbacher and E. Ruoslahti, "Cell Attachment Activity of Fibronectin Can Be Duplicated by Small Synthetic Fragments of the Molecule", *Nature,* vol. 309, no. 5963, pp. 30-33, 1984.

[27] F. Gelain, D. Bottai, A. Vescovi, and S. Zhang, "Designer self-assembling peptide nanofiber scaffolds for adult mouse neural stem cell 3-dimensional cultures", *PLoS One,* vol. 1, p. e119, 2006.

[28] S. Zhang, "Fabrication of novel biomaterials through molecular self-assembly", *Nature Biotechnology,* vol. 21, no. 10, pp. 1171-1178, 2003.

[29] G. A. Silva *et al.*, "Selective differentiation of neural progenitor cells by high-epitope density nanofibers", *Science,* vol. 303, no. 5662, pp. 1352-1355, 2004.

[30] V. M. Tysseling-Mattiace *et al.*, "Self-assembling nanofibers inhibit glial scar formation and promote axon elongation after spinal cord injury", *Journal of Neuroscience,* vol. 28, no. 14, pp. 3814-3823, 2008.

[31] T. Y. Cheng, M. H. Chen, W. H. Chang, M. Y. Huang, and T. W. Wang, "Neural stem cells encapsulated in a functionalized self-assembling peptide hydrogel for brain tissue engineering", *Biomaterials,* vol. 34, no. 8, pp. 2005-2016, 2013.

[32] J. B. Bard and E. D. Hay, "The behavior of fibroblasts from the developing avian cornea. Morphology and movement in situ and in vitro", *Journal of Cell Biology,* vol. 67, no. 2, pp. 400-418, 1975.

[33] N. L. Halliday and J. J. Tomasek, "Mechanical properties of the extracellular matrix influence fibronectin fibril assembly in vitro", *Experimental Cell Research,* vol. 217, no. 1, pp. 109-117, 1995.

[34] A. J. Engler, S. Sen, H. L. Sweeney, and D. E. Discher, "Matrix elasticity directs stem cell lineage specification", *Cell*, vol. 126, no. 4, pp. 677-689, 2006.

[35] P. C. Georges, W. J. Miller, D. F. Meaney, E. S. Sawyer, and P. A. Janmey, "Matrices with compliance comparable to that of brain tissue select neuronal over glial growth in mixed cortical cultures", *Biophysical Journal*, vol. 90, no. 8, pp. 3012-3018, 2006.

[36] K. Saha *et al.*, "Substrate modulus directs neural stem cell behavior", *Biophysical Journal*, vol. 95, no. 9, pp. 4426-4438, 2008.

[37] A. P. Balgude, X. Yu, A. Szymanski, and R. V. Bellamkonda, "Agarose gel stiffness determines rate of DRG neurite extension in 3D cultures", *Biomaterials*, vol. 22, no. 10, pp. 1077-1084, 2001.

[38] G. J. Her, H. C. Wu, M. H. Chen, M. Y. Chen, S. C. Chang, and T. W. Wang, "Control of three-dimensional substrate stiffness to manipulate mesenchymal stem cell fate toward neuronal or glial lineages", *Acta Biomaterialia*, vol. 9, no. 2, pp. 5170-5180, 2013.

[39] R. Bellamkonda, J. P. Ranieri, N. Bouche, and P. Aebischer, "Hydrogel-based three-dimensional matrix for neural cells", *Journal of Biomedical Materials Research Part A*, vol. 29, no. 5, pp. 663-671, 1995.

[40] B. Pardo and P. Honegger, "Differentiation of rat striatal embryonic stem cells in vitro: monolayer culture vs. three-dimensional coculture with differentiated brain cells", *Journal of Neuroscience Research,* vol. 59, no. 4, pp. 504-512, 2000.

[41] H. Peretz, A. E. Talpalar, R. Vago, and D. Baranes, "Superior survival and durability of neurons and astrocytes on 3-dimensional aragonite biomatrices", *Tissue Engineering,* vol. 13, no. 3, pp. 461-472, 2007.

[42] C. Cunha, S. Panseri, O. Villa, D. Silva, and F. Gelain, "3D culture of adult mouse neural stem cells within functionalized self-assembling peptide scaffolds", *International Journal of Nanomedicine,* vol. 6, pp. 943-955, 2011.

[43] M. J. Dalby, M. O. Riehle, H. Johnstone, S. Affrossman, and A. S. Curtis, "In vitro reaction of endothelial cells to polymer demixed nanotopography", *Biomaterials,* vol. 23, no. 14, pp. 2945-2954, 2002.

[44] J. O. Gallagher, K. F. McGhee, C. D. Wilkinson, and M. O. Riehle, "Interaction of animal cells with ordered nanotopography", *IEEE Transactions on NanoBioscience,* vol. 1, no. 1, pp. 24-28, 2002.

[45] M. J. Dalby, M. O. Riehle, H. J. Johnstone, S. Affrossman, and A. S. Curtis, "Polymer-demixed nanotopography: control of fibroblast spreading and proliferation", *Tissue Engineering,* vol. 8, no. 6, pp. 1099-1108, 2002.

[46] M. J. Dalby, S. J. Yarwood, M. O. Riehle, H. J. Johnstone, S. Affrossman, and A. S. Curtis, "Increasing fibroblast response to materials using nanotopography: morphological and genetic measurements of cell response to 13-nm-high polymer demixed islands", *Experimental Cell Research,* vol. 276, no. 1, pp. 1-9, 2002.

[47] A. Ferrari *et al.*, "Nanotopographic control of neuronal polarity", *Nano Letters,* vol. 11, no. 2, pp. 505-511, 2011.

[48] A. L. Hodgkin and A. F. Huxley, "A quantitative description of membrane current and its application to conduction and excitation in nerve", *The Journal of Physiology,* vol. 117, no. 4, pp. 500-544, 1952.

[49] K. A. Chang *et al.*, "Biphasic electrical currents stimulation promotes both proliferation and differentiation of fetal neural stem cells", *PLoS One,* vol. 6, no. 4, p. e18738, 2011.

[50] Y. J. Huang, H. C. Wu, N. H. Tai, and T. W. Wang, "Carbon nanotube rope with electrical stimulation promotes the differentiation and maturity of neural stem cells", *Small,* vol. 8, no. 18, pp. 2869-2877, 2012.

[51] N. A. Kotov *et al.*, "Nanomaterials for neural interfaces", *Advanced Materials,* vol. 21, no. 40, pp. 3970-4004, 2009.

[52] M. Kabiri *et al.*, "Neural differentiation of mouse embryonic stem cells on conductive nanofiber scaffolds", *Biotechnology Letters*, vol. 34, no. 7, pp. 1357-1365, 2012.

[53] M. Sever *et al.*, "Regenerative effects of peptide nanofibers in an experimental model of Parkinson's disease", *Acta Biomaterialia*, vol. 46, pp. 79-90, 2016.

[54] O. Union, "Health at a Glance: Europe", ed: OECD Publishing, 2010.

[55] L. M. de Lau and M. M. Breteler, "Epidemiology of Parkinson's disease", *The Lancet Neurology*, vol. 5, no. 6, pp. 525-535, 2006.

[56] T. M. Dawson and V. L. Dawson, "Molecular pathways of neurodegeneration in Parkinson's disease", *Science*, vol. 302, no. 5646, pp. 819-822, 2003.

[57] N. Lev, E. Melamed, and D. Offen, "Apoptosis and Parkinson's disease", *Progress in Neuro-Psychopharmacology and Biological Psychiatry*, vol. 27, no. 2, pp. 245-250, 2003.

[58] N. A. Tatton, "Increased caspase 3 and Bax immunoreactivity accompany nuclear GAPDH translocation and neuronal apoptosis in Parkinson's disease", *Experimental Neurology*, vol. 166, no. 1, pp. 29-43, 2000.

[59] W. G. Tatton, R. Chalmers-Redman, D. Brown, and N. Tatton, "Apoptosis in Parkinson's disease: signals for neuronal degradation", *Annals of Neurology,* vol. 53 Suppl 3, pp. S61-70; discussion S70-2, 2003.

[60] K. Venderova and D. S. Park, "Programmed cell death in Parkinson's disease", *Cold Spring Harbor Perspectives in Medicine,* vol. 2, no. 8, pp. a009365, 2012.

[61] Y. Liu *et al.*, "Targeting Caspase-3 as Dual Therapeutic Benefits by RNAi Facilitating Brain-Targeted Nanoparticles in a Rat Model of Parkinson's Disease", *Plos One,* vol. 8, no. 5, pp. e62905, 2013.

[62] C. Ossig and H. Reichmann, "Treatment Strategies in Early and Advanced Parkinson Disease", *Neurologic Clinics,* vol. 33, no. 1, pp. 19-37, 2015.

[63] F. I. Tarazi, Z. T. Sahli, M. Wolny, and S. A. Mousa, "Emerging therapies for Parkinson's disease: From bench to bedside", *Pharmacology & Therapeutics,* vol. 144, no. 2, pp. 123-133, 2014.

[64] M. G. Kaplitt *et al.*, "Safety and tolerability of gene therapy with an adeno-associated virus (AAV) borne GAD gene for Parkinson's disease: an open label, phase I trial", *Lancet,* vol. 369, no. 9579, pp. 2097-2105, 2007.

[65] M. H. Fu *et al.*, "Stem cell transplantation therapy in Parkinson's disease", *Springerplus,* vol. 4, no. 1, pp 597, 2015.

[66] Y. H. Zhong and R. V. Bellamkonda, "Biomaterials for the central nervous system", *Journal of the Royal Society Interface*, vol. 5, no. 26, pp. 957-975, 2008.

[67] B. Mammadov, M. Sever, M. O. Guler, and A. B. Tekinay, "Neural differentiation on synthetic scaffold materials", *Biomaterials Science,* vol. 1, no. 11, pp. 1119-1137, 2013.

[68] M. Durbeej, "Laminins", *Cell and Tissue Research*, vol. 339, no. 1, pp. 259-268, 2010.

[69] N. J. Gardiner, "Integrins and the Extracellular Matrix: Key Mediators of Development and Regeneration of the Sensory Nervous System", *Developmental Neurobiology,* vol. 71, no. 11, pp. 1054-1072, 2011.

[70] M. Manthorpe, E. Engvall, E. Ruoslahti, F. M. Longo, G. E. Davis, and S. Varon, "Laminin Promotes Neuritic Regeneration from Cultured Peripheral and Central Neurons", *Journal of Cell Biology,* vol. 97, no. 6, pp. 1882-1890, 1983.

[71] H. Colognato and P. D. Yurchenco, "Form and function: The laminin family of heterotrimers", *Developmental Dynamics,* vol. 218, no. 2, pp. 213-234, 2000.

[72] R. J. Riopelle and K. E. Dow, "Functional Interactions of Neuronal Heparan-Sulfate Proteoglycans with Laminin", *Brain Research,* vol. 525, no. 1, pp. 92-100, 1990.

[73] M. A. Decoster and G. H. Devries, "Evidence That the Axolemmal Mitogen for Cultured Schwann-Cells Is a Positively Charged, Heparan-Sulfate Proteoglycan-Bound, Heparin-Displaceable Molecule", *Journal of Neuroscience Research*, vol. 22, no. 3, pp. 283-288, 1989.

[74] K. Forsten-Williams, C. L. Chu, M. Fannon, J. A. Buczek-Thomas, and M. A. Nugent, "Control of Growth Factor Networks by Heparan Sulfate Proteoglycans", *Annals of Biomedical Engineering*, vol. 36, no. 12, pp. 2134-2148, 2008.

[75] D. A. Pye, R. R. Vives, P. Hyde, and J. T. Gallagher, "Regulation of FGF-1 mitogenic activity by heparan sulfate oligosaccharides is dependent on specific structural features: differential requirements for the modulation of FGF-1 and FGF-2", *Glycobiology*, vol. 10, no. 11, pp. 1183-1192, 2000.

[76] R. Sasisekharan, Z. Shriver, G. Venkataraman, and U. Narayanasami, "Roles of heparan-sulphate glycosaminoglycans in cancer", *Nature Reviews Cancer*, vol. 2, no. 7, pp. 521-528, 2002.

[77] H. G. Cui, M. J. Webber, and S. I. Stupp, "Self-Assembly of Peptide Amphiphiles: From Molecules to Nanostructures to Biomaterials", *Biopolymers*, vol. 94, no. 1, pp. 1-18, 2010.

[78] K. Tashiro *et al.*, "A Synthetic Peptide Containing the Ikvav Sequence from the a-Chain of Laminin Mediates Cell Attachment, Migration, and Neurite

Outgrowth", *Journal of Biological Chemistry,* vol. 264, no. 27, pp. 16174-16182, 1989.

[79] V. M. Tysseling *et al.*, "Self-assembling peptide amphiphile promotes plasticity of serotonergic fibers following spinal cord injury", *Journal of Neuroscience Research,* vol. 88, no. 14, pp. 3161-3170, 2010.

[80] G. Paxinos, K. W. Ashwell, and I. Tork, *Atlas of the developing rat nervous system*. Academic Press, 2013.

[81] M. Cansev, I. H. Ulus, L. Wang, T. J. Maher, and R. J. Wurtman, "Restorative effects of uridine plus docosahexaenoic acid in a rat model of Parkinson's disease", *Neuroscience Research,* vol. 62, no. 3, pp. 206-209, 2008.

[82] D. Kirik, C. Rosenblad, and A. Bjorklund, "Characterization of behavioral and neurodegenerative changes following partial lesions of the nigrostriatal dopamine system induced by intrastriatal 6-hydroxydopamine in the rat", *Experimental Neurology,* vol. 152, no. 2, pp. 259-277, 1998.

[83] D. Kirik, C. Rosenblad, and A. Bjorklund, "Preservation of a functional nigrostriatal dopamine pathway by GDNF in the intrastriatal 6-OHDA lesion model depends on the site of administration of the trophic factor", *European Journal of Neuroscience,* vol. 12, no. 11, pp. 3871-3882, 2000.

[84] T. Schallert and J. L. Tillerson, "Intervention strategies for degeneration of dopamine neurons in parkinsonism", in *Central nervous system diseases*: Springer, 2000, pp. 131-151.

[85] M. Lundblad, M. Andersson, C. Winkler, D. Kirik, N. Wierup, and M. A. Cenci, "Pharmacological validation of behavioural measures of akinesia and dyskinesia in a rat model of Parkinson's disease", *European Journal of Neuroscience,* vol. 15, no. 1, pp. 120-132, 2002.

[86] M. Olsson, G. Nikkhah, C. Bentlage, and A. Bjorklund, "Forelimb Akinesia in the Rat Parkinson Model - Differential-Effects of Dopamine Agonists and Nigral Transplants as Assessed by a New Stepping Test", *Journal of Neuroscience,* vol. 15, no. 5, pp. 3863-3875, 1995.

[87] U. Ungerstedt, "6-Hydroxy-dopamine induced degeneration of central monoamine neurons", *European Journal of Neuroscience,* vol. 5, no. 1, pp. 107-110, 1968.

[88] S. Moore and S. Thanos, "The concept of microglia in relation to central nervous system disease and regeneration", *Progress in Neurobiology,* vol. 48, no. 4-5, pp. 441-460, 1996.

[89] W. E. Thomas, "Brain Macrophages - Evaluation of Microglia and Their Functions", *Brain Research Reviews,* vol. 17, no. 1, pp. 61-74, 1992.

[90] M. Hamanoue, N. Takemoto, K. Matsumoto, T. Nakamura, K. Nakajima, and S. Kohsaka, "Neurotrophic effect of hepatocyte growth factor on central nervous system neurons in vitro", *Journal of Neuroscience Research,* vol. 43, no. 5, pp. 554-564, 1996.

[91] T. Miwa, S. Furukawa, K. Nakajima, Y. Furukawa, and S. Kohsaka, "Lipopolysaccharide enhances synthesis of brain-derived neurotrophic factor in cultured rat microglia", *Journal of Neuroscience Research,* vol. 50, no. 6, pp. 1023-1029, 1997.

[92] J. Zhang *et al.*, "Neuron-derived IgG protects dopaminergic neurons from insult by 6-OHDA and activates microglia through the Fe gamma RI and TLR4 pathways", *International Journal of Biochemistry & Cell Biology,* vol. 45, no. 8, pp. 1911-1920, 2013.

[93] B. Mammadov *et al.*, "Sciatic nerve regeneration induced by glycosaminoglycan and laminin mimetic peptide nanofiber gels", *Rsc Advances,* vol. 6, no. 112, pp. 110535-110547, 2016.

[94] S. Ichihara, Y. Inada, and T. Nakamura, "Artificial nerve tubes and their application for repair of peripheral nerve injury: an update of current concepts", *Injury-International Journal of the Care of the Injured,* vol. 39, pp. 29-39, 2008.

[95] X. Navarro, M. Vivo, and A. Valero-Cabre, "Neural plasticity after peripheral nerve injury and regeneration", *Progress in Neurobiology,* vol. 82, no. 4, pp. 163-201, 2007.

[96] M. J. Barton, J. W. Morley, M. A. Stoodley, A. Lauto, and D. A. Mahns, "Nerve repair: toward a sutureless approach", *Neurosurgical Review,* vol. 37, no. 4, pp. 585-595, 2014.

[97] T. I. Lanaras, H. E. Schaller, and N. Sinis, "Brachial plexus lesions: 10 years of experience in a center for microsurgery in Germany", *Microsurgery,* vol. 29, no. 2, pp. 87-94, 2009.

[98] G. Lundborg, "A 25-year perspective of peripheral nerve surgery: evolving neuroscientific concepts and clinical significance", *The Journal of Hand Surgery,* vol. 25, no. 3, pp. 391-414, 2000.

[99] J. W. Fawcett and R. J. Keynes, "Peripheral nerve regeneration", *Annual Review of Neuroscience,* vol. 13, pp. 43-60, 1990.

[100] S. Hall, "Nerve repair: A neurobiologist's view", *Journal of Hand Surgery-British and European Volume,* vol. 26, no. 2, pp. 129-136, 2001.

[101] K. Torigoe, H. F. Tanaka, A. Takahashi, A. Awaya, and K. Hashimoto, "Basic behavior of migratory Schwann cells in peripheral nerve regeneration", *Experimental Neurology,* vol. 137, no. 2, pp. 301-308, 1996.

[102] G. R. Evans, "Challenges to nerve regeneration", *Journal of Reconstructive Microsurgery,* vol. 19, no. 3, pp. 312-318, 2000.

[103] R. Kaewkhaw, A. M. Scutt, and J. W. Haycock, "Integrated culture and purification of rat Schwann cells from freshly isolated adult tissue", *Nature Protocols,* vol. 7, no. 11, pp. 1996-2004, 2012.

[104] D. Otto, K. Unsicker, and C. Grothe, "Pharmacological Effects of Nerve Growth-Factor and Fibroblast Growth-Factor Applied to the Transectioned Sciatic-Nerve on Neuron Death in Adult-Rat Dorsal-Root Ganglia", *Neuroscience Letters,* vol. 83, no. 1-2, pp. 156-160, 1987.

[105] K. M. Rich, T. D. Alexander, J. C. Pryor, and J. P. Hollowell, "Nerve Growth-Factor Enhances Regeneration through Silicone Chambers", *Experimental Neurology,* vol. 105, no. 2, pp. 162-170, 1989.

[106] M. Sever, B. Mammadov, M. Gecer, M. O. Guler, and A. B. Tekinay, "Nanomaterials for Neural Regeneration", *Therapeutic Nanomaterials,* p. 33, 2016.

[107] M. C. LaPlaca, V. N. Vernekar, J. T. Shoemaker, and D. K. Cullen, "Three-dimensional neuronal cultures", *Methods in bioengineering: 3D tissue engineering,* pp. 187-204, 2010.

[108] C. E. Schmidt and J. B. Leach, "Neural tissue engineering: strategies for repair and regeneration", *Annual Review of Biomedical Engineering,* vol. 5, pp. 293-347, 2003.

[109] M. Sever, I. Uyan, A. B. Tekinay, and M. O. Guler, "Bioactive Nanomaterials for Neural Engineering", in *Neural Engineering*: Springer, pp. 181-206, 2016.

[110] B. Ananthanarayanan, L. Little, D. V. Schaffer, K. E. Healy, and M. Tirrell, "Neural stem cell adhesion and proliferation on phospholipid bilayers functionalized with RGD peptides", *Biomaterials,* vol. 31, no. 33, pp. 8706-8715, 2010.

[111] J. C. Schense, J. Bloch, P. Aebischer, and J. A. Hubbell, "Enzymatic incorporation of bioactive peptides into fibrin matrices enhances neurite extension", *Nature Biotechnology,* vol. 18, no. 4, pp. 415-419, 2000.

[112] T. T. Yu and M. S. Shoichet, "Guided cell adhesion and outgrowth in peptide-modified channels for neural tissue engineering", *Biomaterials,* vol. 26, no. 13, pp. 1507-1514, 2005.

[113] K. Husmann, S. Carbonetto, and M. Schachner, "Distinct sites on tenascin-C mediate repellent or adhesive interactions with different neuronal cell types", *Cell Adhesion and Communication,* vol. 3, no. 4, pp. 293-310, 1995.

[114] K. Husmann, A. Faissner, and M. Schachner, "Tenascin Promotes Cerebellar Granule Cell-Migration and Neurite Outgrowth by Different Domains in the

Fibronectin Type-Iii Repeats", *Journal of Cell Biology*, vol. 116, no. 6, pp. 1475-1486, 1992.

[115] Y. Zhang, P. N. Anderson, G. Campbell, H. Mohajeri, M. Schachner, and A. R. Lieberman, "Tenascin-C expression by neurons and glial cells in the rat spinal cord: changes during postnatal development and after dorsal root or sciatic nerve injury", *Journal of Neurocytology*, vol. 24, no. 8, pp. 585-601, 1995.

[116] J. Schweitzer, T. Becker, J. Lefebvre, M. Granato, M. Schachner, and C. G. Becker, "Tenascin-C is involved in motor axon outgrowth in the trunk of developing zebrafish", *Developmental Dynamics*, vol. 234, no. 3, pp. 550-566, 2005.

[117] Y. M. Yu *et al.*, "The extracellular matrix glycoprotein tenascin-C promotes locomotor recovery after spinal cord injury in adult zebrafish", *Neuroscience*, vol. 183, pp. 238-250, 2011.

[118] S. Meiners, M. S. A. Nur-E-Kamal, and M. L. T. Mercado, "Identification of a neurite outgrowth-promoting motif within the alternatively spliced region of human tenascin-C", *Journal of Neuroscience*, vol. 21, no. 18, pp. 7215-7225, 2001.

[119] M. Sever, B. Mammadov, M. O. Guler, and A. B. Tekinay, "Tenascin-C mimetic Peptide nanofibers direct stem cell differentiation to osteogenic lineage", *Biomacromolecules*, vol. 15, no. 12, pp. 4480-4487, 2014.

[120] K. L. Niece, J. D. Hartgerink, J. J. J. M. Donners, and S. I. Stupp, "Self-assembly combining two bioactive peptide-amphiphile molecules into nanofibers by electrostatic attraction", *Journal of the American Chemical Society,* vol. 125, no. 24, pp. 7146-7147, 2003.

[121] L. A. Greene and A. S. Tischler, "Establishment of a noradrenergic clonal line of rat adrenal pheochromocytoma cells which respond to nerve growth factor", *Proceedings of the National Academy of Sciences,* vol. 73, no. 7, pp. 2424-2428, 1976.

[122] D. Vaudry, P. J. Stork, P. Lazarovici, and L. E. Eiden, "Signaling pathways for PC12 cell differentiation: making the right connections", *Science,* vol. 296, no. 5573, pp. 1648-1649, 2002.

[123] M. K. Lee, J. B. Tuttle, L. I. Rebhun, D. W. Cleveland, and A. Frankfurter, "The expression and posttranslational modification of a neuron-specific beta-tubulin isotype during chick embryogenesis", *Cytoskeleton,* vol. 17, no. 2, pp. 118-132, 1990.

[124] J. R. Menezes and M. B. Luskin, "Expression of neuron-specific tubulin defines a novel population in the proliferative layers of the developing telencephalon", *Journal of Neuroscience,* vol. 14, no. 9, pp. 5399-5416, 1994.

[125] E. M. Fykse *et al.*, "Relative properties and localizations of synaptic vesicle protein isoforms: the case of the synaptophysins", *Journal of Neuroscience,* vol. 13, no. 11, pp. 4997-5007, 1993.

[126] B. Marqueze-Pouey, W. Wisden, M. L. Malosio, and H. Betz, "Differential expression of synaptophysin and synaptoporin mRNAs in the postnatal rat central nervous system", *Journal of Neuroscience*, vol. 11, no. 11, pp. 3388-3397, 1991.

[127] T. S. Lewis, P. S. Shapiro, and N. G. Ahn, "Signal transduction through MAP kinase cascades", *Advances in Cancer Research, Vol 74*, vol. 74, pp. 49-139, 1998.

[128] S. P. Bruder, D. J. Fink, and A. I. Caplan, "Mesenchymal stem cells in bone development, bone repair, and skeletal regeneration therapy", *Journal of Cellular Biochemistry*, vol. 56, no. 3, pp. 283-294, 1994.

[129] A. I. Caplan, "Mesenchymal stem cells", *Journal of Orthopaedic Research*, vol. 9, no. 5, pp. 641-650, 1991.

[130] W. J. Li, R. Tuli, X. Huang, P. Laquerriere, and R. S. Tuan, "Multilineage differentiation of human mesenchymal stem cells in a three-dimensional nanofibrous scaffold", *Biomaterials*, vol. 26, no. 25, pp. 5158-5166, 2005.

[131] N. Jaiswal, S. E. Haynesworth, A. I. Caplan, and S. P. Bruder, "Osteogenic differentiation of purified, culture-expanded human mesenchymal stem cells in vitro", *Journal of Cellular Biochemistry*, vol. 64, no. 2, pp. 295-312, 1997.

[132] B. D. Boyan, T. W. Hummert, D. D. Dean, and Z. Schwartz, "Role of material surfaces in regulating bone and cartilage cell response", *Biomaterials*, vol. 17, no. 2, pp. 137-146, 1996.

[133] N. A. Bullett, D. P. Bullett, F. E. Truica-Marasescu, S. Lerouge, F. Mwale, and M. R. Wertheimer, "Polymer surface micropatterning by plasma and VUV-photochemical modification for controlled cell culture", *Applied Surface Science,* vol. 235, no. 4, pp. 395-405, 2004.

[134] S. F. Long, S. Clarke, M. C. Davies, A. L. Lewis, G. W. Hanlon, and A. W. Lloyd, "Controlled biological response on blends of a phosphorylcholine-based copolymer with poly(butyl methacrylate)", *Biomaterials,* vol. 24, no. 23, pp. 4115-4121, 2003.

[135] V. Nelea *et al.*, "Selective inhibition of type X collagen expression in human mesenchymal stem cell differentiation on polymer substrates surface-modified by glow discharge plasma", *Journal of Biomedical Materials Research Part A,* vol. 75a, no. 1, pp. 216-223, 2005.

[136] N. Huebsch *et al.*, "Harnessing traction-mediated manipulation of the cell/matrix interface to control stem-cell fate", *Nature Materials,* vol. 9, no. 6, pp. 518-526, 2010.

[137] Y. R. Shih, K. F. Tseng, H. Y. Lai, C. H. Lin, and O. K. Lee, "Matrix stiffness regulation of integrin-mediated mechanotransduction during osteogenic differentiation of human mesenchymal stem cells", *Journal of Bone and Mineral Research,* vol. 26, no. 4, pp. 730-738, 2011.

[138] M. Aumailley and B. Gayraud, "Structure and biological activity of the extracellular matrix", *Journal of Molecular Medicine,* vol. 76, no. 3-4, pp. 253-265, 1998.

[139] P. Gehron Robey, "The biochemistry of bone", *Endocrinology and Metabolism Clinics of North America,* vol. 18, no. 4, pp. 858-902, 1989.

[140] E. J. Mackie and R. P. Tucker, "Tenascin in Bone Morphogenesis - Expression by Osteoblasts and Cell Type-Specific Expression of Splice Variants", *Journal of Cell Science,* vol. 103, pp. 765-771, 1992.

[141] F. S. Jones and P. L. Jones, "The tenascin family of ECM glycoproteins: Structure, function, and regulation during embryonic development and tissue remodeling", *Developmental Dynamics,* vol. 218, no. 2, pp. 235-259, 2000.

[142] C. A. Pearson, D. Pearson, S. Shibahara, J. Hofsteenge, and R. Chiquetehrismann, "Tenascin - Cdna Cloning and Induction by Tgf-Beta", *Embo Journal,* vol. 7, no. 10, pp. 2977-2981, 1988.

[143] A. I. Alford and K. D. Hankenson, "Matricellular proteins: Extracellular modulators of bone development, remodeling, and regeneration", *Bone,* vol. 38, no. 6, pp. 749-757, 2006.

[144] E. J. Mackie, I. Thesleff, and R. Chiquetehrismann, "Tenascin Is Associated with Chondrogenic and Osteogenic Differentiation In vivo and Promotes

Chondrogenesis In vitro", *Journal of Cell Biology,* vol. 105, no. 6, pp. 2569-2579, 1987.

[145] L. Vakeva, E. Mackie, T. Kantomaa, and I. Thesleff, "Comparison of the Distribution Patterns of Tenascin and Alkaline-Phosphatase in Developing Teeth, Cartilage, and Bone of Rats and Mice", *Anatomical Record,* vol. 228, no. 1, pp. 69-76, 1990.

[146] E. J. Mackie and S. Ramsey, "Modulation of osteoblast behaviour by tenascin", *Journal of Cell Science,* vol. 109, pp. 1597-1604, 1996.

[147] H. Ceylan, S. Kocabey, A. B. Tekinay, and M. O. Guler, "Surface-adhesive and osteogenic self-assembled peptide nanofibers for bioinspired functionalization of titanium surfaces", *Soft Matter,* vol. 8, no. 14, pp. 3929-3937, 2012.

[148] T. Dvir, B. P. Timko, D. S. Kohane, and R. Langer, "Nanotechnological strategies for engineering complex tissues", *Nature Nanotechnology,* vol. 6, no. 1, pp. 13-22, 2011.

[149] S. Kocabey, H. Ceylan, A. B. Tekinay, and M. O. Guler, "Glycosaminoglycan mimetic peptide nanofibers promote mineralization by osteogenic cells", *Acta Biomaterialia,* vol. 9, no. 11, pp. 9075-9085, 2013.

[150] T. D. Sargeant *et al.*, "Hybrid bone implants: Self-assembly of peptide amphiphile nanofibers within porous titanium", *Biomaterials*, vol. 29, no. 2, pp. 161-171, 2008.

[151] T. D. Sargeant, S. M. Oppenheimer, D. C. Dunand, and S. I. Stupp, "Titanium foam-bioactive nanofiber hybrids for bone regeneration", *Journal of Tissue Engineering and Regenerative Medicine*, vol. 2, no. 8, pp. 455-462, 2008.

[152] C. M. Stanford, P. A. Jacobson, E. D. Eanes, L. A. Lembke, and R. J. Midura, "Rapidly Forming Apatitic Mineral in an Osteoblastic Cell-Line (Umr-106-01 Bsp)", *Journal of Biological Chemistry*, vol. 270, no. 16, pp. 9420-9428, 1995.

[153] C. K. Smith, J. M. Withka, and L. Regan, "A Thermodynamic Scale for the Beta-Sheet Forming Tendencies of the Amino-Acids", *Biochemistry*, vol. 33, no. 18, pp. 5510-5517, 1994.

[154] S. Toksoz, R. Mammadov, A. B. Tekinay, and M. O. Guler, "Electrostatic effects on nanofiber formation of self-assembling peptide amphiphiles", *Journal of Colloid and Interface Science*, vol. 356, no. 1, pp. 131-137, 2011.

[155] M. Pevsner-Fischer, S. Levin, and D. Zipori, "The Origins of Mesenchymal Stromal Cell Heterogeneity", *Stem Cell Reviews and Reports*, vol. 7, no. 3, pp. 560-568, 2011.

[156] H. H. Chang, M. Hemberg, M. Barahona, D. E. Ingber, and S. Huang, "Transcriptome-wide noise controls lineage choice in mammalian progenitor cells", *Nature*, vol. 453, no. 7194, pp. 544, 2008.

[157] E. Wright *et al.*, "The Sry-Related Gene Sox9 Is Expressed during Chondrogenesis in Mouse Embryos", *Nature Genetics*, vol. 9, no. 1, pp. 15-20, 1995.

[158] T. Yamashiro *et al.*, "Possible roles of Runx1 and Sox9 in incipient intramembranous ossification", *Journal of Bone and Mineral Research*, vol. 19, no. 10, pp. 1671-1677, 2004.

[159] Z. Huang, E. R. Nelson, R. L. Smith, and S. B. Goodman, "The sequential expression profiles of growth factors from osteroprogenitors to osteoblasts in vitro", *Tissue Engineering*, vol. 13, no. 9, pp. 2311-2320, 2007.

[160] J. E. Aubin, "Regulation of osteoblast formation and function", *Reviews in Endocrine and Metabolic Disorders*, vol. 2, no. 1, pp. 81-94, 2001.

[161] C. D. Hoemann, H. El-Gabalawy, and M. D. Mckee, "In vitro osteogenesis assays: Influence of the primary cell source on alkaline phosphatase activity and mineralization", *Pathologie Biologie*, vol. 57, no. 4, pp. 318-323, 2009.